nature portfolio

Peer Review File

Alveolar stem cells transdifferentiate to drive bronchiolar regeneration

Corresponding Author: Professor Bin Zhou

Any redactions in this file are there to maintain patient confidentiality, the confidentiality of unpublished data, or to remove third-party material.

This file contains all reviewer reports in order by version, followed by all author rebuttals in order by version.

Attachments originally included by the reviewers as part of their assessment can be found at the end of this file.

Version 0:

Reviewer comments:

Referee #1

(Remarks to the Author)
The manuscript explores the potential of alveolar type 2 (AT2) cells to contribute to bronchiolar epithelial regeneration following injury to club cells. By employing multiple lineage tracing strategies across different injury models, the authors report that AT2 cells can relocate into the bronchiolar compartment and acquire club cell-like characteristics. In addition, single-cell RNA sequencing is used to suggest roles for Notch signaling in differentiation and for integrin-mediated mechanisms in facilitating cell migration.

While the study presents observations that are of potential interest, several conceptual and methodological aspects remain insufficiently developed. The principal concerns are summarized below:

On the mechanism of injury sensing by AT2 cells: A key conceptual question that is not addressed in the manuscript concerns the ability of AT2 cells, situated in the alveolar region, to detect injury at a spatially distant site such as the bronchiole. The nature of this injury-sensing mechanism, and the subsequent initiation of directed migration, remains undefined. Inclusion of experimental data addressing this point would substantially enhance the mechanistic coherence of the study.

The proposed alignment between Cldn4-expressing AT2 cells in mice and AT0 cells in the human lung is presented as an important translational link. However, this comparison lacks functional substantiation and is currently based on limited marker overlap. Further validation ideally involving human tissue or functional assays would be required to support the relevance of this analogy in regenerative contexts.

The authors report that AT2 cells are capable of migrating into injured bronchioles. However, the evidence provided to support this claim is limited to rare observations without robust quantification. The mechanistic plausibility of AT2 cells crossing anatomical barriers such as the basal lamina or bronchioalveolar stem cell (BASC) niches is not addressed. Greater experimental support is necessary to establish this migration as a consistent and biologically meaningful event.

What is the “tunnel-like” structure? It is proposed that AT2 cells traverse the bronchiolar wall via tunnel-like structures, as visualized in Figure 6b. However, the identification of these structures is based solely on DAPI staining, which does not permit accurate interpretation of tissue architecture. Furthermore, the quantification in Figure 6c indicates a progressive increase in tunnel structures up to 8 weeks post-injury, which appears to contradict earlier figures (2G and 3G) showing that the bronchiolar epithelium is largely restored by 4 weeks. This inconsistency warrants clarification.

The manuscript would benefit from experiments assessing whether AT2 cells, particularly those with activated Notch signaling, can adopt club cell identities under defined in vitro conditions. Such data would provide a more direct demonstration of the plasticity inferred from in vivo observations.

The identification of a transient AT2 subpopulation expressing Cldn4 and exhibiting multipotency toward both AT1 and club cell fates is an interesting hypothesis derived from single-cell transcriptomic data. However, this model remains speculative in the absence of corroborating lineage tracing or fate-mapping evidence. Additional experimental validation is required to confirm the existence and functional relevance of this transitional state.

In Extended Data Figure 6, both Ager-creER and Hopx-dreER drivers are shown to label AT1 as well as AT2 cells. Consequently, the triple-recombinase system is likely to mark a broader epithelial population than stated in the main text. The assertion that this system specifically labels Hopx+Ager+ AT1 cells (page 7) is questionable. If AT2 cells are also labeled, the interpretation of negative findings related to their migration must be revisited.

(Remarks on code availability)

Referee #2

(Remarks to the Author)
In this manuscript, regenerative plasticity from AT2 cells to distal airway epithelium driven by Notch and ITGB1 signaling is demonstrated using highly sophisticated lineage tracing models. The manuscript is technically almost perfect and very clearly written. It does add novel insights. On the other hand however, regenerative plasticity between most cell types in the lung has now been firmly established in mouse lineage tracing models. This manuscript definitely adds a novel regenerative plasticity trajectory, but does not provide a conceptual leap.

Specific comments.

1. In all lineage tracing studies, except in those involving AT1 cells, promiscuous labeling or spontaneous recombination are not taken into account. The Jackson website, for example, mentions 10-25% spontaneous recombination in the Sftpc-CreERT model (https://www.jax.org/strain/028054), although it is not mentioned in which cells this recombination takes place. To what extent this would affect the conclusions of this manuscript remains to be seen, but it might be worth verifying this, or at least acknowledging this issue. No-tamoxifen controls would be the experiment to do. With only one airway typically showing, the data presented do not exclude spontaneous recombination as a confounding variable.

2. The lineage tracing data seem clear-cut. However, it is not immediately clear how the statistical analysis was performed. 5 mice are typically used, but how many airways/fields were quantified? Were the data pooled per mouse?

3. Given the black-and-white phenotypes with respect to lineage tracing and DT-induced injury, what were the functional repercussions? Such studies are entirely missing. For example, if the Scgb1a1-DTR model is nearly 100% efficient, is lung function or histology somehow affected? And what happens when regeneration is partially blocked, for example by interfering with Notch and ITGB1 signaling?

4. Fig. 1a, Extended data 3a-d: A confetti reporter is used to demonstrate clonality. However, it seems that only RFP+ cells are shown. It is unclear how this proves clonality.

5. Throughout the manuscript, the authors demonstrate AT1 cells in bronchioles after injury as evaluated by staining for AGER. This is surprising. It might be helpful to complement with other markers. AT1 cells were also identified in scRNAseq, but these data obviously do not provide spatial information. It might also be of interest to see if in uninjured (or perhaps in older) mice, AT1 cells are observed in bronchioles.

6. Fig. 4c: Lysotracker stains most cells, not just AT2 cells. Using this marker to exclude mature AT2 cells might not be entirely valid.

7. Extended data 7h-j: Differential expression of specific gene signatures is analyzed here. It is not made clear how these signatures were determined. Furthermore, Extended Data 7i shows a similar Notch signature in both subsets, contrary to what is claimed in the text (line 303-305). This is important as most of the remainder of manuscript focuses on Notch signaling.

8. Along the same lines, Extended data 9,f,g, Fig. 4j,n,o focus on Notch signaling. However, expression of Notch receptors and of canonical Notch target genes is not shown.

9. The authors try to link their findings to human lung regeneration, where secretory-like cells in the distal respiratory airways (SCGB3A2+SFTPB+SCGB1A1-) may be derived from AT2 cells (ref. 37). However, another paper suggested that these cells in fact differentiate into AT2 cells (Basil et al, Nature 2022, which is not cited), and another paper using hPSC-derived models indicates that these cells may be AT1 precursors (Pezet et al., Nat Biotechnol, 2025, also not cited). Another paper (Habermann et al., Sci Adv 2021, not cited either) places such cells in between AT2 and AT1 cells. Furthermore, also not acknowledged is the fact that the respiratory airways found in larger mammals are absent in rodents. The extrapolation to human data is therefore a bit tenuous.

(Remarks on code availability)

Referee #3

(Remarks to the Author)
In this manuscript, Liu and colleagues provide compelling evidence that alveolar epithelial cells type-2 (AT2) can sense the loss of airway club cells and migrate to replenish them in vivo. While multiple studies have previously showed that airway/bronchiolar epithelial cells migrate to distal lung upon severe injury. Now this manuscript provides evidence that distal alveolar cells can migrate to bronchioles to replenish club cells after their ablation. The authors used a suite of intersectional lineage tracing mouse models coupled with club cell ablation or chemical injury models to demonstrate the plasticity of AT2s. The authors claim that AT2-linegae derived cells contribute to Club, AT2, and BASCs after injury via transbronchial "tunnels". Further, the authors combine these lineage tracing models with genetic perturbation to modulate notch and Itgb1. Using scRNA-seq profiling approaches, the authors claim that AT2s go through a molecular defined transient cell state prior to generating club, ciliated cells, and AT2 and found enrichment of ligand-receptor interactions mediating notch signaling. The authors went on to use genetic perturbation models to increase or decrease notch signaling and loss of Itgb1.
In summary, this manuscript further expands on the widely described cell plasticity during injury repair in lungs. They used mouse models with multiple alleles to definitively demonstrate the contribution of specific cell populations. A major concern is that the signaling pathways they targeted are either very general or they focus on downstream cell fate specification once AT2s migrate to the bronchiolar luminal side. I suggest the authors address the following comments/concerns to make this manuscript more meaningful.

Major comments:
1. Functional properties of AT2-lineage derived bronchiolar epithelial cells:
In Fig-2, they show AT2-derived cells sustain up to 6 months post naphthalene. Do they function as club cells? Do they respond to a secondary injury and generate club cells and ciliated cells? Do AT2-lineage derived cells retain any epigenetic memory? Use ATAC-seq. Similarly, are AT2-lineage derived ciliated cells function similarly as the native ciliated cells?
2. Contribution of rare p63+ distal bronchiolar epithelium:
Previous studies found a rare population of p63+ cells in the distal bronchioles expand extensively and generate "pods after H1N1-PR8 infection and to some extent in bleomycin-induced injury models. In Extended Data Fig-4, the authors used p63-lineage tracing models. However, this reviewer questions whether their tamoxifen regimen was sufficient to label these rare p63+ cells in the distal airways? Additionally, recent studies showed the presence of SCGB3A2+ve SCGB1A1-ve cells in small airways and they convert to p63+ basal cells in H1N1-PR8 infected cells. Therefore, authors need to check the relative contribution of different cell sources.
3. Communication between ciliated cells and transient cells via Notch:
Based on the data in Fig-5n-U, the authors concluded that notch receptor and ligand interaction between "transient cell" and ciliated cell controls the fate of migrated AT2 cells. However, current data doesn't show whether the interaction between ciliated cells and "transient cells" is mediated by Notch ligand and receptor. The authors need to specifically delete Notch2 and Jag2 in Ciliated cells and transient cells, respectively. Current work targets Notch receptors in AT2s and its dependents but not specifically the transient cells.
4. Trans-bronchial migration of AT2 cells via "tunnels":
Based on the static image data in Fig-6b, the authors state that AT2s migrate to the airway surface via "tunnels". However, current images don't show a clear "tunnel" like structure instead they look like "channels". It would be very informative to visualize these passages in 3-dimensional view. Further, what regulates "Tunnel" formation? Is the basement membrane completely disassembled or patchy disorganization under the bronchiolar epithelium after club cell loss? Have the authors found upregulation of any ECM degrading proteases in transcriptome data?
5. What are the mechanisms that initiate AT2s to sense the loss of club cells and drive their migration? Currently, the authors focused on Itgb1and Notch and found that disruption of these pathways block AT2s migration and fate specification during and after migration, respectively. However, loss of Itgb1 blocks various cellular processes besides migration including cell attachment to the basement membrane and their replication. Therefore, the phenotype described here is not very specific to migration. Similarly, as mentioned above (#3), it is important to modulate notch in specific cell states that are in contact with ciliated cells rather than all AT2s. Lack of specificity can obscure the conclusions.
6. Based on the current data, AT2s contribute to multiple cell populations within lung epithelium, which suggests that AT2s are multipotent. Authors need to discuss this further and emphasize this in the results and discussion sections.
7. There are some AT2-lineage derived AT1s in bronchioles Fig-1m and 2l. What is the fate of these cells at late times?
8. scRNA-seq data in Fig-4S shows that very few AT2-lineage derived cells contribute to Ciliated cells at 6 months compared to 4 months. Are they lost by 6 months and replenished by other lineages (BASCs or club cells)?
9. Are AT2-lineage derived cells indispensable? In Sftpc-DreER/Rbpj-KO lungs, does the lung have any defects in regeneration and physiology. Same in ITGB1-KO?
10. How far AT2-lineage derived cells migrate along bronchioles? Show images from different branches.
11. In Fig-2l, the authors show Acetylated tubulin to identify ciliated cells. While this is a specific marker of ciliated cells, its not clear whether cilia belong to AT2-lineage derived cells? FOXJ1 would be a better marker to confirm AT2-labeled cells make ciliated cells.
12. How long does it take to fully replenish the lost club cells in bronchioles?

Minor comments:
1. In Fig-5u and in text, the authors referred the process of conversion of AT2 cells into club cells as "Differentiation". Based on classical definition, this should be called "Transdifferentiation". Authors should review the nomenclature and change that accordingly.

(Remarks on code availability)

Version 1:

Reviewer comments:

Referee #1

(Remarks to the Author)
In the reviewed manuscript, Liu et al. demonstrate that AT2 cells can migrate to the bronchioles and transdifferentiate into club cells, ciliated cells, and AT1 cells, using multiple lineage-tracing approaches across different injury models. To investigate the regulatory mechanisms governing AT2 cell transdifferentiation, single-cell sequencing was performed, revealing a transient cell population characterised by high Cldn4 expression between club and AT2 cells. Further analyses indicated that Notch signalling is activated during this transdifferentiation process, and that inhibition of the Notch pathway blocks AT2 cell fate conversion. In addition, ciliated cells were shown to express the Notch ligands Jag1/2, whereas AT2 cells express the corresponding receptors during this process. Finally, the authors propose that immune cells secrete Spp1, which binds to Itgb1 on AT2 cells and promotes their migration towards the bronchioles.
Although the study presents an interesting concept, the current evidence remains insufficient to fully support several key conclusions:
1. In this manuscript, most immunostaining used to quantify the proportions of AT2 and club cells relies on single-marker staining. However, as noted by the authors, BASCs located at the BADJ co-express both AT2 and club cell markers and can differentiate into club cells following injury. Therefore, double-marker staining is essential to ensure that lineage-labelled cells are accurately identified as bona fide AT2 or club cells. A similar concern applies to the organoid culture experiments.
2. To demonstrate AT2 cell migration toward the bronchioles, the authors present examples of AT2 cell clones (route 1) and putative channels (route 2). In route 1, lineage-labelled cells could also localise to the BADJ and differentiate into BASCs. In route 2, AT2 cells may transiently reside in this region or migrate away from it; thus, the data in Extended Fig. 3f do not provide clear evidence to support the direction of migration as the arrow showed. Furthermore, in Fig. 1o, it is unclear how lineage-labelled cells observed in the bronchioles can be definitively assigned to either route 1 or route 2 based solely on immunostaining. In addition, in Fig. 1p, the authors propose that the channel is formed by AT1 cells, yet no direct evidence is provided to confirm that these channel-forming cells are indeed AT1 cells.
3. On page 5, the authors state that only a small proportion of BASCs are detected following injury repair. This raises an important question: if AT2 cells can migrate to the bronchioles via the BADJ and subsequently differentiate into club cells, why do they not first adopt a BASC state, given that BASCs are both anatomically and developmentally closer to AT2 cells than club cells? The authors should address this point directly to strengthen the biological plausibility of their model.
4. The authors report that all Scgb1a1^{+} cells are ablated , and excluding alternative sources of club cells, including basal cells, neuroendocrine cells, and AT1 cells. However, in Fig. 1j and 1k, approximately 20% of club cells are negative for AT2 lineage tracing. Additional evidence is required to clarify the origin of these AT2 lineage-negative club cells.
5. Club cells and ciliated cells are arranged in an alternating pattern within the bronchioles. Based on the authors' model, migrating AT2 cells would frequently encounter ciliated cells and potentially differentiate into club cells. However, the quantification data indicate that the majority of lineage-labelled cells remain as AT2 or AT1 cells. This apparent discrepancy should be clarified to improve the coherence of the proposed model.
6. The authors state that AT2 cells can differentiate into AT1 cells within the bronchioles and exclude the possibility that AT1 cells migrate into this region. However, in Fig. 2j and Extended Fig. 2i, j, some AT1 cells do not express RFP, indicating that they are not derived from the AT2 lineage. These seemingly contradictory observations require further clarification.
7. In the injury models used, club cells are specifically ablated by genetic or chemical methods, whereas ciliated cells remain intact. The authors also show that AT2 cells can differentiate into AT1 cells upon migration to the bronchioles. Given that AT1 cells have a substantially larger surface area, this raises the question of how ciliated cells are accommodated within regions covered by AT1 cells. If ciliated cells are also lost, this would call into question the validity of the injury models employed. The authors should address this issue explicitly.
8. The interaction strength between peribronchial fibroblasts and AT2 cells appears to be substantially greater than that between immune cells and AT2 cells. Therefore, investigating signalling pathways mediated by peribronchial fibroblasts may be more relevant for understanding AT2 cell migration. The authors should justify their focus on immune-derived signals to improve the interpretability of their findings.

(Remarks on code availability)

Referee #2

(Remarks to the Author)
The authors addressed all my technical concerns, and then some. It is a tour-de-force. There is no doubt that the observed trajectories occur in mice.

The connection to human lung regeneration remains tenuous however, as this extrapolation is based on expression of Cldn4 in both the transitional cells studied here and in AT0 cells in the data of the Tata group (Nature 2022). The trajectory

of the heterogenuous TRB population in humans is furthermore quite controversial, which does not help the argument, and the authors picked the one trajectory that fits their argument. The only way to resolve this issue is to do studies on well-characterized and pure human cells, and correlate with rigorous trajectory analysis in human lung injury. This is admittedly beyond the scope of this already very extensive manuscript.

(Remarks on code availability)

Referee #3

(Remarks to the Author)
All my prior concerns were addressed and congratulations to the authors for accomplishing this.

(Remarks on code availability)
NA

Version 2:

Reviewer comments:

Referee #1

(Remarks to the Author)
My comments have been fully addressed. I have no further comments.

(Remarks on code availability)

Open Access This Peer Review File is licensed under a Creative Commons Attribution 4.0 International License, which permits use, sharing, adaptation, distribution and reproduction in any medium or format, as long as you give appropriate credit to the original author(s) and the source, provide a link to the Creative Commons license, and indicate if changes were made.
In cases where reviewers are anonymous, credit should be given to 'Anonymous Referee' and the source.
The images or other third party material in this Peer Review File are included in the article's Creative Commons license, unless indicated otherwise in a credit line to the material. If material is not included in the article's Creative Commons license and your intended use is not permitted by statutory regulation or exceeds the permitted use, you will need to obtain permission directly from the copyright holder.
To view a copy of this license, visit https://creativecommons.org/licenses/by/4.0/

Response Letter to Reviewers

We sincerely thank the reviewers for their valuable time and insightful comments. Their constructive suggestions have greatly helped us enhance the quality of our manuscript. Below, we provide point-by-point responses to their comments. The reviewers' original remarks are in black text, and our responses follow in blue text. The references cited in our responses are listed at the end of this letter. Additionally, Figures to Reviewers 1-8 are attached at the end of this document.

Referees' comments:

Referee #1 (Remarks to the Author):

The manuscript explores the potential of alveolar type 2 (AT2) cells to contribute to bronchiolar epithelial regeneration following injury to club cells. By employing multiple lineage tracing strategies across different injury models, the authors report that AT2 cells can relocate into the bronchiolar compartment and acquire club cell-like characteristics. In addition, single-cell RNA sequencing is used to suggest roles for Notch signaling in differentiation and for integrin-mediated mechanisms in facilitating cell migration.

While the study presents observations that are of potential interest, several conceptual and methodological aspects remain insufficiently developed. The principal concerns are summarized below:

Author's Response: We thank the reviewer for recognizing the potential interest of our observations and for their constructive critique of the conceptual and methodological aspects that require further development. In the revised manuscript, we have systematically addressed each of the concerns raised, as detailed below. The additional experiments and clarifications have, we believe, substantially strengthened the conceptual foundation and methodological rigor of our study.

On the mechanism of injury sensing by AT2 cells: A key conceptual question that is not addressed in the manuscript concerns the ability of AT2 cells, situated in the alveolar region, to detect injury at a spatially distant site such as the bronchiole. The nature of this injury-sensing mechanism, and the subsequent initiation of directed migration, remains undefined. Inclusion of experimental data addressing this point would substantially enhance the mechanistic coherence of the study.

Author's Response: We thank the reviewer for raising this important conceptual question. In our original study, the mechanisms by which AT2 cells sense distal bronchiolar injury and initiate directed migration were not fully elucidated. To systematically characterize the cellular response to bronchiolar injury, we established a high-resolution lung transcriptional atlas using scRNA-seq on PBS-treated (control) and DT-treated *Scgb1a1-DTR-GFP* mice. Unsupervised clustering and UMAP visualization of the integrated dataset identified 27 distinct cell populations, including epithelial, endothelial, stromal, and immune lineages (Extended Data Fig. 15a, c). Overlay of samples by condition (Extended Data Fig. 15b) revealed broad overlap between PBS and DT groups for most populations, but also highlighted injury-specific cell expansion in localized clusters. Specifically, DT-injured lungs exhibited massive infiltration of innate immune cells, primarily a

sharp rise in neutrophils, accompanied by robust expansion of peribronchiolar fibroblasts, suggesting the formation of a highly active inflammatory and stromal microenvironment (Extended Data Fig. 15d).

Building upon this cellular census, we investigated whether these compositional shifts translated into functional alterations in the signaling network. Comparative CellChat analysis revealed a global expansion of signaling intensity following injury, with neutrophils, NK cells, monocytes, alveolar macrophages, and peribroncholar fibroblasts shifting toward active signaling hubs (Fig. 7a). Notably, the directionality of these interactions shifted markedly toward AT2 cells after DT treatment, identifying neutrophils, monocytes, and peribronchiolar fibroblasts as the predominant injury-induced signal sources (Fig. 7b). To identify potential chemotactic cues orchestrating AT2 cell recruitment for bronchial repair, we used CellChat to quantify relative information flow across ligand-receptor pathways, enabling systematic comparison of signaling dynamics between homeostatic and injured states. This analysis revealed a consistent and robust induction of SPP1 signaling targeting AT2 cells, primarily emanating from diverse immune cell populations following DT-mediated bronchial damage (Extended Data Fig. 15e). In contrast, peribronchiolar fibroblasts did not show a discernible injury-induced enhancement in chemotactic signaling (Extended Data Fig. 15e). SPP1 is a well-characterized secreted chemotactic factor that binds to integrins and CD44 receptors on the cell surface, activating multiple pathways–including PI3K/AKT/mTOR, Rho/Cdc42, and RAS/MAPK–to promote proliferation and migration of recipient cells (Pang et al., *Pharmacol Res*, 2019; Yim et al., *Immunol Rev*, 2022; Li et al., *Int J Cancer*, 2025) (Extended Data Fig. 15h).

These findings suggest that the rapid infiltration of myeloid cells serves as a signal amplifier, secreting high levels of Spp1 to establish a chemotactic gradient following DT-induced bronchial injury. This biochemical bridge effectively traverses the spatial gap between the injured bronchioles and the adjacent alveolar regions. Ligand–receptor interaction analysis further revealed that DT treatment significantly intensified interaction probabilities between immune cells-derived SPP1 and specific integrin heterodimers (e.g., *Itgav+Itgb6* and *Itga5+Itgb1*) on AT2 cells (Fig. 7c). Activation of the Spp1-Integrin axis appeared to prime downstream PI3K/AKT/mTOR, Rho/Cdc42, and RAS/MAPK signaling, as evidenced by marked upregulation of migration-related and S-phase gene signatures in AT2 cells following injury (Extended Data Fig. 15h,i). Consistent with this migratory phenotype, expression of key Rho GTPases, including *Rhoa*, *Rac1*, and *Cdc42*, was significantly elevated and positively correlated with migration signaling scores (Extended Data Fig. 15j,k). Collectively, we propose that the rapid infiltration of $Spp1^{high}$ immune cells establishes a chemotactic gradient, serving as the critical “injury-sensing” signal. This gradient triggers downstream activation of PI3K/AKT, Rho, and RAS pathways in AT2 cells, initiating their directed migration toward the bronchioles.

Our scRNA-seq analysis revealed a response of multiple cell types to DT injury, with the most pronounced interaction strength changes observed in the immune compartments (Fig. 7a). Specifically, cell-cell communication signaling analysis identified SPP1 as a central ligand, primarily secreted by immune cells and potentially signaling to AT2 cells via specific ligand-receptor interactions (Fig. 7c and Extended Data Fig. 15e). While these data suggest that SPP1-mediated chemotaxis may drive the recruitment of AT2 cells toward the injured bronchioles, scRNA-seq lacks the spatial resolution to confirm whether these signaling events are localized to the injury site. To determine whether these responsive immune cells are strategically positioned to

establish a chemotactic gradient for AT2 migration, we performed high-resolution spatial transcriptomic sequencing (Stereo-seq) on lung tissues from *Scgb1a1-DTR-GFP* mice at day 7 post-DT injury, with wildtype mice as controls. Initially, we identified major lung cell types in both control and DT groups, including immune cells, peribronchiolar fibroblasts, pericytes, smooth muscle cells, endothelial cells, AT1 cells, AT2 cells, and ciliated cells (Fig. 7d). To characterize the regionalized response to bronchial injury, we utilized H&E staining on sister sections to delineate airway and alveolar structures, subsequently defining "peribronchiolar region" (within ~200 μm of the bronchi) and "alveolar region" for localized transcriptomic analysis (Extended Data Fig. 16a). We observed a significant (~3-fold) and localized increase in immune cell infiltration within the peribronchiolar region following DT injury (Fig. 7e). To identify the molecular signals potentially driving AT2 recruitment, we employed Hotspot analysis to identify spatially coherent gene modules. Under homeostasis, gene modules associated with leukocyte activation and chemokine signaling (e.g., Modules 7 and 20) showed no specific correlation with bronchial structures (Extended Data Fig. 16b,c). In contrast, DT-injured lungs exhibited the emergence of modules related to leukocyte activation and chemotaxis (e.g., Modules 9 and 26), which were highly concentrated within the bronchial lumen and peribronchiolar areas (Extended Data Fig. 16b,c and Fig. 7 h). Notably, module 9 was enriched for pro-inflammatory and chemokine-related genes such as *Spp1* and *Ccl6*. Concurrently, module 26 was characterized by the expression of key mediators of chemokine response and leukocyte chemotaxis (e.g. *Cxcl9* and *Ccl17*). Consistently, *Spp1* expression was significantly upregulated in peribronchiolar immune cells after DT injury (Fig. 7f). Moreover, we observed a profound enrichment of chemotaxis-related gene sets in immune cells localized within the peribronchiolar regions after DT-induced injury (Fig. 7g). Collectively, these spatial findings complement our single-cell data by demonstrating that bronchial injury triggers a localized accumulation of immune cells that secrete potent chemotactic factors such as SPP1. This localized inflammatory microenvironment likely serves as key mediators that transmit bronchial injury signals to AT2 cells and establish the chemotactic gradient necessary to drive their directed migration.

To test this hypothesis, we first validated SPP1 expression in immune cells by immunostaining. Lungs from *Scgb1a1-DTR-GFP* mice were collected on days 3, 7, 14, and 28 following DT injury (Extended Data Fig. 17a). Compared with PBS-treated controls, a large number of $CD45^+$ immune cells infiltrated the bronchial lumen after injury and showed high SPP1 expression (Fig. 7i and Extended Data Fig. 17b). Quantification revealed that the mean fluorescence intensity of SPP1 in infiltrated immune cells (yellow arrows) was significantly higher than that in peribronchiolar $CD45^+$ immune cells (white arrows, Fig. 7i,j). The number of immune cells infiltrating the bronchial lumen decreased over time after injury. During the first 7 days following DT treatment, immune cells rapidly responded to injury and infiltrated the bronchial lumen, whereas after day 7, infiltration rapidly declined. Accordingly, we defined the first 7 days as the early injury-response stage and the period after day 7 as the late injury-response stage (Fig. 7k). Using *Sftpc-CreER;R26-tdT;Scgb1a1-DTR-GFP* mice to trace AT2 cell lineage (AT2-tracer1) migration toward the bronchi following DT injury, we found that tdT^+ AT2 lineage cells began migrating toward the bronchiole as early as the early response stage, and the proportion of the bronchiole covered by migrated tdT^+ cells increased with repair time (red line, Fig. 7l and Extended Data Fig. 17d). Immune cell infiltration peaked during the early response phase (blue line), suggesting that SPP1 secreted by these immune cells induces AT2 cell lineage migration (Fig. 7l).

We found that after DT injury, AT2 lineage cells enter the bronchiole via two routes: the natural bronchioalveolar duct junction (BADJ, route 1) and channels formed by AT2 cells through the bronchiolar wall (route 2) (Fig. 1n-p). Further immunofluorescence staining of lung sections from *Sftpc-CreER;R26-tdT;Scgb1a1-DTR-GFP* mice on day 3 post-DT injury revealed that infiltrating $SPP1^{+}MMP9^{+}$ immune cells were distributed near migrating AT2-derived cells at both the terminal bronchioles (adjacent to the BADJ) and channel sites, suggesting that these immune cells may participate in AT2 cell migration toward the bronchioles (Extended Data Fig. 17h-j). We then examined an alternative bronchiolar injury model induced by naphthalene. In wild-type mice treated with naphthalene, we similarly observed massive infiltration of $SPP1^{high}$ immune cells into the bronchiolar lumen, with the number of infiltrated cells gradually decreasing as repair progressed (Extended Data Fig. 17k-n). Based on the immune cell response, we again defined the first 7 days as the early response stage and the period after day 7 as the late response stage (Extended Data Fig. 17n). We used *Scgb1a1-CreER;Sftpc-DreER;R26-NR* mice to specifically examine the contribution of ZsG^{+} AT2 cells (AT2-tracer2) to the bronchiolar epithelium following naphthalene injury. Immunostaining and statistical analysis revealed that ZsG^{+} cells began migrating to the bronchiolar epithelium during the early stage when immune cell infiltration was high, and that their coverage of the bronchiolar epithelium increased with repair time (Extended Data Fig. 17o-q). Together, these findings suggest a correlation between $SPP1^{high}$ immune cells and AT2 cell migration.

We next performed *in vitro* scratch and Transwell migration assays to determine whether SPP1 secreted by immune cells promotes AT2 cell migration. Using the AT2 cell line (MLE-12), we found that wound closure was detectable 24 hours after scratching, and quantitative analysis showed that the addition of recombinant SPP1 significantly accelerated wound closure (Extended Data Fig. 18a,b). To further confirm the pro-migratory effect of SPP1, we conducted Transwell migration assays. MLE-12 cells were seeded into the upper chamber of Transwell inserts, and recombinant SPP1 was added to the lower chamber as a chemoattractant. After 16 hours of incubation, non-migrated cells were removed from the upper surface of the membrane, while migrated cells on the lower surface were fixed, stained with crystal violet, and counted under a microscope. Consistent with the scratch assay results, recombinant SPP1 also enhanced cell migration in the Transwell assay (Extended Data Fig. 18c,d). To further verify that soluble factors secreted by immune cells drive cell migration, we added immune cells to the lower chamber and found that this markedly increased MLE-12 cell migration. Moreover, the addition of an SPP1 inhibitor significantly suppressed this immune-cell-induced migratory effect (Extended Data Fig. 18e-g). Together, these *in vitro* data demonstrate that SPP1 secreted by immune cells promotes alveolar epithelial cell migration.

Next, we validated the regulatory role of SPP1 *in vivo*. We treated *Sftpc-CreER;R26-tdT;Scgb1a1-DTR-GFP* mice with DT and administered an SPP1 inhibitor every other day. Lungs were collected at 4 weeks after DT injury for analysis (Fig. 7m). Immunostaining and statistical analysis showed that, compared with the control group, the coverage of tdT^{+} cells migrating to the bronchioles was significantly reduced in the SPP1 inhibitor-treated group (Fig. 7n.o). In addition, the *Scgb1a1-CreER;Sftpc-DreER;R26-NR* mice were subjected to naphthalene injury and treated with the SPP1 inhibitor (Extended Data Fig. 18h). Analysis of lung samples collected on day 28 similarly revealed that SPP1 inhibition significantly reduced the coverage of ZsG^{+} cells migrating to the bronchiole (Extended Data Fig. 18i,j). Together, these experiments demonstrate that SPP1

secreted by immune cells acts as a chemoattractant for AT2 cell migration toward injured bronchioles (Fig. 7p).

Our scRNA-seq analysis revealed a robust interaction between immune cell-derived *Spp1* and the integrin receptor *Itgb1* expressed on AT2 cells (Fig. 7c). To further test whether *Itgb1* regulates AT2 cell migration, we performed *in vitro* scratch assays and found that addition of an anti-integrin β1 antibody significantly inhibited wound closure (Extended Data Fig. 18k,l). Moreover, Transwell assays demonstrated that adding the anti-integrin β1 antibody significantly reduced cell migration from the upper to the lower chamber (Extended Data Fig. 18m,n). To extend these findings *in vivo*, we used *Sftpc-CreER;R26-tdT;Scgb1a1-DTR-GFP;Itgb1*$^{flox/flox}$ mice to specifically knock out *Itgb1* in AT2 cells. We collected lungs 28 days after DT injury and performed immunostaining and statistical analyses (Fig. 7q). Compared with control mice (*Sftpc-CreER;R26-tdT;Scgb1a1-DTR-GFP;Itgb1*$^{flox/+}$ mice), *Itgb1* knockout significantly reduced AT2 cell migration toward the bronchioles (Fig. 7r,s). These data indicate that AT2 cells rely on the receptor Itgb1 to receive chemotactic signals, thereby responding to bronchial damage by migrating to the affected area.

In summary, through the series of new experiments described above, we propose that following bronchiolar injury (DT and naphthalene models), a large number of immune cells infiltrate the bronchiolar lumen and express SPP1. Secreted SPP1 diffuses to form a concentration gradient centered on the bronchioles. This SPP1 acts as a ligand that binds to integrin receptors on peribronchiolar AT2 cells, thereby initiating their directional migration toward the bronchiolar region with high SPP1 concentration (Fig. 7u and Extended Data Fig. 20). These data and discussion have been added to the revised manuscript. For details, please refer to revised Figure 7, Extended Data Figs. 15-18; Page 17, line 498; and Pages 18-20 of the revised manuscript.

The proposed alignment between Cldn4-expressing AT2 cells in mice and AT0 cells in the human lung is presented as an important translational link. However, this comparison lacks functional substantiation and is currently based on limited marker overlap. Further validation ideally involving human tissue or functional assays would be required to support the relevance of this analogy in regenerative contexts.

Author's Response: We thank the reviewer for this insightful suggestion. In the first version of the manuscript, we linked our mouse findings to human lung regeneration based on the following observations. In a human single-cell study (Murthy et al., *Nature*, 2022) on the terminal and respiratory bronchioles (TRBs, a structure absent in mice), a population of AT0 cells was identified that co-express SFTPC and SCGB3A2. Pseudotime analysis and *in vitro* organoid culture showed that human AT2 cells can transition into secretory cells and AT1 cells through the AT0 intermediate state (Murthy et al., *Nature*, 2022). In parallel, our mouse data revealed high expression of *Cldn4* in the transient state during both AT2-to-AT1 and AT2-to-club transitions, with a lineage trajectory similar to that observed in humans (Fig. 4c,d). When we re-analyzed the single-cell data from Murthy et al., 2022, we found that the AT0 cells in the trajectory of AT2-to-secretory cell differentiation also highly expressed *CLDN4* (Extended Data Fig. 11b-e). Based on these similarities, we speculated that the mouse AT2-to-club transition may resemble the human AT2-to-secretory cell transition with respect to cellular state changes, and that mouse Cldn4^{+}

transient cells might correspond to human CLDN4$^+$ AT0 cells. However, we acknowledge that the absence of respiratory bronchioles in mice represents an anatomical divergence that makes a direct functional analogy inappropriate. Therefore, we have reduced the emphasis on this comparison and included a revised discussion in the manuscript.

As suggested by the reviewer, we have performed functional assays in mice, including genetic tracing of *Cldn4*$^+$ intermediate cells specifically derived from AT2 cells and functional examination of the role of *Cldn4* in directing AT2 cell contribution to bronchiolar repair. Please note that because the Reviewer specifically raised questions regarding the fate and function of Cldn4$^+$ transient cells in the sixth question, only the key data are presented here. Please refer to our response to the sixth question for detailed data. We first generated a *Cldn4*-loxP-Stop-loxP-Dre (abbreviated as *Cldn4-LSL-Dre*) line (Fig. 4j) and another AT2-specific genetic tool, *Lamp3*-CreER (Extended Data Fig. 12a). We then combined these two tools to investigate the fate of transient cells. To this end, we generated *Lamp3-CreER;Scgb1a1-DTR-GFP;Cldn4-LSL-Dre;R26-rox-stop-rox-loxP-stop-loxP-tdTomato* quadruple-positive mice (Fig. 4k). The *R26-rox-stop-rox-loxP-stop-loxP-tdTomato* (abbreviated as *R26-RSR-LSL-tdT*) reporter requires dual recombinase activity: tdTomato is expressed only after both stop cassettes are excised by Dre-rox and Cre-loxP recombination (Fig. 4l). The tracing principle is as follows. Upon tamoxifen induction, *Lamp3-CreER* excises the LSL stop sequence in the *Cldn4*-LSL-Dre locus specifically in AT2 cells, converting it to *Cldn4*-Dre (step 1). It also excises one stop cassette (LSL) in *R26-RSR-LSL-tdT* to generate *R26-RSR-tdT* (step 1). Subsequently, when AT2-derived transient cells express *Cldn4* after DT injury, the activated *Cldn4* promoter drives Dre expression, which excises the second stop cassette (RSR) in *R26-RSR-tdT* (step 2), resulting in specific tdT labeling of AT2-derived Cldn4$^+$ cells (Fig. 4l). Because club cells express GFP, those derived from Cldn4$^+$ transient cells co-express tdT and GFP, appearing yellow. For *in vivo* validation, we treated mice with tamoxifen and DT (with PBS as vehicle) and collected lung samples at week 4 post-injury (Fig. 4k). Immunostaining showed minimal tdT signal in control mice (Fig. 4m). In contrast, after DT injury, we detected abundant newly generated GFP$^+$Scgb1a1$^+$ club cells that also expressed tdT, confirming genetic tracing of AT2-derived Cldn4$^+$ transient cells and their contribution to club cells after injury (Fig. 4n). We also detected tdT$^+$ AGER$^+$ cells in the bronchioles. Further quantification of tdT$^+$ cell lineages in the bronchiolar epithelium showed that club cells, AT1 cells, and AT2 cells accounted for 56.55 ± 4.54%, 14.05 ± 3.13%, and 7.48 ± 2.06% of the total, respectively (Fig. 4p). These fate-mapping data demonstrate that AT2 cells pass through a Cldn4$^+$ transient stage, which subsequently gives rise to both club cells and AT1 cells, consistent with our previous pseudotime analysis (Fig. 4d). To further validate the functional role of Cldn4 in AT2 cell contribution to the bronchiolar epithelium, we developed a conditional knockout tool, *Cldn4*-flox (Fig. 4q). We generated *Sftpc-CreER;R26-tdT;Scgb1a1-DTR-GFP;Cldn4*$^{flox/+}$ (control) and *Sftpc-CreER;R26-tdT;Scgb1a1-DTR-GFP;Cldn4* $^{flox/flox}$ (experimental) mice (Fig. 4r). After tamoxifen and DT treatment, AT2 cells were specifically traced and *Cldn4* was knocked out (Fig. 4r and Extended Data Fig. 12k,l). At 4 weeks post-DT, immunostaining and statistical analysis showed that *Cldn4* knockout significantly reduced the proportion of AT2 cells contributing to club cells (Fig. 4s,t and Extended Data Fig. 12m). Furthermore, *Cldn4* knockout also significantly reduced the proportion of AT1 cells among AT2-derived bronchiolar cells and decreased bronchiolar epithelial coverage (Fig. 4u-w and Extended Data Fig. 12n). In summary, these genetic fate-mapping and functional analyses demonstrate that Cldn4$^+$ intermediate cells derived from AT2 cells not only

contribute to the bronchiolar epithelium but also functionally promote AT2 cell-mediated epithelial repair (Fig. 4x).

Although the above experiments confirmed the role of Cldn4 in the transition of AT2 cells into club and AT1 cells, we still lack direct evidence demonstrating functional similarity between human CLDN4$^+$ AT0 cells and mouse Cldn4$^+$ transient cells. Therefore, we have made the following revisions to the manuscript. First, we explicitly acknowledge the anatomical differences between human and mouse distal airways, stating that direct extrapolation from mouse to human is not warranted. Second, we have toned down statements that directly equate mouse AT2-to-club conversion with human secretory cell differentiation. Instead, we discuss the similarity of AT2 cell differentiation trajectories between the two species: in mice, AT2 cells transition via a transient state into club and AT1 cells; in humans, AT2 cells transition via AT0 cells into secretory and AT1 cells. We also highlight the molecular similarity of CLDN4 as a conserved intermediate marker. Third, we note that the mouse AT2 differentiation trajectories have been validated by our genetic lineage tracing and functional studies, and we underscore that the core value of the mouse model lies in providing causal mechanistic evidence. We believe these revisions provide a more balanced and rigorous discussion that respects both the power and the limitations of mouse genetic models for understanding human lung biology. These data and discussion have been added to the revised manuscript. For details, please refer to revised Figure 4, Extended Data Figs. 11 and 12; Page 13, Paragraph 2; Page 14, Paragraphs 1-2; Page 22, Paragraph 2, Line 654; and Page 23 of the revised manuscript.

The authors report that AT2 cells are capable of migrating into injured bronchioles. However, the evidence provided to support this claim is limited to rare observations without robust quantification. The mechanistic plausibility of AT2 cells crossing anatomical barriers such as the basal lamina or bronchioalveolar stem cell (BASC) niches is not addressed. Greater experimental support is necessary to establish this migration as a consistent and biologically meaningful event.

Response: We thank the reviewer for raising this important point. In our original manuscript, we reported that AT2 cells can migrate and contribute to bronchiolar regeneration in both DT-induced and naphthalene-induced bronchiolar injury models. To provide an in-depth description of the migration mechanism, we have now performed additional experiments and quantitative analyses to support this migratory process. First, we present immunostaining scan images of lung sections to illustrate that AT2 cell migration is not a rare observation. These images readily show that the majority of bronchiolar epithelium contains genetically traced AT2 cell lineages (Extended Data Fig. 3a,b and Fig. 1 to Reviewers). We then investigated the routes of AT2 cell migration toward the bronchiole following injury. Using *Sftpc-CreER;R26-tdT;Scgb1a1-DTR-GFP* mice, we administered DT to specifically ablate Scgb1a1$^+$ club cells and BASCs. We detected tdT-traced AT2 cells migrating into the bronchioles and contributing to club cells (Fig. 1d-m). We found that AT2 cell lineages enter the bronchiole via two routes after injury: (1) the natural bronchioalveolar duct junction (BADJ, route 1), and (2) channels formed by AT2 cells through the bronchial wall

into the bronchiolar lumen (route 2) (Fig. 1n-p).

To examine the migration mechanism in detail, we re-collected lungs at multiple time points following DT injury (days 3, 7, 14, 28, and 8 weeks post-DT) for sectional immunostaining and quantitative analysis of AT2 cell migration (Fig. 1f). In PBS-treated control mice, no tdT signal was detected in the distal bronchioles (Fig. 1g). On day 3 post-DT, immunostaining analysis of lung sections revealed tdT^+ cells initiating migration toward the bronchiole through the BADJ (route 1, white arrowheads) as well as directly through formed bronchiolar wall channels (route 2); however, no transdifferentiation into club cells had yet occurred at this stage (Fig. 1n). Immunostaining and statistical analysis on days 7, 14, 28, and 8 weeks post-DT showed that tdT^+ club cells were detectable on day 7, and the coverage of the bronchiolar epithelium by tdT^+ cells increased as repair progressed (Extended Data Fig. 3a-d). At all these time points, tdT^+ cells were detected along both route 1 and route 2 on lung sections (Extended Data Fig. 3c-e), suggesting AT2 cell lineages employ both routes to enter the bronchioles. However, we observed a marked difference in the frequency with which these two routes were used. We defined a "route 1 event" when tdT^+ cells were located at the distal bronchioles near the BADJ, and a "route 2 event" when channel structures were detected on the bronchiolar wall (Fig. 1n,p). By quantifying the proportion of bronchioles exhibiting route 1 and route 2 events at different time points, we observed a difference in the cumulative proportions. The proportion of route 1 events increased rapidly from day 3 to day 28 post-injury, reaching 92.08 ± 3.39% by 8 weeks, which coincided with the rapid increase in tdT^+ cell coverage of the bronchiolar epithelium (Fig. 1o,p and Extended Data Fig. 3c,d). In contrast, although route 2 events were detectable as early as day 3 post-DT (Fig. 1n), their proportion increased only slightly over time, and by 8 weeks, channel structures were detected in 9.65 ± 1.12% of bronchioles (Fig. 1o,p and Extended Data Fig. 3e,f). These data suggest that AT2 cell lineages primarily contribute to the bronchiolar epithelium via route 1 (BADJ), with route 2 as serving as a supplementary route for epithelial cell contribution. We acknowledge that due to the lack of continuous *in vivo* live monitoring of cell migration over time, the current quantification provides only a rough estimate but not a precise quantitative measurement of the two migration routes.

To investigate how AT2 cells cross anatomical barriers into the bronchiolar region, we characterized the expression of matrix-remodeling enzymes during the early injury response (day 7 post-DT). Our scRNA-seq analysis revealed an upregulation of matrix metalloproteinases (MMPs) following DT-mediated damage. Notably, MMP14, a key enzyme for membrane-associated proteolytic activity and pericellular extracellular matrix (ECM) degradation, was significantly induced in AT2 cells, peribronchiolar fibroblasts, and smooth muscle cells (SMCs). Concurrently, infiltrating immune cells showed a localized surge in MMP9 expression (Extended Data Fig. 17e, f). These findings suggest that the injured microenvironment undergoes a systemic enzymatic remodeling, in which immune- and stromal-derived MMPs degrade the peribronchiolar matrix and basal lamina, potentially creating a permissive path for AT2 cell migration into the bronchioles. Immunostaining of lung sections from *Scgb1a1-DTR-GFP* mice on day 3 post-DT injury also

revealed that immune cells infiltrating the bronchiole expressed high levels of both SPP1 and MMP9, indicating a dual role: inducing AT2 cell migration and facilitating channel formation (Extended Data Fig. 17g). Further immunostaining of lung sections from *Sftpc-CreER;R26-tdT;Scgb1a1-DTR-GFP* mice on day 3 post-DT injury revealed that infiltrating SPP1^{+}MMP9^{+} immune cells were distributed near migrating AT2-derived cells at both the terminal bronchioles (adjacent to the BADJ) and channel sites (Extended Data Fig. 17h-j). In our previous response, we hypothesized that immune cells may regulate AT2 cell migration toward the bronchioles via the SPP1-Itgb1 axis (Fig. 7). As the BADJ serves as a natural conduit connecting the bronchioles and alveoli, AT2 cells may directly traverse the BADJ to enter the bronchioles, resulting in a relatively high frequency of usage of this route (Fig. 1o). Regarding channel formation, we propose that injury-induced infiltrating immune cells, through the secretion of MMP9 and SPP1, may degrade the peribronchiolar extracellular matrix while simultaneously inducing AT2 cell migration, thereby forming channels that guide AT2 cells toward the bronchial lumen. Additionally, injury-induced MMP14 expression in AT2 cells, peribronchiolar fibroblasts, and SMCs may also contribute to ECM degradation. Together with immune cells-derived MMP9, this proteolytic activity may collectively facilitate AT2 cell migration. These findings support the idea that route 1 may be directly used for AT2 cell migration, in contrast to route 2, which requires active ECM remodeling (Fig. 1p).

We also used *Scgb1a1-CreER;Sftpc-DreER;R26-NR* mice to evaluate the AT2 cell migration toward the bronchioles following naphthalene injury. Lung samples were collected on days 3, 7, 14, and 28 post-injury for immunostaining and statistical analysis (Extended Data Fig. 8b). At none of these time points did we detect channel structures formed by ZsG^{+} AT2 cell lineages on the bronchiolar wall (Extended Data Fig. 8c,d). However, by day 7 post-injury, ZsG^{+} cells were detectable at the distal bronchioles (near the BADJ), indicating that after naphthalene injury, AT2 cells migrate to the bronchioles through the BADJ route (Extended Data Fig. 8e). Immunostaining and quantitative analysis across time points further showed that the coverage of the bronchiolar epithelium by ZsG^{+} cells increased with repair time (Extended Data Fig. 8e,f). We speculate that the difference in AT2 cell migration routes between the DT and naphthalene injury models may be related to the severity of tissue injury. Previous studies have shown that after naphthalene injury, some naphthalene-resistant Scgb1a1^{+} cells survive (Reynolds et al., *Am J Pathol*, 2000). These cells are distributed near NE cells and the BADJ (i.e., BASCs) and can serve as reserve stem cells to participate in bronchial epithelial repair (Rawlins et al., *Cell Stem Cells*, 2009; Liu et al., *Nat Genet*, 2019). In contrast, the DT model induces ablation of all Scgb1a1^{+} cells, including resistant club cells and BASCs. This more severe injury may create an environment that promotes the formation of channel structures, thereby accelerating AT2 cell participation in bronchiolar repair. We have added these data and related discussion to the revised manuscript. Because our Extended Data Figures now total 20 after revision, we have included the panoramic immunofluorescence scans of the lung in the Figures to Reviewers. These data, along with the review comments and our response, can be considered for publication at the reviewer and editor's discretion. For details, please refer to

revised Figs. 1 and 7, Extended Data Figs. 3,8,15,17, Fig. 1 to Reviewers; Page 6, Paragraph 2; Page 9, Paragraph 2, Line 241; Page 17, Paragraph 1; Page 18-19; Page 20; Page 21, Paragraph 1 of the revised manuscript.

What is the “tunnel-like” structure? It is proposed that AT2 cells traverse the bronchiolar wall via tunnel-like structures, as visualized in Figure 6b. However, the identification of these structures is based solely on DAPI staining, which does not permit accurate interpretation of tissue architecture. Furthermore, the quantification in Figure 6c indicates a progressive increase in tunnel structures up to 8 weeks post-injury, which appears to contradict earlier figures (2G and 3G) showing that the bronchiolar epithelium is largely restored by 4 weeks. This inconsistency warrants clarification.

Response: We thank the reviewer for raising this important concern. In our original manuscript, we used the term "tunnel" to describe the structures through which AT2 cells traverse the bronchiolar wall in the DT injury model. To more accurately reflect their structural properties, we have renamed them "channels" throughout the revised manuscript. To address the concern regarding identification based solely on DAPI staining, we have incorporated PDGFRa staining, which marks peribronchiolar mesenchymal fibroblasts and provides a clear positional reference and structural boundary for the channels. Immunostaining for tdT, DAPI, and PDGFRa on lung sections at various time points post-DT injury showed that PDGFRa clearly delineates the bronchiolar wall and peribronchiolar fibroblasts (Fig. 1n and Extended Data Fig. 3e). At channel sites, we observed small gaps in the bronchiolar wall where the basement membrane appeared disrupted, directly connecting the bronchiolar lumen to the alveolar space (Extended Data Fig. 3e, white arrows). Moreover, the channels are surrounded by a continuous sleeve of PDGFRa$^+$ cells, indicating that they are organized, well-defined structures (Extended Data Fig. 3e). Importantly, the inner side of the channels is lined by tdT$^+$ AT2-derived cells without invasion by PDGFRa$^+$ cells (Fig. 1n and Extended Data Fig. 3e), demonstrating that the channels are actively formed by migrating AT2 cell lineages rather than by mesenchymal ingrowth. In addition, *Z*-stack scanning and 3D reconstruction of thick lung sections further visualized channel structures connecting the alveolar region and the bronchiolar lumen (Extended Data Fig. 3f and Supplemental movie 1).

Regarding the temporal dynamics of channel formation, we previously reported that channel structures continued to increase up to 8 weeks post-DT injury. However, through additional immunostaining and careful re-quantification, we found that channels increase during the first 4 weeks after DT, but their proportion no longer increases from 4 weeks to 8 weeks post-injury (Fig. 1o). These data suggest that once repair reaches a certain stage, new channel formation ceases, and the pre-existing channels are stably maintained following AT2 cell migration.

We also note that Figures 2 and 3 show the naphthalene-induced bronchiolar injury model, which differs from the DT model and is not suitable for direct comparison regarding channel formation. For example, we did not detect channel structures in the naphthalene injury model. Moreover, we found that the recovery speed of bronchiolar club cells differs the two models.

Immunostaining and statistical analysis showed that club cell recovery after naphthalene injury is faster than in the DT model (Fig. 2 to Reviewers). This is likely because some resistant Scgb1a1$^+$ cells survive after naphthalene injury and can participate in bronchiolar repair (Reynolds et al., *Am J Pathol*, 2000; Rawlins et al., *Cell Stem Cell*, 2009; Liu et al., *Nat Genet*, 2019) , whereas DT ablates all Scgb1a1$^+$ cells, resulting in more severe injury. Furthermore, in our naphthalene injury model, club cells were not fully restored at 4 weeks post-injury. In fact, it required 6 months of repair for the distribution density of club cells to become fully indistinguishable from that of control mice (Fig. 2 to Reviewers). We have added these data and discussion to the revised manuscript. For details, please refer to revised Figure 1, Extended Data Figure 3; Page 6, Paragraph 2; Page 9, Line 242; Page 21, Paragraph 1 of the revised manuscript.

The manuscript would benefit from experiments assessing whether AT2 cells, particularly those with activated Notch signaling, can adopt club cell identities under defined in vitro conditions. Such data would provide a more direct demonstration of the plasticity inferred from in vivo observations.
Response: We thank the reviewer for the suggestion to test whether AT2 cells, particularly those with activated Notch signaling, can adopt club cell identities *in vitro*. Accordingly, we performed a series of *in vitro* experiments to examine the AT2 cell plasticity. We first administered tamoxifen to *Sftpc-CreER;R26-tdT;Scgb1a1-DTR-GFP* mice, and tdT$^+$GFP$^-$ AT2 cells and tdT$^-$GFP$^+$ club cells were isolated by FACS for *in vitro* organoid culture (Fig. 3a,b to Reviewers and Fig. 1d). When AT2 cells were cultured in AT2 medium or club cells in club medium, both AT2 and club cell organoids formed and grew normally, as assessed by colony-forming efficiency (CFE) and organoid size (Fig. 3c,d to Reviewers). However, when AT2 cells were cultured directly in club medium, organoid formation capacity was significantly reduced, and the cells did not transdifferentiate into club cells (Fig. 3c,d to Reviewers). Given that our *in vivo* experiments revealed AT2-to-club cell conversion after bronchiolar injury, we next induced DT injury in mice to elicit AT2 cell damage responses and examined the fate plasticity of injury-induced AT2 cells *in vitro*. On day 7 post-DT, tdT$^+$GFP$^-$ AT2 cells were sorted and cultured in club medium (Fig. 5t). Again, we did not detect AT2-to-club transdifferentiation (Fig. 5t-x), indicating that the club medium alone is insufficient to drive fate conversion of AT2 cells isolated from the injured lung. These data suggest that the *in vitro* environment cannot accurately recapitulate the intricate *in vivo* microenvironment. We then adopted the reviewer's specific suggestion to test whether activation of the Notch signaling pathway could induce transdifferentiation. Our *in vivo* results have already shown that overexpression of NICD in AT2 cells using *Sftpc-CreER;R26-tdT;Scgb1a1-DTR-GFP;R26-NICD* mice promoted AT2-to-club conversion (Fig. 5j-m). Therefore, we administered tamoxifen and DT to *Sftpc-CreER;R26-tdT;Scgb1a1-DTR-GFP;R26-NICD* mice, and on day 7 post-DT, tdT$^+$GFP$^-$ AT2 cells were sorted and cultured in club medium (Fig. 5t). In this revised experiment, we detected a large number of GFP$^+$ cells (indicating club cells) that were also tdT$^+$, confirming that they were derived from AT2 cells (Fig. 5t-y). Quantification showed that approximately 60% of tdT$^+$ organoids expressed GFP (Fig. 5x). Section staining of organoids further confirmed that the GFP$^+$ organoids derived from AT2 cells co-expressed club cell marker Scgb1a1, validating their club cell identity (Extended Data Fig. 13y,z). Moreover, compared with controls, NICD overexpression significantly increased both organoid size and formation efficiency, indicating that Notch activation not only promotes AT2-to-club conversion but also enhances organoid formation capacity (Fig. 5v,w). Together, these

experiments demonstrate that achieving AT2-to-club transdifferentiation *in vitro* is challenging. The current culture microenvironment is insufficient; stronger drivers, such as activation of Notch signaling, are required. We have added these new experimental data and discussion to the revised manuscript. Because our Extended Data Figures now total 20 after revision, we have included some organoid data in the Figure to reviewers. These data can be considered for publication, along with review comments and response, at the reviewer and editor's discretion. For details, please refer to revised Fig. 5, Extended Data Fig. 13, Fig. 3 to Reviewers; Page 15, Line 438; Page 22, Line 645 of the revised manuscript.

The identification of a transient AT2 subpopulation expressing Cldn4 and exhibiting multipotency toward both AT1 and club cell fates is an interesting hypothesis derived from single-cell transcriptomic data. However, this model remains speculative in the absence of corroborating lineage tracing or fate-mapping evidence. Additional experimental validation is required to confirm the existence and functional relevance of this transitional state.

Response: We thank the reviewer for raising this critical point regarding lineage tracing of Cldn4^{+} transient cells. Our previous data showed that after naphthalene injury in *Scgb1a1-CreER;Sftpc-DreER;R26-TLR* mice, specifically labeled ZsG^{+} tdT^{-} AT2 cells contributed to club cells (Fig. 3a-h). Single-cell transcriptomic data further revealed a population of *Cldn4*-expressing transient cells during the AT2-to-club transition, and pseudotime analysis suggested that these transient cells could differentiate into both club cells and AT1 cells (Fig. 4a-f). However, direct *in vivo* genetic evidence supporting the fate of these transient cells was lacking. To address this, we constructed a new dual recombinase-based lineage tracing system during revision. Because the two reporter systems used to specifically label AT2 cells in the naphthalene injury model (*R26-NR* in Figure 2 and the *R26-TLR* in Figure 3) already occupied both Cre and Dre recombinases, it was technically challenging to use the naphthalene injury model to further trace AT2-derived Cldn4^{+} transient cells with a third orthogonal recombinase. We therefore chose to use the DT injury model here to examine the fate of these cells during bronchiolar repair. Pseudotime analysis of scRNA-seq data from *Scgb1a1-DTR-GFP* mice at day 7 post-DT indeed showed upregulation of *Cldn4* during the evolution from AT2 to club cells (Fig. 4i).

To specifically trace AT2-derived Cldn4^{+} transient cells, we generated a *Cldn4-LSL-Dre* knock-in line by inserting a loxP-Stop-loxP-WPRE-polyA sequence into the 5'UTR of the Cldn4 locus (Fig. 4j). However, the *Sftpc-CreER* line (Jackson Lab, strain #028054) exhibits approximately 40% leakage of tdT expression without tamoxifen induction (Fig. 4a,b to Reviewers), This leakiness would lead to premature *Cldn4-Dre* generation in AT2 cells before injury, resulting in labeling of any Cldn4-expressing cells in the history from development to homeostasis, which would compromise the specificity of tracing injury-induced Cldn4^{+} transient cells. To overcome this issue, we generated a new AT2-specific Cre tool with minimal leakiness, based on another characteristic AT2 marker, Lamp3. We constructed the *Lamp3-CreER* knock-in line by inserting a 2A-CreER sequence into the 3'UTR of the *Lamp3* gene locus (Extended Data Fig. 12a). To validate this line, we treated *Lamp3-CreER;R26-tdT* mice with tamoxifen or corn oil (control). One week later, lungs sections were analyzed (Extended Data Fig. 12b). In the control group, only a very small fraction ($0.07 \pm 0.04\%$) of AT2 cells were labeled, indicating minimal leakiness. In contrast, in the tamoxifen group, nearly all ($99.73 \pm 1.10\%$) Sftpc^{+}Lamp3^{+}AT2 cells were specifically labeled, demonstrating high efficiency of the new AT2-CreER line (Extended Data Fig. 12c-h). We next

generated *Lamp3-CreER;R26-tdT;Scgb1a1-DTR-GFP* triple-positive mice, designated AT2-tracer5 (Extended Data Fig. 12i), which functions similarly to the *Sftpc-CreER;R26-tdT;Scgb1a1-DTR-GFP* mice (AT2-tracer1, Fig. 1d,e). DT treatment specifically ablates Scgb1a1$^+$ club cells and BASCs, allowing specific tracing of Lamp3$^+$ AT2 cells (Extended Data Fig. 12i). As expected, immunostaining of lung sections collected 4 weeks after DT injury showed that tdT$^+$ AT2 cells migrate to the bronchioles and differentiate into GFP$^+$Scgb1a1$^+$ club cells, thereby participating in bronchiolar repair (Extended Data Fig. 12j).

We then combined the *Lamp3-* and *Cldn4-* based genetic tools to investigate the fate of transient cells. We generated *Lamp3-CreER;Scgb1a1-DTR-GFP;Cldn4-LSL-Dre;R26-rox-stop-rox-loxP-stop-loxP-tdTomato* (abbreviated as *R26-RSR-LSL-tdT*) quadruple-positive mice (Fig. 4k). The *R26-RSR-LSL-tdT* reporter requires dual recombinase activity: only after excision of both stop cassettes by Dre-rox and Cre-loxP recombinations does the tdTomato become expressed (Fig. 4l). The tracing principle is as follows: upon tamoxifen induction of the quadruple-positive mice, *Lamp3-CreER* excise the LSL stop sequence in *Cldn4-LSL-Dre* locus specifically in AT2 cells, converting it to *Cldn4-Dre* (step 1). It also excises one stop cassette (LSL) in *R26-RSR-LSL-tdT* to generate *R26-RSR-tdT* (step 1). Subsequently, when AT2 -derived transient cells express Cldn4 after DT injury, the activated Cldn4 promoter drives Dre expression, which excises the second stop cassette (RSR) in *R26-RSR-tdT* (step 2), resulting in specific tdT labeling of AT2-derived Cldn4$^+$ cells (Fig. 4l). Because club cells express GFP, the club cells derived from Cldn4$^+$ transient cells will co-express tdT and GFP, appearing yellow. For *in vivo* validation, we treated mice with tamoxifen and DT (with PBS as vehicle) and collected lung samples at week 4 post-injury (Fig. 4k). Immunostaining showed minimal tdT signal in control mice, indicating that the *Cldn4* promoter is inactive in AT2 cells under steady-state conditions (Fig. 4m). In contrast, after DT injury, we detected abundant newly generated GFP$^+$Scgb1a1$^+$ club cells in the bronchioles that were also tdT$^+$, confirming genetic tracing of AT2-derived Cldn4$^+$ transient cells and their contribution to club cells after injury (Fig. 4n). Statistical analysis revealed that 62.10 ± 6.16% of newly formed bronchiolar club cells after DT injury originated from Cldn4$^+$ transient cells (Fig. 4o). We also detected tdT$^+$ AGER$^+$ cells in the bronchioles. In addition, residual Sftpc$^+$ AT2 cells labeled with tdT were also observed in the bronchial epithelium; we speculate that these may represent AT2 cells undergoing the Cldn4$^+$ stage or having reverted from the Cldn4$^+$ transient state back to the AT2 cells (Fig. 4n). Further quantification of the tdT$^+$ cell lineages in the bronchiolar epithelium showed that club cells, AT1 cells, and AT2 cells accounted for 56.55 ± 4.54%, 14.05 ± 3.13%, and 7.48 ± 2.06% of the total, respectively (Fig. 4p). These fate-mapping data demonstrate that AT2 cells do pass through Cldn4$^+$ transient cell stage, which subsequently give rise to both club cells and AT1 cells, consistent with our previous pseudotime analysis (Fig. 4d).

To further validate the functional role of Cldn4 in AT2 cell contribution to the bronchiolar epithelium, we developed a conditional knockout tool, *Cldn4-flox* (Fig. 4q). We generated *Sftpc-CreER;R26-tdT;Scgb1a1-DTR-GFP;Cldn4$^{flox/+}$* (control group) and *Sftpc-CreER;R26-tdT;Scgb1a1-DTR-GFP;Cldn4$^{flox/flox}$* (experimental group) mice (Fig. 4r). After tamoxifen and DT treatment, AT2 cells were specifically traced and *Cldn4* was knocked out (Fig. 4r). RT-qPCR on FACS-sorted tdT$^+$GFP$^-$ AT2 cells confirmed that *Cldn4* expression was significantly reduced compared with controls (Extended Data Fig. 12k,l). At 4 weeks post-DT, immunostaining and statistical analysis showed that Cldn4 knockout significantly reduced the proportion of AT2 cells contributing to club cells (control vs. experimental: 65.94 ± 6.50% vs. 25.49 ± 3.54%) (Fig. 4s,t and

Extended Data Fig. 12m). Furthermore, Cldn4 knockout also significantly reduced the proportion of AT1 cells among AT2-derived bronchiolar cells (control vs. experimental: 21.11 ± 2.74% vs. 8.82 ± 1.56%), and decreased the coverage of the bronchiolar epithelium (control vs. experimental: 54.47 ± 5.84% vs. 19.42 ± 4.45%) (Fig. 4u-w and Extended Data Fig. 12n).

In summary, through these genetic fate-mapping and functional analyses, we demonstrate that Cldn4$^+$ intermediate cells derived from AT2 cells not only contribute to the bronchiolar epithelium but also functionally promote AT2 cell-mediated epithelial repair (Fig. 4x). We have added these data and discussion in the revised manuscript. For details, please refer to revised Figure 4, Extended Data Figure 12; Page 13, Paragraph 2; Page 14, Paragraph 1; Page 22, Paragraph 2 of the revised manuscript.

In Extended Data Figure 6, both Ager-creER and Hopx-dreER drivers are shown to label AT1 as well as AT2 cells. Consequently, the triple-recombinase system is likely to mark a broader epithelial population than stated in the main text. The assertion that this system specifically labels Hopx+Ager+ AT1 cells (page 7) is questionable. If AT2 cells are also labeled, the interpretation of negative findings related to their migration must be revisited.

Response: We thank the reviewer for raising this technical question. We first apologize for any confusion caused by the incomplete description of the dual-recombinase system for labeling of Hopx$^+$Ager$^+$ AT1 cells in Extended Data Fig. 7 (original Extended Data Fig. 6), especially given the multiple genetic systems employed in our study. To clarify, the system used for precise AT1 lineage tracing in Extended Data Fig. 7 is the *Rosa26-rox-stop-rox-loxp-stop-loxp-tdTomato* (*R26-RSR-LSL-tdT*) reporter. In this design, tdTomato expression is activated only upon concurrent Dre-rox and Cre-loxP recombination, thereby enabling the genetic targeting of double-positive cell populations. We acknowledge that the original figure lacked supporting quantification, and we have now added statistical data in the revised manuscript. Our quantification confirms that the single-recombinase systems—*Ager-CreER;R26-tdT* or *Hopx-2A-DreER;R26-RSR-tdT*—are not specific for AT1 cells and can ectopically label a subset of AT2 cells (Extended Data Fig. 7a-d), and the proportions of ectopically labeled AT2 cells are 21.06 ± 2.48% and 0.11 ± 0.02%, respectively (Extended Data Fig. 7a-d). Critically, in the *Hopx-2A-DreER;Ager-CreER;R26-RSR-LSL-tdT* triple-positive mice, the *in vivo* labeling specificity for AT1 cells is greatly enhanced. The incidence of ectopic AT2 cell labeling is exceedingly low (0.02 ± 0.01%), and these few events were randomly distributed across lung lobes (Extended Data Fig. 7e-g). Therefore, using this intersectional strategy, we were able to specifically label Hopx$^+$Ager$^+$ AT1 cells with tdT while achieving virtually no labeling of AT2 cells.

Subsequently, by subjecting *Hopx-2A-DreER;Ager-CreER;R26-RSR-LSL-tdT;Scgb1a1-DTR-GFP* mice to DT injury, or *Hopx-2A-DreER;Ager-CreER;R26-RSR-LSL-tdT* mice to naphthalene injury, we investigated the fate of the labeled AT1 cells following bronchial injury (Extended Data Fig. 7h-m and Fig. 3p-s). In both models, we did not observe any tdT$^+$ cells in the bronchial epithelium. These data indicate that resident AT1 cells do not contribute to the bronchial epithelium during injury repair. We have added these experimental data and discussion to the revised manuscript. For details, please refer to revised Figure 3, Extended Data Fig. 7, Page 8, Paragraph 2 of the revised manuscript.

Referee #2 (Remarks to the Author):

In this manuscript, regenerative plasticity from AT2 cells to distal airway epithelium driven by Notch and ITGB1 signaling is demonstrated using highly sophisticated lineage tracing models. The manuscript is technically almost perfect and very clearly written. It does add novel insights. On the other hand however, regenerative plasticity between most cell types in the lung has now been firmly established in mouse lineage tracing models. This manuscript definitely adds a novel regenerative plasticity trajectory, but does not provide a conceptual leap.

Author's Response: We thank the reviewer for acknowledging the technical quality and novelty of our work. In response to the concerns regarding conceptual advance, we have now incorporated new experimental data that significantly clarify the concept of AT2 cell contribution to distal airway epithelium and its underlying regulatory mechanisms. We believe that with these revisions, the revised manuscript now provides a solid conceptual advance in the field of lung regeneration.

Specific comments.

1. In all lineage tracing studies, except in those involving AT1 cells, promiscuous labeling or spontaneous recombination are not taken into account. The Jackson website, for example, mentions 10-25% spontaneous recombination in the Sftpc-CreERT model (https://www.jax.org/strain/028054), although it is not mentioned in which cells this recombination takes place. To what extent this would affect the conclusions of this manuscript remains to be seen, but it might be worth verifying this, or at least acknowledging this issue. No-tamoxifen controls would be the experiment to do. With only one airway typically showing, the data presented do not exclude spontaneous recombination as a confounding variable.

Response: We thank the reviewer for raising this important technical point regarding the potential leakiness of our genetic tools. As the reviewer noted, we utilized multiple inducible genetic lineage tracing lines in this study, but did not initially address possible promiscuous labeling or spontaneous recombination under steady-state, no-tamoxifen conditions. We have now systematically evaluated each key genetic line and assess whether such labeling could affect our conclusions in the revised manuscript.

First, for the *Sftpc-CreER;R26-tdT* mice (used in Figure 1), immunostaining of adult lungs without tamoxifen treatment revealed spontaneous recombination, with leaky tdT^+ signals detected in the alveolar region (Fig. 4a,b to Reviewers). Statistical analysis showed that 38.56 ± 4.15% of AT2 cells were labeled by tdTomato (tdT) (Fig. 4a,b to Reviewers), which is consistent with the spontaneous recombination reported on the Jackson website (https://www.jax.org/strain/028054) . This spontaneous recombination occurred exclusively within $Sftpc^+$ cells and did not label other cell types, confirming specificity for AT2 cells. Similarly, using another Sftpc-based tool, *Sftpc-DreER;R26-RSR-tdT*, we detected spontaneous labeling in 25.32 ± 2.56% of AT2 cells without tamoxifen induction (Fig. 4c,d to Reviewers), suggesting that the Sftpc promoter drives comparable strong expression of recombinases regardless of the recombinase variant. In naphthalene-injured *Sftpc-CreER;R26-tdT* mice without prior tamoxifen induction, these leakily labeled $Sftpc^+$ cells migrated to the bronchiole and differentiated into club cells (Fig. 4e,f to Reviewers). Similarly, DT treatment of *Sftpc-CreER;R26-tdT;Scgb1a1-DTR-GFP* mice without prior tamoxifen also showed

contributions from leakily labeled AT2 cells to bronchiolar club cells (Fig. 4g,h to Reviewers). We also examined spontaneous recombination in the *Sftpc-CreER;R26-Confetti;Scgb1a1-DTR-GFP* mice used for AT2 clonal analysis. In the absence of tamoxifen induction, reporter leakage was detected in only 0.04 ± 0.02% of AT2 cells (Fig. 4i-k to Reviewers). The stop cassette (pGK-Neo-pA) upstream of *R26-Confetti* is approximately 2 kb in length (Snippert et al., *Cell*, 2010), which is substantially longer than the stop cassette used in *R26-tdT*. This longer cassette likely makes Cre-loxP recombination more difficult, explaining the much lower leakage rate with *R26-Confetti*, compared to *R26-tdT*. In DT-injured *Sftpc-CreER;R26-Confetti;Scgb1a1-DTR-GFP* mice without prior tamoxifen, we detected no labeled AT2 cell lineages in the bronchioles (Fig. 4l,m to Reviewers). In summary, although *Sftpc-CreER* exhibits substantial spontaneous recombination, the leakily labeled cells are strictly restricted to AT2 cells. We did not detect any leakily labeled AT2 cells migrating to bronchioles before injury. Therefore, even though the migration of labeled-AT2 cells observed in these no-tamoxifen experiments partially resembles that seen in our prior tamoxifen-based studies, this does not compromise our conclusions that AT2 cells migrate to bronchioles specifically after injury. In addition, during the revision, we generated a new AT2-specific Cre tool with minimal leakiness based on another characteristic AT2 marker, Lamp3. We constructed the *Lamp3-CreER* knock-in line by inserting a 2A-CreER sequence into the 3'UTR of the *Lamp3* gene locus (Extended Data Fig. 12a). To validate this line, we treated *Lamp3-CreER;R26-tdT* mice with tamoxifen or corn oil (control). One week later, lung sections were analyzed (Extended Data Fig. 12b). In the control group, only a very small fraction (0.07 ± 0.04%) of AT2 cells were labeled, indicating minimal leakiness. In contrast, in the tamoxifen group, nearly all (99.73 ± 1.10%) Sftpc$^+$Lamp3$^+$ AT2 cells were specifically labeled, demonstrating the high efficiency of the new AT2-CreER line (Extended Data Fig. 12c–h). We next generated *Lamp3-CreER;R26-tdT;Scgb1a1-DTR-GFP* triple-positive mice, designated AT2-tracer5 (Extended Data Fig. 12i), which functions similarly to the *Sftpc-CreER;R26-tdT;Scgb1a1-DTR-GFP* mice (AT2-tracer1, Fig. 1d,e). DT treatment specifically ablated Scgb1a1$^+$ club cells and BASCs, allowing specific tracing of Lamp3$^+$ AT2 cells (Extended Data Fig. 12i). As expected, immunostaining of lung sections collected 4 weeks after DT injury showed that tdT$^+$ AT2 cells migrated to the bronchioles and differentiated into GFP$^+$Scgb1a1$^+$ club cells, thereby participating in bronchiolar repair (Extended Data Fig. 12j). These data further confirm that the AT2-to-club cell transition we observed indeed occurs.

We next examined the spontaneous recombination in *p63-DreER;R26-RSR-tdT* mice (used in Extended Data Fig. 5). Immunostaining of adult lung sections showed no tdT expression without tamoxifen induction (Fig. 5a,b to Reviewers). DT treatment of adult *p63-DreER;R26-RSR-tdT;Scgb1a1-DTR-GFP* mice also did not induce any tdT expression (Fig. 5c,d to Reviewers), demonstrating no detectable leakiness for *P63-DreER*. We also assessed the spontaneous recombination in *Ascl1-CreER;R26-tdT* mice (in Extended Data Fig. 6). Analysis of adult lungs without tamoxifen treatment revealed tdT leakiness into neuroendocrine (NE) cells, with 44.45 ± 5.97% of NE cells expressing tdT (Fig. 5e,f to Reviewers). DT treatment of adult *Ascl1-CreER;R26-tdT* mice without tamoxifen showed that tdT-labeled NE cells could contribute to neighboring club cells (Fig. 5g,h to Reviewers). In summary, we systematically investigated promiscuous labeling and spontaneous recombination in all inducible genetic tracing lines used in this study, including *Sftpc-CreER*, *Scgb1a1-CreER*, *Sftpc-DreER*, *p63-DreER*, and *Ascl1-CreER*. We found that most of these lines exhibited varying degrees of spontaneous recombination, but this

occurred specifically in their intended target cells and not as promiscuous labeling of other cell type. Importantly, this does not compromise the conclusions drawn from our experiments.

We next detected that adult *Scgb1a1-CreER;Sftpc-DreER;R26-NR* mice (used in Figure 2) also expressed ZsGreen (ZsG) and tdT signals without tamoxifen treatment (Fig. 6a-d to Reviewers). Immunostaining and quantification analysis showed that 7.09 ± 1.25% of Sftpc$^+$ cells expressed ZsG, while 3.89 ± 0.82% Scgb1a1$^+$ cells expressed tdT (Fig. 6a-d to Reviewers). In naphthalene-induced injury of *Scgb1a1-CreER;Sftpc-DreER;R26-NR* mice without prior tamoxifen, these spontaneous recombination-labeled Sftpc lineage migrated to the bronchiole and differentiate into club cells (Fig. 6e,f to Reviewers). Additionally, we found that adult *Scgb1a1-CreER;Sftpc-DreER;R26-TLR* mice (used in Figure 3) also exhibited ZsG and tdT signals without tamoxifen (Fig. 6g-j to Reviewers). Immunostaining and statistical analysis showed that 25.35 ± 3.98% of Sftpc$^+$ cells expressed ZsG, while 9.43 ± 2.08% Scgb1a1$^+$ cells expressed tdT (Fig. 6g-j to Reviewers). In naphthalene-induced injury of these mice without prior tamoxifen, the labeled Sftpc$^+$ cells contributed to bronchiolar club cells (Fig. 6k,l to Reviewers). Because the spontaneous recombination in these no-tamoxifen experiments labeled the same target cell types (Sftpc$^+$ or Scgb1a1$^+$ cells) as intended with tamoxifen treatment, this does not compromise our conclusions.

Spontaneous recombination without tamoxifen in inducible genetic tools is unavoidable. Our team has also detected spontaneous recombination in many other inducible tracing tools. We speculate that the higher rate of spontaneous recombination in lung epithelial cells may result from excessively strong promoter activity, leading to cytoplasmic accumulation of CreER/DreER and increased frequency of leaky nuclear entry. However, we empirically observed that using reporter mice containing longer stop sequences can reduce spontaneous recombination by making recombination more difficult. For example, the stop sequences between the two loxP sites in the *R26-tdT*, *R26-TLR*, and *R26-NR* reporter mice are approximately 900 bp, 1700 bp, and 2660 bp, respectively (Fig. 6m to Reviewers). While 65.83 ± 5.63% of Scgb1a1$^+$ cells underwent spontaneous recombination in adult *Scgb1a1-CreER;R26-tdT* mice (Fig. 6n-p to Reviewers), the proportion decreased to approximately 4% and 9% in *Scgb1a1-CreER;R26-NR* and *Scgb1a1-CreER;R26-TLR* mice, respectively (Fig. 6d,j to Reviewers). This suggests that if spontaneous recombination occurs with an inducible recombination tool, changing the reporter line may help mitigate it under certain conditions.

Additionally, as the reviewer pointed out, most fields of view in our previous data contained only a single airway, which could be confounded by spontaneous recombination,. To demonstrate that the AT2-to-club transition observed after bronchiolar injury is not a sporadic event, we have added panoramic scans of immunostaining of lung sections in the revised manuscript. These scans, which contain multiple bronchial fields, were collected 28 days after DT injury in *Sftpc-CreER;R26-tdT;Scgb1a1-DTR-GFP* mice and after naphthalene injury in *Scgb1a1-CreER;Sftpc-DreER;R26-NR* mice (Extended Data Fig. 3a and Fig. 1 to Reviewers). In both injury models, traced AT2 cells were detected migrating into the majority of bronchioles to participate in injury repair. Quantification showed that 71.21 ± 6.29% of the distal bronchial epithelium was populated by tdT$^+$ cell lineages at 28 days after DT injury (Extended Data Fig. 3b). Furthermore, immunostaining and statistical analysis of lungs collected at different time points after DT injury revealed that the coverage of the bronchiolar epithelium by tdT-labeled AT2 cells increased with repair time (Extended Data Fig. 3c-e). Similarly, analysis of different time points after naphthalene injury

showed that the coverage of the bronchiolar epithelium by ZsG-labeled AT2 cells also increased with repair time (Extended Data Fig. 8b-f).

Collectively, these data sufficiently demonstrate that our conclusions are robust and reliable, and that spontaneous recombination does not affect our findings. Because our Extended Data Figures now total 20 after revision, we have included leakiness examination of each mouse line in the Figure to reviewers. These data can be considered for publication, along with review comments and response, at the reviewer and editor's discretion. We have added these data and discussion in the revised manuscript. For details, please refer to revised Figs. 1,4,5,6 to Reviewers, Extended Data Figs. 3,8,12; Page 13, Line 367; Page 21, Line 608 of the revised manuscript.

2. The lineage tracing data seem clear-cut. However, it is not immediately clear how the statistical analysis was performed. 5 mice are typically used, but how many airways/fields were quantified? Were the data pooled per mouse?

Response: We thank the reviewer for raising this important point and agree that clarity regarding statistical methods and data aggregation is crucial for interpreting the experimental results. In our study, we typically used n = 5 mice as independent biological replicates. For quantification, all five lung lobes from each mouse were analyzed. From each mouse, we examined at least 10 non-consecutive lung tissue sections. Within each section, a minimum of five 10× fields containing airways were analyzed, resulting in the assessment of at least 50 fields per mouse. For statistical analysis, the data from all fields for each mouse were first averaged to generate a single composite value per animal (e.g., the percentage of lineage-positive cells). Thus, the statistical sample size (n) refers to the number of mice (n=5 in this case), not the total number of airways or fields. Statistical tests were performed using GraphPad Prism (v9.3.1) on these per-mouse data points. Data normality (Shapiro-Wilk test) and homogeneity of variance (F-test) were assessed first. Comparisons between two groups were performed using unpaired two-tailed Student's *t*-tests (for data with equal variance) or Welch's *t*-tests (for unequal variance). Non-normal data were analyzed using the Mann-Whitney U test. For comparisons across multiple groups, one-way ANOVA with Tukey's test (for normal data) or the Kruskal-Wallis test with Dunn's test (for non-normal data) was applied. Data are presented as mean ± SD, as indicated in the figure legends. Significance thresholds are defined as $*p < 0.05$, $**p < 0.01$, $***p < 0.001$, and $****p < 0.0001$; "ns" denotes no significance. The number of independent biological replicates, specific quantification methods, and exact *P* values are provided in the respective figures and legends. We have updated these statistical methods in the revised manuscript. For details, please refer Page 40, Paragraph 2 of the revised manuscript.

3. Given the black-and-white phenotypes with respect to lineage tracing and DT-induced injury, what were the functional repercussions? Such studies are entirely missing. For example, if the Scgb1a1-DTR model is nearly 100% efficient, is lung function or histology somehow affected? And what happens when regeneration is partially blocked, for example by interfering with Notch and ITGB1 signaling?

Response: We thank the reviewer for raising this important point regarding function and histology analysis. Our previous experiments using lineage tracing and the DT model yielded clear and convincing results, but we lacked an assessment of lung function or histology. Club cells, as airway secretory and progenitor cells in bronchioles, play multiple physiological roles in maintaining airway homeostasis, repairing injury, regulating lung mechanics, and defending against infection

(Hao et al., *Physiological Reviews*, 2025; Blackburn et al., *Am J Physiol Lung Cell Mol Physiol*, 2023). Therefore, in the revised manuscript, we have added multidimensional assessments of bronchiolar tissue structure, cell proliferation, pulmonary function parameters, and host defense to systematically evaluate the functional and histological consequences of the DT model.

In the DT model, we used *Scgb1a1-DTR-GFP* mice to specifically ablate GFP$^+$Scgb1a1$^+$ cells (club cells and BASCs). Immunostaining and quantification confirmed the high efficiency of this ablation strategy (Extended Data Fig. 2a-f). First, we evaluated the impact of Scgb1a1$^+$ cell ablation on bronchiolar tissue structure. Lung sections were collected at multiple time points after DT injury (days 3, 7, 14, and 28) and subjected to H&E staining and statistical analysis (Extended Data Fig. 13g). Compared with the control group (PBS-treated), bronchiolar wall thickness began to increase in response to injury on day 3 and gradually decreased over time as repair progressed (Extended Data Fig. 13h,i). Furthermore, PDGFRa and Ki67 immunostaining and quantification revealed that injury stimulated the activation and proliferation of PDGFRa$^+$ peribronchiolar mesenchymal cells, leading to adventitial thickening (Extended Data Fig. 13j-l). Our scRNA-seq analysis revealed that peribronchiolar fibroblasts from day 7 DT-injured lungs significantly upregulated a wide range of ECM-related genes, including multiple collagens (*Col1a1*, *Col3a1*, *Col4a1*, *Col6a1*, etc.), as well as *Tnc*, *Postn*, and *Vim* (Extended Data Fig. 15f). Gene set enrichment analysis confirmed enhanced extracellular matrix organization (Extended Data Fig. 15g). These molecular changes provide a mechanistic basis for the adventitial thickening and airway wall remodeling seen after club cell ablation, consistent with our histological observations. As repair continued, the proportion of proliferating peribronchiolar mesenchymal cells gradually decreased, and the thickness of the mesenchymal layer gradually recovered (Extended Data Fig. 13j-l). Together, these data indicate that club cell ablation induces structural remodeling of the bronchioles.

Next, we used a pulmonary function testing system to assess the impact of club cell ablation-induced airway remodeling on lung respiratory function. We measured six expiratory parameters for lung function. (1) Functional residual capacity (FRC): reflects alveolar inflation or small airway ventilation. A reduced value suggests expiratory limitation or small airway obstruction. (2) Peak expiratory flow/forced vital capacity (PEF/FVC): indicates the degree of airway obstruction. A reduced ratio suggests expiratory limitation, often seen in small airway dysfunction or bronchial wall thickening. (3) Maximal mid-expiratory flow/FVC (MMEF/FVC): represents the flow rate during the middle 50% of the forced expiratory curve and reflects small airway function. A reduced ratio indicates increased small airway resistance. (4) Forced expiratory volume in 100 ms/FVC (FEV100/FVC): a commonly used indicator of airway obstruction in mouse lung function tests. A reduced ratio suggests increased airway resistance and expiratory limitation. (5) Forced expiratory volume in 75 ms/FVC (FEV75/FVC): reflects the very early, rapid phase of expiration and is sensitive to changes in small airway resistance. A reduced ratio indicates obstruction during the initial phase of expiration. (6) Airway hyperresponsiveness to acetylcholine challenge: assessed by measuring inspiratory resistance. An increase in inspiratory resistance indicates enhanced airway hyperresponsiveness, increased sensitivity of airway smooth muscle to contractile stimulation, and airway narrowing. We performed *in vivo* measurements in living *Scgb1a1-DTR-GFP* mice on day 7 after DT injury, with PBS-treated mice as controls, to capture real-time pulmonary function (Extended Data Fig. 13m). Compared with the control group, the DT group showed a significant increase in FRC and significant decreases in PEF/FVC, MMEF/FVC, FEV100/FVC, and FEV75/FVC (Extended Data Fig. 13n). In addition, airway hyperresponsiveness was significantly

increased in the DT group (Extended Data Fig. 13o). These data demonstrate that DT-induced Scgb1a1$^+$ cell ablation leads to airway remodeling, airway obstruction, and significant impairment of lung respiratory function, suggesting that structural airway remodeling contributes to the observed pulmonary function deficits in mice.

We also evaluated whether Scgb1a1$^+$ cell ablation affects pulmonary antibacterial defense. Previous studies have reported that club cells promote the clearance of *Pseudomonas aeruginosa* (*P. aeruginosa*) infection by secreting antimicrobial proteins (Sahu et al., *Sci. Immunol*, 2023; Guan et al., *J. Adv. Res*, 2025). Therefore, we examined the efficiency of pulmonary *P. aeruginosa* clearance in the DT model. *Scgb1a1-DTR-GFP* mice were first subjected to DT injury (PBS-treated as controls). Seven days later, mice were infected via the trachea with *P. aeruginosa* at a dose of 2×10^5 Colony-Forming Unit (CFU)/g. After 24 hours, lungs were collected, homogenized, and plated on *P. aeruginosa* selective medium. Following 12-16 hours of culture, samples were analyzed (Extended Data Fig. 13p). Photographs and statistical analysis of single colonies showed that the CFU count in the DT group was significantly higher than that in the control group, indicating that Scgb1a1$^+$ cell ablation severely impaired *P. aeruginosa* clearance (Extended Data Fig. 13q,r). In summary, DT-induced Scgb1a1$^+$ cell ablation leads to bronchiolar structural remodeling, impaired lung respiratory function, and reduced pathogen clearance, demonstrating significant alterations in tissue structure and lung function.

Having established that club cell ablation causes structural and functional deficits, we next asked whether blocking AT2-to-club cell regeneration affects the recovery of these parameters. We found that specific knockout of either *Rbpj* or *Itgb1* in AT2 cells significantly inhibited AT2 contribution to club cells. To determine whether partial blockade of club cell regeneration delays the restoration of lung tissue structure and function, we performed comparative analyses of the pulmonary parameters described above in both knockout models. We first used *Sftpc-CreER;R26-tdT;Scgb1a1-DTR-GFP;Rbpj$^{flox/flox}$* mice (knockout group) to delete the *Rbpj* gene specifically in AT2 cells, with *Sftpc-CreER;R26-tdT;Scgb1a1-DTR-GFP;Rbpj$^{flox/+}$* mice as controls. Lung function was assessed on day 28 after DT injury (Extended Data Fig. 13s). Compared with the control group, the knockout group exhibited significantly higher FRC, significantly lower PEF/FVC, MMEF/FVC, FEV100/FVC, and FEV75/FVC, and significantly enhanced airway hyperresponsiveness (Fig. 5n-p and Extended Data Fig. 13t). In addition, *P. aeruginosa* infection experiments revealed significantly higher CFU counts in the experimental group compared with controls (Fig. 5q-s). These pulmonary function data indicate that blocking club cell regeneration significantly delays functional recovery. Consistent with these functional deficits, histological analysis revealed structural abnormalities. Immunostaining and statistical analysis of lung sections showed that the peribronchiolar mesenchymal layer was significantly thicker in the knockout group than in the control group (Extended Data Fig. 13u,v). H&E staining and quantification also revealed significantly increased bronchial wall thickness in the knockout group (Extended Data Fig. 13w,x). These histological findings suggest that impaired club cell regeneration leads to persistent activation of the peribronchiolar mesenchymal layer, thereby slowing its return to baseline. We next evaluated the impact of *Itgb1* knockout on lung tissue structure and function. Experimental mice were *Sftpc-CreER;R26-tdT;Scgb1a1-DTR-GFP;Itgb1$^{flox/flox}$*, and control mice were *Sftpc-CreER;R26-tdT;Scgb1a1-DTR-GFP;Itgb1$^{flox/+}$*. Mice were subjected to DT injury and analyzed on day 28 (Extended Data Fig. 18o). Lung function measurements showed that, compared with controls, the *Itgb1* knockout group had significantly higher FRC and airway hyperresponsiveness, and

significantly lower PEF/FVC, MMEF/FVC, FEV100/FVC, and FEV75/FVC (Extended Data Fig. 18p,q). Histological assessment of lung sections also revealed that the peribronchiolar mesenchymal layer and bronchial wall thickness were significantly increased in the *Itgb1* knockout group compared with controls (Extended Data Fig. 18r-u). Moreover, *P. aeruginosa* clearance was significantly impaired in the *Itgb1* knockout group relative to controls (Extended Data Fig. 18v-x).

In summary, our findings demonstrate that club cell ablation leads to bronchial structural remodeling and pulmonary dysfunction, and that impaired club cell regeneration resulting from Notch and Itgb1 knockout delays the recovery of bronchial structure and lung function. We have added these experimental data and discussion to the revised manuscript. For details, please refer to revised Fig. 5, Extended Data Figs. 2,13,15,18; Page 5, Paragraph 1; Page 15, Paragraph 2; Page 20, Paragraph 1 and Line 588 of the revised manuscript.

4. Fig. 1a, Extended data 3a-d: A confetti reporter is used to demonstrate clonality. However, it seems that only RFP+ cells are shown. It is unclear how this proves clonality.

Response: We thank the reviewer for raising this important technical point. We used *Sftpc-CreER;R26-Confetti;Scgb1a1-DTR-GFP* mice to perform clonal analysis, demonstrating that AT2 cells can contribute to bronchial epithelial regeneration at the single-cell level after DT-mediated depletion of club cells and BASCs (Fig. 1q-u). The Confetti reporter system stochastically labels AT2 cells with one of four fluorescent proteins: nGFP, YFP, RFP, or mCFP. We acknowledge that showing only RFP^+ clones in the original submission did not fully illustrate the principle of clonal expansion. Therefore, in the revised manuscript we have added representative images of clones expressing the other three fluorescent colors (Extended Data Fig. 4). To first confirm sparse single-cell labeling, the adult *Sftpc-CreER;R26-Confetti* mice were induced with a low dose of tamoxifen (0.025mg/g) (Extended Data Fig. 4a). Immunostaining on lung sections collected one week later showed rare AT2 cells were labeled with nGFP, YFP, RFP, or mCFP (Extended Data Fig. 4b). Next, *Sftpc-CreER;R26-Confetti;Scgb1a1-DTR-GFP* mice were given tamoxifen followed by a three-week washout period, then treated with DT. Lungs were analyzed eight weeks later (Extended Data Fig. 4c). Immunostaining analysis revealed clones of single colors from all four fluorescent proteins, demonstrating clonally that AT2-derived cells had migrated into bronchiolar regions and contributed to club cells (Extended Data Fig. 4d,e). We further quantified the proportion of each fluorescent clone among the total clones analyzed: $nGFP^+$ accounted for 19.44 ± 2.05%, YFP^+ for 27.77 ± 2.36%, RFP^+ for 38.01 ± 2.89%, and $mCFP^+$ for 14.78 ± 3.50% (Extended Data Fig. 4f). These data demonstrate that AT2 cells participate in bronchiolar repair via monoclonal expansion as a general phenomenon, not limited to any specific reporter color. We have added these new experimental data and discussion in the revised manuscript. For details, please refer to revised Fig. 1, Extended Data Fig. 4; Page 6, Paragraph 3 of the revised manuscript.

5. Throughout the manuscript, the authors demonstrate AT1 cells in bronchioles after injury as evaluated by staining for AGER. This is surprising. It might be helpful to complement with other markers. AT1 cells were also identified in scRNAseq, but these data obviously do not provide spatial information. It might also be of interest to see if in uninjured (or perhaps in older) mice, AT1 cells are observed in bronchioles.

Response: We thank the reviewer for raising this important suggestion. We used two bronchiolar injury models, the DT model and the naphthalene injury model, to trace AT2 cell participation in

bronchiolar repair. We found that after migrating into the bronchi, AT2 cells differentiated not only into club cells but also partially into AT1 cells, as demonstrated by AGER staining (Figs. 1j, 2j, 3j). As the reviewer correctly pointed out, relying on a single AT1 cell marker is not sufficiently rigorous. Therefore, in the revised manuscript, we have added two additional classical AT1 cell markers, T1a (PDPN) and Hopx, for cell type confirmation. For the DT model, we performed immunostaining on lung sections from *Sftpc-CreER;R26-tdT;Scgb1a1-DTR-GFP* mice at 28 days after DT injury. The results showed that a subset of tdT^+, flattened AT2-derived bronchiolar epithelial cells expressed T1a and Hopx (Extended Data Fig. 2i,j, white arrows). For the naphthalene injury model, we performed immunostaining on lung sections from *Scgb1a1-CreER;Sftpc-DreER;R26-NR* mice and *Scgb1a1-CreER;Sftpc-DreER;R26-TLR* mice at 28 days after naphthalene injury. We confirmed that a subset of ZsG^+, flattened AT2-derived bronchial epithelial cells also expressed T1a and Hopx (Extended Data Fig. 8a,r, white arrows). Together, these data demonstrate the presence of AT1 cells within the AT2-derived bronchial epithelium. We previously sorted ZsG^+tdT^- AT2 cell lineages from *Scgb1a1-CreER;Sftpc-DreER;R26-TLR* mice at 28 days after naphthalene injury for scRNA-seq analysis and detected ZsG^+tdT^- AT1 cells from the AT2 lineage (Fig. 4a-c). Through pseudotime analysis, we inferred that these genetically labeled AT1 cells likely originate from AT2 cells (Fig. 4d, green arrow). We agree with the reviewer that the single-cell data cannot provide spatial information (Fig. 4c). We therefore performed immunostaining to reveal the spatial distribution of these AT1 cells. AT1 cells are normally distributed in the alveolar region, and we readily detected ZsG^+tdT^- AT1 cells in the alveolar region, which are derived from differentiation of their progenitor AT2 cells (Extended Data Fig. 8s, white arrows). In addition, some ZsG^+tdT^- AT1 cells were located in the bronchiolar epithelium, representing the AT2-derived bronchiolar AT1 cells identified in our study (Fig. 3j and Extended Data Fig. 8r).

As suggested by the reviewer, we also examined whether AT1 cells are present in the bronchial epithelium of uninjured or aged mice. We induced tamoxifen in young uninjured (8-10 weeks old) or aged (55-75 weeks old) *Sftpc-CreER;R26-tdT;Scgb1a1-DTR-GFP* mice (Fig. 8a-c to Reviewers), *Scgb1a1-CreER;Sftpc-DreER;R26-NR* mice (Fig. 8d-f to Reviewers), and *Scgb1a1-CreER;Sftpc-DreER;R26-TLR* mice (Fig. 8g-i to Reviewers). One week later, lung sections were collected for immunostaining and statistical analysis. We did not detect any AT1 cells in the bronchial epithelium from any of these mice, indicating that under steady-state conditions, AT1 cells reside only in the alveolar region and do not ectopically appear in the bronchial region (Fig. 8 to Reviewers). We have added these experimental data and discussion in the revised manuscript. Because our Extended Data Figures now total 20 after revision, we have included the examination of AT1 cells in uninjured or older mice in the Figure to reviewers. These data can be considered for publication, along with review comments and response, at the reviewer and editor's discretion. For details, please refer to revised Figure 1,2,3, Extended Data Fig. 2,8, Fig. 8 to Reviewers, Page 5, Line 128; Page 9, Line 237; Page 10, Line 279 of the revised manuscript.

6. Fig. 4c: Lysotracker stains most cells, not just AT2 cells. Using this marker to exclude mature AT2 cells might not be entirely valid.

Response: We thank the reviewer for raising this technical question. In our previous Figure 4c (now moved to Extended Data Fig. 10a), we used Lysotracker to exclude the majority of mature AT2 cells due to the lack of flow cytometry antibodies specifically targeting AT2 cells. Lysotracker is a cell-permeable fluorescent dye that stains acidic organelles (primarily lysosomes) in live cells. In

the lung, cell types with high lysosomal activity mainly include immune cells and AT2 cells. To enrich for AT2-derived transient cells and club cells, we implemented a sequential gating strategy. First, we gated on $CD45^{-}Ter119^{-}$ cells to exclude all immune cells and erythrocytes (Extended Data Fig. 10a, first gating strategy). Because we used *Scgb1a1-CreER;Sftpc-DreER;R26-TLR* mice, in which AT2 cell lineages are labeled as $ZsG^{+}tdT^{-}$ (Fig. 3a), we next gated on $ZsG^{+}tdT^{-}$ cells (Extended Data Fig. 10a, second gating strategy). Within this gate, the cell population was already restricted to AT2 cell lineages. At this stage, the majority of $ZsG^{+}tdT^{-}$ are alveolar AT2 cells, which are not our cells of interest. Our goal was to enrich the relatively rare AT2-derived transient cells and club cells from this bulk population of alveolar AT2 cells. Therefore, we further sorted Lysotracker-negative cells from this population (third gating strategy). Because mature AT2 cells retain high lysosomal activity and are Lysotracker-positive, this step effectively excluded the majority of mature AT2 cells from the $ZsG^{+}tdT^{-}$ population. Collectively, this sequential sorting strategy allowed us to effectively enrich for AT2-derived transient cells and club cells, and our single-cell analysis results confirmed the success of this approach (Fig. 4a-d). We have added an explanation of the sorting strategy in the revised manuscript. For details, please refer to revised Extended Data Figs.10 and 19; Page 78, Line 2253 of the revised manuscript.

7. Extended data 7h-j: Differential expression of specific gene signatures is analyzed here. It is not made clear how these signatures were determined. Furthermore, Extended Data 7i shows a similar Notch signature in both subsets, contrary to what is claimed in the text (line 303-305). This is important as most of the remainder of manuscript focuses on Notch signaling.

We thank the reviewer for these comments. The original Extended Data Fig. 7h-j has been moved to Extended Data Fig. 10j-l in the revised manuscript. To clarify, the signatures used in this manuscript were derived from three complementary sources: (1) cell-type-specific markers identified via differential expression analysis (DEA) of previous scRNA-seq data (Liu et al., *Nat Genet*, 2019); (2) well-established markers for PATS cells and functional pathways retrieved from literature (Kobayashi et al., *Nat Cell Biol*, 2020; Strunz et al., *Nat Commun*, 2020) and Gene Ontology (GO) databases (https://geneontology.org); and (3) lineage-specific chromatin accessibility peaks identified from single-cell multiome ATAC-seq data. All gene sets and genomic coordinates for these signatures have been consolidated into Supplementary Table 1: signature_table.csv for full transparency. We also thank the reviewer for carefully reading our manuscript and pointing out the inconsistency between the figure and the text. The original Extended Data Fig. 7i (now Extended Data Fig. 10k) shows that both AT2-derived and BASC-derived transient cells exhibit upregulated Notch signatures, with no statistically significant difference in enrichment scores between the two subsets. Our original text incorrectly suggested a difference. Accordingly, we have revised the text to accurately reflect the data: “Upon entering the transient state, BASC-tracer cells continued to display a higher club cell signature; however, their Notch signature and pre-alveolar type 1 transitional state (PATS) signature showed no significant difference compared to AT2-tracer3 cells.” This correction has been made in the revised manuscript (Page 12, Paragraph 2, Line 332). We apologize for the oversight and thank the reviewer for helping us improve the accuracy of our presentation.

8. Along the same lines, Extended data 9,f,g, Fig. 4j,n,o focus on Notch signaling. However, expression of Notch receptors and of canonical Notch target genes is not shown.

Response: We thank the reviewer for requesting direct evidence of Notch receptor and canonical target gene expression. First, the original Extended Data Fig. 9f,g and Fig. 4j,n,o have now been moved to Extended Data Fig. 14e,f, Fig. 4h, and Extended Data Fig. 10g,h in the revised manuscript, respectively. To address the reviewer's question, we re-analyzed our scRNA-seq data of AT2-tracer3 and BASC-tracer cells sorted from *Scgb1a1-CreER;Sftpc-DreER;R26-TLR* mice at 4 weeks after naphthalene injury (Fig. 4d,h and Extended Data Fig. 10c-h). Through analysis of AT2-derived cells, we observed sustained upregulation of Notch receptors (*Notch1*, *Notch2*), the ligand *Jag1*, and the canonical downstream target gene *Hes1* throughout the transition to club cells. *Jag2* was upregulated in the transient state but decreased in club cells, whereas another target gene, *Hey1*, showed transient downregulation in the transient state followed by an increase in club cells (Extended Data Fig. 14c). In BASC-derived transient cells, Notch receptors (*Notch1*, *Notch2*), the ligand *Jag1*, and the target gene *Hes1* were consistently upregulated. *Jag2* displayed a transient decrease in the intermediate state before rising again in club cells (Extended Data Fig. 14d). These data provide direct molecular evidence that Notch receptors (*Notch1/2*) and the canonical target gene *Hes1* are activated in transient cells during AT2-to-club and BASC-to-club differentiation. The dynamic expression of *Jag2* and *Hey1* suggests a finely tuned Notch signaling response rather than a simple binary on/off switch, which may reflect lineage-specific regulatory mechanisms. We have added these data and discussion to the revised manuscript. For details, please refer to revised Fig. 4, Extended Data Figs. 10 and 14, Page 16, Paragraph 2 of the revised manuscript.

9. The authors try to link their findings to human lung regeneration, where secretory-like cells in the distal respiratory airways (SCGB3A2+SFTPB+SCGB1A1-) may be derived from AT2 cells (ref. 37). However, another paper suggested that these cells in fact differentiate into AT2 cells (Basil et al, Nature 2022, which is not cited), and another paper using hPSC-derived models indicates that these cells may be AT1 precursors (Pezet et al., Nat Biotechnol, 2025, also not cited). Another paper (Habermann et al., Sci Adv 2021, not cited either) places such cells in between AT2 and AT1 cells. Furthermore, also not acknowledged is the fact that the respiratory airways found in larger mammals are absent in rodents. The extrapolation to human data is therefore a bit tenuous.

Response: We thank the reviewer for raising these important points. In the first version of the manuscript, we linked our mouse findings to human lung regeneration based on the following observations. In a human single-cell study (Murthy et al., *Nature*, 2022) on the terminal and respiratory bronchioles (TRBs, a structure absent in mice), a population of AT0 cells was identified that co-express SFTPC and SCGB3A2. Pseudotime analysis and *in vitro* organoid culture showed that human AT2 cells can transition into AT1 cells and secretory cells through the AT0 intermediate state (Murthy et al., *Nature*, 2022). In parallel, our mouse data revealed high expression of *Cldn4* in the transient state during both AT2-to-AT1 and AT2-to-club transitions, with a lineage trajectory similar to that observed in humans. When we re-analyzed the single-cell data from Murthy et al., 2022, we found that the AT0 cells in the trajectory of AT2-to-secretory cell differentiation also highly expressed *CLDN4*. Based on these similarities, we speculated that the mouse AT2-to-club transition may resemble the human AT2-to-secretory cell transition with respect to cellular state changes, and that mouse Cldn4^{+} transient cells might correspond to human CLDN4^{+} AT0 cells. We acknowledge that we currently have no direct genetic or functional evidence to support this conclusion.

We acknowledge the following points raised by the reviewer and have corrected the manuscript accordingly. First, the human lung contains TRBs whereas the mouse lacks this anatomical structure. This difference limits direct extrapolation of cellular dynamics from mice to humans, and we now explicitly acknowledge this limitation in the revised manuscript. Second, we omitted several key references, including Basil et al., (*Nature*, 2022), Pezet et al., (*Nat Biotechnol*, 2025), and Habermann et al., (*Sci Adv*, 2021). These studies present different views on the differentiation potential of secretory cells in human respiratory bronchioles: Basil et al. proposed that respiratory airway secretory (RAS) cells can differentiate into AT2 cells, whereas Pezet et al. and Habermann et al. suggested that these cells may be AT1 precursors or represent an intermediate state between AT2 and AT1. The omission of these references made our original discussion appear less balanced. We have now cited and discussed these studies in the revised manuscript.

After carefully reviewing these studies, we believe that these different observations are not in conflict with our mouse data but can be integrated from a broader perspective. Importantly, our single-cell data revealed two differentiation trajectories in the mouse: (1) AT2 → Cldn4^{+} transient → club, and (2) AT2 → Cldn4^{+} transient → AT1 (Fig. 4d). The second trajectory (AT2 → transient → AT1) is highly consistent with the following human studies: Murthy et al also showed an AT2-AT0-AT1 trajectory (not only the AT2-AT0-TRB-SC trajectory); Pezet et al. (2025), using a human PSC-derived model, indicated that these cells are AT1 precursors; and Habermann et al. (2021) placed such cells in an intermediate state between AT2 and AT1. Therefore, although mice lack respiratory bronchioles, the capacity of AT2 cells to differentiate into AT1 cells through a Cldn4^{+}/AT0-like intermediate state shows remarkable similarity in molecular signatures and lineage relationships to human studies. Regarding the observation by Basil et al. (2022) that RAS cells can differentiate into AT2 cells, this direction appears different from our observed AT2-to-club differentiation. However, this may reflect species-specific repair strategies at the bronchioalveolar junction.

Notably, in the revised manuscript we have used *in vivo* genetic lineage tracing and conditional gene knockout to directly demonstrate the cell fate and functional significance of these two trajectories (Fig. 4). Specifically, we generated a *Cldn4-loxP-Stop-loxP-Dre* (abbreviated as *Cldn4-LSL-Dre*) knock-in mouse via homologous recombination (Fig. 4j). We also generated another AT2-specific genetic tool based on the *Lamp3* gene, *Lamp3-CreER* (Extended Data Fig. 12a). After tamoxifen induction in adult *Lamp3-CreER;R26-tdT* mice, we observed that only $0.07 \pm 0.04\%$ of AT2 cells were leakily labeled in the control group, whereas $99.73 \pm 1.10\%$ of Sftpc^{+}Lamp3^{+} AT2 cells were efficiently and specifically labeled in the tamoxifen group, indicating successful generation of a new AT2 tracer line (Extended Data Fig. 12b-h). We then combined the *Lamp3*- and *Cldn4*- based genetic tools to investigate the fate of transient cells. We generated *Lamp3-CreER;Scgb1a1-DTR-GFP;Cldn4-LSL-Dre;R26-rox-stop-rox-loxP-stop-loxP-tdTomato* (abbreviated as *R26-RSR-LSL-tdT*) quadruple-positive mice (Fig. 4k). The *R26-RSR-LSL-tdT* reporter requires dual recombinase activity: only after excision of both stop cassettes by Dre-rox and Cre-loxP recombinations does the tdTomato become expressed (Fig. 4l). The tracing principle is as follows: upon tamoxifen induction of the quadruple-positive mice, *Lamp3-CreER* excise the LSL stop sequence in *Cldn4-LSL-Dre* locus specifically in AT2 cells, converting it to *Cldn4-Dre* (step 1). It also excises one stop cassette (LSL) in *R26-RSR-LSL-tdT* to generate *R26-RSR-tdT* (step 1). Subsequently, when AT2 -derived transient cells express Cldn4 after DT injury, the activated Cldn4 promoter drives Dre expression, which excises the second stop cassette (RSR) in

R26-RSR-tdT (step 2), resulting in specific tdT labeling of AT2-derived Cldn4$^+$ cells (Fig. 4l). Because club cells express GFP, the club cells derived from Cldn4$^+$ transient cells will co-express tdT and GFP, appearing yellow. For *in vivo* validation, we treated mice with tamoxifen and DT (with PBS as vehicle) and collected lung samples at week 4 post-injury (Fig. 4k). Immunostaining showed minimal tdT signal in control mice, indicating that the *Cldn4* promoter is inactive in AT2 cells under steady-state conditions (Fig. 4m). In contrast, after DT injury, we detected abundant newly generated GFP$^+$Scgb1a1$^+$ club cells in the bronchioles that were also tdT$^+$, confirming genetic tracing of AT2-derived Cldn4$^+$ transient cells and their contribution to club cells after injury (Fig. 4n). Statistical analysis revealed that 62.10 ± 6.16% of newly formed bronchiolar club cells after DT injury originated from Cldn4$^+$ transient cells (Fig. 4o). We also detected tdT$^+$ AGER$^+$ cells in the bronchioles. In addition, residual Sftpc$^+$ AT2 cells labeled with tdT were also observed in the bronchial epithelium; we speculate that these may represent AT2 cells undergoing the Cldn4$^+$ stage or having reverted from the Cldn4$^+$ transient state back to the AT2 cells (Fig. 4n). Further quantification of the tdT$^+$ cell lineages in the bronchiolar epithelium showed that club cells, AT1 cells, and AT2 cells accounted for 56.55 ± 4.54%, 14.05 ± 3.13%, and 7.48 ± 2.06% of the total, respectively (Fig. 4p). These fate-mapping data demonstrate that AT2 cells do pass through Cldn4$^+$ transient cell stage, which subsequently give rise to both club cells and AT1 cells, consistent with our previous pseudotime analysis (Fig. 4d).

To further validate the functional role of Cldn4 in AT2 cell contribution to the bronchiolar epithelium, we developed a conditional knockout tool, *Cldn4-flox* (Fig. 4q). We generated *Sftpc-CreER;R26-tdT;Scgb1a1-DTR-GFP;Cldn4$^{flox/+}$* (control group) and *Sftpc-CreER;R26-tdT;Scgb1a1-DTR-GFP;Cldn4$^{flox/flox}$* (experimental group) mice (Fig. 4r). After tamoxifen and DT treatment, AT2 cells were specifically traced and *Cldn4* was knocked out (Fig. 4r). RT-qPCR on FACS-sorted tdT$^+$GFP$^-$ AT2 cells confirmed that *Cldn4* expression was significantly reduced compared with controls (Extended Data Fig. 12k,l). At 4 weeks post-DT, immunostaining and statistical analysis showed that Cldn4 knockout significantly reduced the proportion of AT2 cells contributing to club cells (control vs. experimental: 65.94 ± 6.50% vs. 25.49 ± 3.54%) (Fig. 4s,t and Extended Data Fig. 12m). Furthermore, Cldn4 knockout also significantly reduced the proportion of AT1 cells among AT2-derived bronchiolar cells (control vs. experimental: 21.11 ± 2.74% vs. 8.82 ± 1.56%), and decreased the coverage of the bronchiolar epithelium (control vs. experimental: 54.47 ± 5.84% vs. 19.42 ± 4.45%) (Fig. 4u-w and Extended Data Fig. 12n). In summary, through these genetic fate-mapping and functional analyses, we demonstrate that Cldn4$^+$ intermediate cells derived from AT2 cells not only contribute to the bronchiolar epithelium but also functionally promote AT2 cell-mediated epithelial repair (Fig. 4x). Together, these This genetic evidence provides causal mechanistic insight that is difficult to obtain from human transcriptomic inference alone, highlighting the unique value of mouse models for dissecting conserved regenerative mechanisms.

Based on the above data and discussion, we have made the following revisions to the manuscript. First, we have added citations to Basil et al. (2022), Pezet et al. (2025), and Habermann et al. (2021) in the Discussion. We also explicitly acknowledge the anatomical differences between human and mouse distal airways, stating that direct extrapolation from mouse to human is not warranted. Second, we have toned down statements that directly equate mouse AT2-to-club conversion with human secretory cell differentiation. Instead, we emphasize the consistency of the two differentiation trajectories (especially AT2 → transient → AT1) across species, as well as the

molecular similarity of CLDN4 as a conserved intermediate marker. Third, we highlight the two trajectories validated by our genetic lineage tracing and functional studies, and we note that the core value of the mouse model lies in providing causal mechanistic evidence. We believe that these revisions provide a more balanced and rigorous discussion that respects both the power and the limitations of mouse genetic models for understanding human lung biology. We have added these data and discussion to the revised manuscript. For details, please refer to revised Fig. 4, Extended Data Figs. 11 and 12; Page 13, Paragraph 2; Page 14, Paragraph 2; Page 22, Paragraph 2; Page 23, Paragraph 1 of the revised manuscript.

Referee #3 (Remarks to the Author):

In this manuscript, Liu and colleagues provide compelling evidence that alveolar epithelial cells type-2 (AT2) can sense the loss of airway club cells and migrate to replenish them in vivo. While multiple studies have previously showed that airway/bronchiolar epithelial cells migrate to distal lung upon severe injury. Now this manuscript provides evidence that distal alveolar cells can migrate to bronchioles to replenish club cells after their ablation. The authors used a suite of intersectional lineage tracing mouse models coupled with club cell ablation or chemical injury models to demonstrate the plasticity of AT2s. The authors claim that AT2-linegae derived cells contribute to Club, AT2, and BASCs after injury via transbronchial “tunnels”. Further, the authors combine these lineage tracing models with genetic perturbation to modulate notch and Itgb1. Using scRNA-seq profiling approaches, the authors claim that AT2s go through a molecular defined transient cell state prior to generating club, ciliated cells, and AT2 and found enrichment of ligand-receptor interactions mediating notch signaling. The authors went on to use genetic perturbation models to increase or decrease notch signaling and loss of Itgb1.
In summary, this manuscript further expands on the widely described cell plasticity during injury repair in lungs. They used mouse models with multiple alleles to definitively demonstrate the contribution of specific cell populations. A major concern is that the signaling pathways they targeted are either very general or they focus on downstream cell fate specification once AT2s migrate to the bronchiolar luminal side. I suggest the authors address the following comments/concerns to make this manuscript more meaningful.
Response: We sincerely thank the reviewer for recognizing the novelty and technical rigor of our work. We also appreciate the constructive concern regarding the general nature of the signaling pathways studied and the focus on post-migration cell fate specification. In the original manuscript, we agree that the mechanisms underlying AT2 migration and the characterization of the transient intermediate state were not sufficiently addressed. To directly address these points, we have substantially revised the manuscript and added new experimental data that strengthen the mechanistic depth and overall conclusions. Our detailed point-by-point responses to the reviewer's comments are as follows.

Major comments:
1. Functional properties of AT2-lineage derived bronchiolar epithelial cells:
In Fig-2, they show AT2-derived cells sustain up to 6 months post naphthalene. Do they function as club cells? Do they respond to a secondary injury and generate club cells and ciliated cells? Do

AT2-lineage derived cells retain any epigenetic memory? Use ATAC-seq. Similarly, are AT2-lineage derived ciliated cells function similarly as the native ciliated cells?

Response: We thank the reviewer for raising these important functional questions. In Fig. 2, using *Scgb1a1-CreER;Sftpc-DreER;R26-NR* mice, we specifically labeled AT2 cells as $ZsG^{+}tdT^{-}$ and tracked their fate after naphthalene-induced airway injury (Fig. 2a-e). At 4 weeks post-injury, AT2-lineage cells had migrated into the bronchioles and differentiated into club cells and AT1 cells (Fig. 2f-k). These AT2-derived club cells persisted for up to 6 months after injury, and by that time point, we also observed AT2-derived ciliated cells (Fig. 2l-n). To address whether these persistent AT2-derived club cells are functionally equivalent to native club cells, we assessed their proliferation and differentiation capacity in response to a secondary airway injury, as suggested by the reviewer. *Scgb1a1-CreER;Sftpc-DreER;R26-NR* mice were treated with tamoxifen, followed three weeks later by naphthalene injury. After a 6-month repair period, the experimental group received a second naphthalene injury, while the control group received vehicle (corn oil). Lungs were collected two weeks later (Extended Data Fig. 8g). Immunostaining and statistical analysis for ZsG, tdT, Scgb1a1, and Ki67 on lung sections showed that the proportion of $ZsG^{+}Scgb1a1^{+}tdT^{-}$ (AT2-derived club) cells expressing Ki67 was significantly higher in the second injury group than in controls, demonstrating that AT2-derived club cells retain the ability to proliferate upon injury (Extended Data Fig. 8h,i). Furthermore, immunostaining for ZsG, tdT, and Foxj1 revealed a significant increase in the proportion of bronchiolar ciliated cells that were ZsG^{+} following secondary injury, indicating that a subset of AT2-derived club cells can differentiate into ciliated cells when stimulated (Extended Data Fig. 8j,k). Together, these *in vivo* genetic data demonstrate that AT2-derived club cells, even after 6 months, retain the classical stem cell functions of native club cells—namely, injury-induced proliferation and differentiation into ciliated cells.

To directly address the reviewer's important questions regarding whether AT2-derived cells truly function as airway cells and whether they retain any "epigenetic memory" of their alveolar origin, we performed single-cell multiome sequencing (joint profiling of ATAC-seq and RNA-seq) on FACS-sorted $ZsG^{+}tdT^{-}$ cells (AT2-derived lineage cells) from *Scgb1a1-CreER;Sftpc-DreER;R26-NR* mice at 4 weeks and 6 months after naphthalene injury. For baseline comparison, we collected tdT^{+} cells (containing homeostatic club cells and their ciliated progeny) and $CD45^{-}Lysotracker^{+}$ enriched AT2 cells from *Scgb1a1-CreER;R26-tdT* mice at 2 months after tamoxifen induction. Weighted Nearest Neighbor (WNN) analysis resolved distinct clusters of AT2, club, and ciliated cells (Extended Data Fig. 8l, left). Importantly, sample-source mapping revealed that AT2-derived cells from injured lungs (Naph-4w and Naph-6m) extensively overlapped with homeostatic club and ciliated populations. These findings demonstrate that the transcriptomic and chromatin accessibility landscapes of AT2-derived cells successfully converge toward those of native airway epithelial cells (Extended Data Fig. 8l, right).

Our transcriptional analysis and functional signature scoring further confirm that AT2-derived cells acquire the characteristic features of their native counterparts (Extended Data Fig. 8m-o). For AT2-derived club cells, the Secretory and Immune Signature score was significantly higher at 6 months than at 4 weeks, showing no statistical difference from native club cells by the later stage (Extended Data Fig. 8m, left). Regarding the Xenobiotic Metabolism Signature, while some differences remained compared to native club cells, the score in AT2-derived club cells exhibited a upward trend from 4 weeks to 6 months (Extended Data Fig. 8m, right). Similarly, for AT2-derived ciliated cells, the Ciliogenesis Signature score at both time points was no longer different from

native ciliated cells (Extended Data Fig. 8n, left). Crucially, the Ciliary Beating Signature score showed a clear upward trend from 4 weeks to 6 months, and by 6 months it was no longer statistically different from that of native ciliated cells. (Extended Data Fig. 8n, right). Morphologically, we further examined the ultrastructure of ZsG^{+} AT2-derived ciliated cells (ZsG protein detected by immunogold labeling) versus ZsG^{-} ciliated cells using electron microscopy at 6 months after naphthalene injury. The results showed that both populations displayed similar mature ciliary structures (Extended Data Fig. 8o).

To quantitatively assess the retention of AT2-specific epigenetic memory, we first identified high-confidence lineage-specific open chromatin regions (peaks) by performing differential accessibility analysis between homeostatic AT2 cells and native club or ciliated cells. We then calculated an epigenetic signature score for each cell using a chromatin module-based approach. Comparing AT2-derived club cells at 4 weeks post-injury, their AT2 signature scores were already significantly lower than those of homeostatic AT2 cells, approaching the levels of native club cells (Fig. 2o); Moreover, no significant difference in AT2 signature scores was observed between the 4-week and 6-month time points. (Fig. 2o). Notably, in AT2-derived ciliated cells, the AT2 signature scores at both 4 weeks and 6 months were no longer statistically different from those of native ciliated cells (Fig. 2p). This is exemplified by the representative AT2-specific peak at the *Sftpc* promoter loci, where the signal was highest in homeostatic AT2 cells but decreased in AT2-derived cells to levels comparable with native airway cells (Extended Data Fig. 8p). Conversely, the epigenetic scores for club-cell-specific signatures in AT2-derived cells were significantly higher than those in homeostatic AT2 cells at both time points (Extended Data Fig. 8q, left).Moreover, the epigenetic scores for ciliated-cell-specific signatures in AT2-derived cells showed an upward trend from 4 weeks to 6 months and was no longer statistically different from those of native ciliated cells at either time point (Extended Data Fig. 8q, right).To further evaluate the robustness of memory retention, we defined an epigenetic memory index, calculated by normalizing the aggregate accessibility of AT2-specific peaks in AT2-derived cells relative to the dynamic range established by homeostatic AT2 cells (100% memory) and corresponding native airway cells (0% memory). We found that the AT2 epigenetic memory index decreased to approximately 30% in AT2-derived club cells and 10% in ciliated cells, and remained stable from 4 weeks to 6 months (Fig. 2q). This suggests that AT2 epigenetic memory drops sharply upon lineage conversion and is stably maintained at a low level, with further reduction occurring during terminal differentiation into ciliated cells via additional gene regulatory remodeling (Fig. 2q).

In summary, our data demonstrate that AT2-derived club and ciliated cells undergo stable epigenetic reprogramming during injury repair, progressively losing their AT2 signature while acquiring airway-specific epigenetic features and functional gene expression programs that closely resemble those of native airway epithelial cells. We have added these data and discussion to the revised manuscript. For details, please refer to revised Fig. 2, Extended Data Fig. 8; Page 9, Paragraph 2; Page 21, Line 608; Page 22, Paragraph 1 of the revised manuscript.

2. Contribution of rare p63+ distal bronchiolar epithelium:

Previous studies found a rare population of p63+ cells in the distal bronchioles expand extensively and generate “pods after H1N1-PR8 infection and to some extent in bleomycin-induced injury models. In Extended Data Fig-4, the authors used p63-lineage tracing models. However, this reviewer questions whether their tamoxifen regimen was sufficient to label these rare p63+ cells in

the distal airways? Additionally, recent studies showed the presence of SCGB3A2+ve SCGB1A1-ve cells in small airways and they convert to p63+ basal cells in H1N1-PR8 infected cells. Therefore, authors need to check the relative contribution of different cell sources.

Response: We thank the reviewer for raising these important points regarding the potential contribution of rare $p63^+$ distal bronchiolar epithelium and $Scgb3a2^+Scgb1a1^-$ cells to airway repair. We first confirmed that our tamoxifen regimen (0.2 mg/g for 4 consecutive days) in *p63-DreER;Rosa26-RSR-tdT* mice efficiently labeled basal cells, achieving 99.26 ± 0.68% labeling efficiency (Extended Data Fig. 5a-c). Using *p63-DreER;Rosa26-RSR-tdT;Scgb1a1-DTR-GFP* mice, we found that after DT-mediated depletion of all $Scgb1a1^+$ cells, *p63-DreER*-labeled cells predominantly contributed to club cells in proximal airways, including the trachea and main bronchi (Extended Data Fig. 5d-h). As noted by the reviewer, previous studies have reported the presence of a rare population of $p63^+$ cells in distal bronchioles that can expand after H1N1-PR8 infection or bleomycin injury (Kumar et al., *Cell*, 2011; Vaughan et al., *Nature*, 2015; Zuo et al., *Nature*, 2015). To examine whether our tamoxifen dosing regimen could label these distal bronchiolar $p63^+$ cells, we performed immunostaining and comprehensive imaging of lung sections. Indeed, we detected rare tdT^+ cells sporadically distributed in distal bronchioles, and these cells expressed the basal cell marker Krt5 (Extended Data Fig. 5b, right). Quantification across 80 non-consecutive lung sections from four mice revealed a total of 6 tdT^+ basal cells (Extended Data Fig. 5c, right). Immunostaining for tdT and GFP on lung sections of *p63-DreER;Rosa26-RSR-tdT;Scgb1a1-DTR-GFP* mice at four weeks after DT treatment showed that these rare $p63^+$ cells formed clonal expansions and differentiated into club cells in distal bronchioles (Extended Data Fig. 5h). Thus, due to their high abundance proximally and scarcity distally, $p63^+$ cells are primarily responsible for the regeneration of club cells in proximal airways, with only a minor contribution to distal bronchiolar repair (Extended Data Fig. 5i,j).

Moreover, we have previously shown that a $p63^+$ intermediate cell state arises during the transdifferentiation of bronchiolar club cells into AT2 cells after bleomycin-induced alveolar injury (Lv et al, *Cell Stem Cell*, 2024). To further validate the sufficiency of our p63-based tracing system to capture such transient basal-like states, we employed a sequential strategy in *p63-DreER;Rosa26-RSR-tdT* mice. Bleomycin injury induction was followed by tamoxifen administration between weeks 1 and 2 post-injury, with tissues harvested two weeks later (Fig. 7a to Reviewers). Immunostaining confirmed that this strategy successfully labels $Krt5^+$ basal-like cells surrounding the bronchioles (Fig. 7b to Reviewers). Subsequent analysis verified that these traced basal-like cells possessed stem/progenitor potential and could differentiate into alveolar AT2 and AT1 cells (Fig. 7c,d to Reviewers). Together, these results confirm that our p63-based tracing system and tamoxifen dosing are sufficient to capture both resident and transient basal cell states.

Regarding the reviewer's comment on the $Scgb3a2^+Scgb1a1^-$ cell population (Beppu et al., *Nat Commun*, 2023), we performed a detailed examination of the presence and repair potential. Through co-immunostaining for Scgb3a2, GFP, and Scgb1a1 on lung sections from *Scgb1a1-DTR-GFP* mice, we identified a small number of $Scgb3a2^+GFP^-Scgb1a1^-$ cells (white arrowheads) within the bronchiolar epithelium (Extended Data Fig. 6a,b). Statistical analysis across 150 fields of view (10× magnification) from three mice revealed 41 such cells randomly distributed along the airways, indicating their low abundance (Extended Data Fig. 6c,d). At 7 days after DT treatment, immunostaining showed that most of $GFP^+Scgb1a1^+$ cells were ablated, whereas $Scgb3a2^+GFP^-Scgb1a1^-$ cells remained (Extended Data Fig. 6e-g). Further immunostaining for

Scgb3a2, GFP, and Ki67, followed by quantitative analysis, showed that a subset of Scgb3a2^{+}GFP^{-} cells (white arrowheads) and Scgb3a2^{+}GFP^{+} cells (yellow arrowheads) expressed Ki67, indicating their proliferation in response to injury (Extended Data Fig. 6h). Notably, the Scgb3a2^{+}Ki67^{+}GFP^{-}Scgb1a1^{-} cells observed after injury likely represent the expansion of surviving Scgb3a2^{+}GFP^{-}Scgb1a1^{-} cells (Extended Data Fig. 6h-j). The regenerated Scgb3a2^{+}GFP^{+}cells post-injury may originate from either Scgb3a2^{+}GFP^{-} cells reacquiring GFP (Scgb1a1) expression or from differentiation of other stem/progenitor cells (e.g., AT2 cells, neuroendocrine cells, or basal cells). Immunostaining for Scgb3a2, GFP, and Krt5 revealed no Krt5^{+} cells adjacent to Scgb3a2^{+}GFP^{-} cells, suggesting that Scgb3a2^{+}GFP^{-} cells may not contribute to basal cells after DT injury (Extended Data Fig. 6i). However, we acknowledge that due to the lack of *Scgb1a1*/*Scgb3a2*-driven dual lineage-tracing tool, we were unable to rigorously assess the *in vivo* fate of Scgb3a2^{+}Scgb1a1^{-} cells or their quantitative contribution to newly formed club cells after bronchiolar injury. This limitation could be addressed in the future when appropriate genetic tracing tools become available.

We have added these data and discussion to the revised manuscript. Because our Extended Data Figures now total 20 after revision, we have included the bleomycin injury data from *p63-DreER;Rosa26-RSR-tdT* mice in the Figure to reviewers. These data can be considered for publication, along with review comments and response, at the reviewer and editor's discretion. For details, please refer to revised Extended Data Figs. 5,6, and Fig. 7 to Reviewers; Page 7, Paragraph 2; Page 8, Line 211; Page 22, Line 637 of the revised manuscript.

3. Communication between ciliated cells and transient cells via Notch:

Based on the data in Fig-5n-U, the authors concluded that notch receptor and ligand interaction between "transient cell" and ciliated cell controls the fate of migrated AT2 cells. However, current data doesn't show whether the interaction between ciliated cells and "transient cells" is mediated by Notch ligand and receptor. The authors need to specifically delete Notch2 and Jag2 in Ciliated cells and transient cells, respectively. Current work targets Notch receptors in AT2s and its dependents but not specifically the transient cells.

Response: We thank the reviewer for raising these important points. The previous Fig. 5n-u has been moved to Fig. 6a-i in the revised manuscript. Through cellular interaction analysis, we detected that ciliated cells established specific Notch signaling pathways with AT2-derived populations via Jag1/2-Notch1/2 ligand-receptor pairs following bronchiolar injury (Fig. 6a). We used DT injury in *Sftpc-DreER;R26-RSR-tdT;Scgb1a1-DTR-GFP;Foxj1-CreER;R26-iDTR* mice to simultaneously ablate Scgb1a1^{+} cells and ciliated cells. Compared with control mice (*Sftpc-DreER;R26-RSR-tdT;Scgb1a1-DTR-GFP*), ciliated cell ablation significantly inhibited the transdifferentiation of AT2 cells into ciliated cells (Fig. 6a-i). We fully agree with the reviewer that ciliated cell ablation experiments do not directly prove a ligand-receptor regulatory relationship between ciliated cells and transient cells. As suggested by the reviewer, we therefore performed cell-type-specific deletion of Notch ligands in ciliated cells and Notch receptors in AT2-derived cells. To address the Reviewer's concern, we redesigned the gene knockout experiment in the revised manuscript. Among all Notch ligand-receptor pairs, the Jag1-Notch2 interaction showed the highest association strength between ciliated cells and transient cells (Fig. 6a), even higher than the Jag2-Notch2 pair suggested by the Reviewer, indicating that Jag1-Notch2 may play a more prominent regulatory role. We therefore selected this pair for subsequent *in vivo* experiments.

We first generated *Foxj1-CreER;R26-tdT* mice and collected lungs after tamoxifen induction for immunofluorescence analysis (Extended Data Fig. 14j). The results showed that tdT$^+$Ace-Tub$^+$ ciliated cells expressed high levels of Jagged1, consistent with the cellular interaction data (Extended Data Fig. 14k and Fig. 6a). To further validate Jagged1 knockout efficiency, we generated *Foxj1-CreER;Jag1$^{flox/flox}$* experimental mice and *Foxj1-CreER;Jag1$^{flox/+}$* control mice. We showed that, compared with control mice, Jagged1 was efficiently eliminated in ciliated cells after tamoxifen induction (Extended Data Fig. 14l,m). To test whether *Jag1* in ciliated cells regulates AT2-to-club cell transdifferentiation, we generated *Sftpc-DreER;R26-RSR-tdT;Scgb1a1-DTR-GFP;Foxj1-CreER;Jag1$^{flox/flox}$* experimental mice, with *Sftpc-DreER;R26-RSR-tdT;Scgb1a1-DTR-GFP;Foxj1-CreER;Jag1$^{flox/+}$* mice as controls (Fig. 6j). The working principle of our strategy is as follows: after tamoxifen induction, ciliated cells specifically delete *Jag1*; Scgb1a1$^-$Sftpc$^+$ AT2 cells are labeled with tdT; Scgb1a1$^+$Sftpc$^-$ club cells are labeled with GFP; and Scgb1a1$^+$Sftpc$^+$ BASCs are labeled with both tdT and GFP. DT treatment specifically ablates both club cells and BASCs, allowing us to assess the effect of ciliated cell-specific *Jag1* knockout on the cell fate of AT2 cell lineages (Fig. 6k,l). Immunostaining and statistical analysis of lungs 4 weeks after DT injury revealed that *Jag1* knockout significantly inhibited the transdifferentiation of AT2-derived cells that had migrated into the bronchioles into club cells (Fig. 6m-o). These data provide direct genetic evidence that ciliated cells regulate AT2-to-club cell transdifferentiation through the Notch ligand Jag1.

Regarding conditional knockout in transient cells, we acknowledge the reviewer's suggestion to specifically delete Notch2 in transient cells. However, performing gene-specific editing in transient cells during cell fate transition presents substantial challenges. To the best of our knowledge, no established technical precedent exists in the current literature that enables efficient and specific gene knockout in such intermediate cell populations. First, the transient nature of intermediate cells: transient cells, such as AT2-derived transitional cells, are highly dynamic and persist only within a narrow temporal window following injury. Their rapid emergence and subsequent disappearance make it difficult to achieve precise spatiotemporal control of gene recombination using inducible systems such as CreER. Second, the lack of stable and specific genetic markers: to date, no gene has been identified that is exclusively and consistently expressed throughout the lifespan of these transient intermediate cells. Even widely utilized markers, such as Krt8 (Strunz et al., *Nat Commun*, 2020), are expressed in only a subset of the transitional state and are therefore unsuitable for precise lineage-restricted knockout. Third, limitations of available mouse tools: no validated CreER mouse line exclusively targeting such transient populations is currently available. Moreover, such a CreER would generally require an orthogonal recombinase to achieve specificity of AT2-derived transient cell targeting. The generation and validation of a new Dre-induced CreER system would require at least two years, while the narrow induction window and potential off-target effects remain an unresolved challenge. Fourth, the risk of false-negative results due to protein persistence represents a biological barrier. Even if all of the above technical obstacles could be overcome, an unavoidable biological issue persists: gene knockout results in deletion of DNA, whereas pre-existing mRNA and functional protein do not disappear immediately. Many proteins possess long half-lives (e.g., days), whereas transient cells exist for only hours to days. Following CreER-induced gene knockout, residual protein may still be sufficient to maintain the gene's function and drive the fate transition of the transient cells. Consequently, even if a gene is critically important for the transition, no phenotype may be observed after knockout (a

false-negative outcome), thereby precluding reliable conclusions. Thus, classical gene knockout strategies are incompatible with the transient nature of these cells, and the field generally adopts lineage-specific knockout in precursor cells to study such populations. Given these technical constraints, we adopted a widely accepted alternative strategy: conditional knockout of *Notch2* in the upstream precursor cells (AT2 cells) using *Sftpc-CreER* combined with lineage tracing, which allows us to assess gene function in the AT2-derived lineage, including the transient cells. We have acknowledged this limitation in the Discussion section of the revised manuscript, and we respectfully hope that the reviewer appreciates the current technical boundaries and accepts our alternative experimental evidence.

To investigate the function of the Notch receptor Notch2, we first generated conditional knockout *Notch2-flox* mice by homologous recombination using CRISPR/Cas9 (Fig. 6p). To achieve specific knockout of *Notch2* in AT2-derived cells, including tdT^+ AT2 cells and tdT^+ transient cells, we further generated *Sftpc-CreER;R26-tdT;Scgb1a1-DTR-GFP;Notch2*$^{flox/flox}$ mice as the experimental group to study the effect of Notch2 deletion on the AT2-to-club cell transition (Fig. 6q,r). We first collected lung tissues at 4 weeks post-DT injury and sorted tdT^+ cells for RT-qPCR analysis (Extended Data Fig. 14o). Notch2 expression was significantly reduced in the experimental group compared with control *Sftpc-CreER;R26-tdT;Scgb1a1-DTR-GFP;Notch2*$^{flox/+}$ mice, indicating that our *Notch2-flox* mice were successfully generated and that Notch2 was efficiently deleted in AT2-derived cells (Extended Data Fig. 14p). Subsequently, immunostaining and statistical analysis of lung sections revealed that, compared with controls, knockout of *Notch2* in AT2 cells and transient cells significantly inhibited their transition into club cells, and this regulatory effect was consistent with the cellular interaction analysis data (Fig. 6a,s-u). These data demonstrate that AT2-derived cells can receive Notch signals from ciliated cells through the Notch2 receptor, thereby promoting their fate transition toward club cells (Fig. 6w). Furthermore, our *Notch2* knockout results are consistent with our previous *Rbpj* knockout findings (Fig. 5), collectively demonstrating the critical role of Notch signaling in the AT2-to-club cell transition.

In summary, we have validated the role of Notch ligand-receptor interactions in regulating bronchiolar club cell regeneration through a refined gene knockout strategy. Specifically, we provide robust *in vivo* genetic evidence demonstrating that ciliated cells regulate AT2-derived club cell regeneration via the Notch ligand Jag1. Furthermore, we show that AT2-derived cells are regulated by the Notch2 receptor during their transition toward club cells. We have acknowledged in the Discussion section the limitation that we could not perform specific gene knockout in transient cells in this experiment. Moreover, owing to the considerable time and resources required, we did not examine the roles of all individual Notch ligands and receptors in AT2-to-club cell conversion—a limitation that we have also discussed in the Discussion section. We have added these new experimental data and the above discussion to the revised manuscript. For details, please refer to revised Fig. 6, Extended Data Fig. 14; Pages 16 and 17; Page 22, Paragraph 1 of the revised manuscript.

4. Trans-bronchial migration of AT2 cells via “tunnels”:

Based on the static image data in Fig-6b, the authors state that AT2s migrate to the airway surface via “tunnels”. However, current images don’t show a clear “tunnel” like structure instead they look like “channels”. It would be very informative to visualize these passages in 3-dimensional view. Further, what regulates “Tunnel” formation? Is the basement membrane completely disassembled

or patchy disorganization under the bronchiolar epithelium after club cell loss? Have the authors found upregulation of any ECM degrading proteases in transcriptome data?

Response: We thank the reviewer for raising these important points regarding AT2 migration. The content originally presented in Fig. 6b has been moved to Fig. 1 in the revised manuscript. In our original manuscript, we used the term "tunnel" to describe the structures through which AT2 cells traverse the bronchiolar wall in the DT injury model. To more accurately reflect their structural properties, we have renamed them "channels" throughout the revised manuscript (Fig. 1n-p). We previously found that AT2 cell lineages enter the bronchiole via two routes after injury: (1) the natural bronchioalveolar duct junction (BADJ, route 1), and (2) channels formed by AT2 cells through the bronchial wall into the bronchiolar lumen (route 2) (Fig. 1n-p). Following the reviewer's suggestion regarding the channels, we have now provided three-dimensional views that more intuitively display the channel structures (white arrows, Extended Data Fig. 3f and Supplementary Movie 1).

To systematically characterize the dynamics of the AT2 migration routes, we collected lungs at multiple time points following DT injury (days 3, 7, 14, 28, and 8 weeks post-DT) for analysis (Fig. 1f). In PBS-treated control mice, no tdT signal was detected in the distal bronchioles (Fig. 1g). On day 3 post-DT, immunostaining analysis of lung sections revealed tdT^+ cells initiating migration toward the bronchiole through the BADJ (route 1, white arrowheads) as well as directly through formed bronchiolar wall channels (route 2) (Fig. 1n). Immunostaining and statistical analysis on days 7, 14, 28, and 8 weeks post-DT showed that the coverage of the bronchiolar epithelium by tdT^+ cells increased as repair progressed (Extended Data Fig. 3a-e). At all these time points, tdT^+ cells were detected along both route 1 and route 2 on lung sections (Extended Data Fig. 3c-e). However, we observed a marked difference in the frequency with which these two routes were used. We defined a "route 1 event" when tdT^+ cells were located at the distal bronchioles near the BADJ, and a "route 2 event" when channel structures were detected on the bronchiolar wall (Fig. 1n,p). By quantifying the proportion of bronchioles exhibiting route 1 and route 2 events at different time points, we observed a difference in the cumulative proportions. The proportion of route 1 events increased rapidly from day 3 to day 28 post-injury, reaching 92.08 ± 3.39% by 8 weeks, which coincided with the rapid increase in tdT^+ cell coverage of the bronchiolar epithelium (Fig. 1o,p and Extended Data Fig. 3c,d). In contrast, although route 2 events were detectable as early as day 3 post-DT (Fig. 1n), their proportion increased only slightly over time, and by 8 weeks, channel structures were detected in 9.65 ± 1.12% of bronchioles (Fig. 1o,p and Extended Data Fig. 3e,f). These data suggest that AT2 cell lineages primarily contribute to the bronchiolar epithelium via route 1 (BADJ), with route 2 serving as a supplementary route for epithelial cell contribution. We acknowledge that due to the lack of continuous *in vivo* live monitoring of cell migration over time, the current quantification provides only a rough estimate but not a precise quantitative measurement of the two migration routes.

To further characterize the channel architecture, we performed PDGFRa co-immunostaining at multiple time points after DT injury (days 3, 7, 14, 28, and 8 weeks post-DT), which marks peribronchiolar mesenchymal fibroblasts and provides a clear positional reference and structural boundary for the channels. Immunostaining at these time points revealed that PDGFRa clearly delineates both bronchiolar wall and peribronchiolar fibroblasts (Fig. 1n and Extended Data Fig. 3e). The channels connect the bronchiolar lumen to the alveolar region and are surrounded by a continuous sleeve of $PDGFRa^+$ cells, indicating that the channels are organized, well-defined

structures. Importantly, the inner side of the channels is lined by tdT$^+$ AT2-derived cells without invasion by PDGFRa$^+$ cells (Fig. 1n and Extended Data Fig. 3e), demonstrating that the channels are actively formed by migrating AT2 cell lineages rather than by mesenchymal ingrowth. Regarding the reviewer's question about basement membrane integrity, we observed small gaps in the bronchial wall at channel sites where the basement membrane appeared disrupted, directly connecting the bronchiolar lumen to the alveolar space. These gaps indicate focal breakdown of the basement membrane rather than complete disassembly (Extended Data Fig. 3e, white arrows). Thus, channels represent localized breaches that allow AT2 cells to migrate from the alveolar region into the bronchiolar lumen. In addition, Z-stack scanning and 3D reconstruction of thick lung sections further visualized channel structures connecting the alveolar region and the bronchiolar lumen (Extended Data Fig. 3f and Supplemental Movie 1).

To investigate what regulates channel formation, we then established a high-resolution lung transcriptional atlas using single-cell RNA-seq on PBS-treated (control) and DT-treated *Scgb1a1-DTR-GFP* mice (day 7 post-DT). Unsupervised clustering and UMAP visualization of the integrated dataset identified 27 distinct cell populations, including epithelial, endothelial, stromal, and immune lineages (Extended Data Fig. 15a,c). Specifically, DT-injured lungs exhibited a massive infiltration of innate immune cells, primarily a sharp rise in neutrophils, accompanied by robust expansion of peribronchiolar fibroblasts, suggesting the formation of a highly active inflammatory and stromal microenvironment (Extended Data Fig. 15d). As the reviewer suggested, we characterized the expression of matrix-remodeling enzymes after bronchiolar injury. Our scRNA-seq analysis revealed an upregulation of matrix metalloproteinases (MMPs) following DT-mediated damage. Notably, MMP14, a key enzyme for membrane-associated proteolytic activity and pericellular extracellular matrix (ECM) degradation, was significantly induced in AT2 cells, peribronchiolar fibroblasts, and smooth muscle cells (SMCs). Concurrently, infiltrating immune cells showed a localized surge in MMP9 expression (Extended Data Fig. 17e,f). These findings suggest that the injured microenvironment undergoes systemic enzymatic remodeling, in which immune- and stromal-derived MMPs degrade the peribronchiolar matrix and basal lamina, potentially creating a permissive path for AT2 cell migration into the bronchioles. Immunostaining of lung sections from *Scgb1a1-DTR-GFP* mice on day 3 post-DT injury also revealed that immune cells infiltrating the bronchiole expressed high levels of both MMP9 and SPP1, indicating a dual role: facilitating channel formation by MMP9 and inducing AT2 cell migration by SPP1 (Extended Data Fig. 17g). In the revised manuscript, we show that immune cell-derived SPP1 promotes AT2 cell migration; detailed data are provided in our response to the reviewer's following question 5. In *Sftpc-CreER;R26-tdT;Scgb1a1-DTR-GFP* mice, tdT$^+$ channel structures were adjacent to immune cells with high MPP9 and SPP1 expression (Extended Data Fig. 17h-j). These data suggest that injury-induced infiltrating immune cells, through MMP9 and SPP1 secretion, may degrade the peribronchiolar ECM while simultaneously inducing AT2 cell migration, thereby forming channels that guide AT2 cells toward the bronchial lumen. Additionally, injury-induced MMP14 expression in AT2 cells, peribronchiolar fibroblasts, and SMCs may also contribute to ECM degradation. Together with immune cell-derived MMP9, this proteolytic activity may collectively facilitate channel formation. We have added these data and discussion to the revised manuscript. For details, please refer to revised Fig. 1, Extended Data Figs. 3,15, 17; Page 6, Paragraph 2; Page 9, Paragraph 2, Line 242; Page 17, Paragraph 1; Page 18-19; Page 20; Page 21, Paragraph 1 of the revised manuscript.

5. What are the mechanisms that initiate AT2s to sense the loss of club cells and drive their migration? Currently, the authors focused on Itgb1and Notch and found that disruption of these pathways block AT2s migration and fate specification during and after migration, respectively. However, loss of Itgb1 blocks various cellular processes besides migration including cell attachment to the basement membrane and their replication. Therefore, the phenotype described here is not very specific to migration. Similarly, as mentioned above (#3), it is important to modulate notch in specific cell states that are in contact with ciliated cells rather than all AT2s. Lack of specificity can obscure the conclusions.

Response: We thank the reviewer for raising these important points. The mechanisms by which AT2 cells detect club cell ablation and trigger directed migration were not fully defined in our initial study. We agree with the Reviewer that, in addition to affecting cell migration, Itgb1 blockade may impact other cellular processes, and further evidence is required to specifically demonstrate the role of Itgb1 in mediating migration.

To systematically characterize the cellular response to bronchiolar injury, we established a high-resolution lung transcriptional atlas using scRNA-seq on PBS-treated (control) and DT-treated *Scgb1a1-DTR-GFP* mice. Unsupervised clustering and UMAP visualization of the integrated dataset identified 27 distinct cell populations, including epithelial, endothelial, stromal, and immune lineages (Extended Data Fig. 15a, c). Overlay of samples by condition (Extended Data Fig. 15b) revealed broad overlap between PBS and DT groups for most populations, but also highlighted injury-specific cell expansion in localized clusters. Specifically, DT-injured lungs exhibited a massive infiltration of innate immune cells, primarily a sharp rise in neutrophils, accompanied by robust expansion of peribronchiolar fibroblasts, suggesting the formation of a highly active inflammatory and stromal microenvironment (Extended Data Fig. 15d).

Building upon this cellular census, we investigated whether these compositional shifts translated into functional alterations in the signaling network. Comparative CellChat analysis revealed a global expansion of signaling intensity following injury, with neutrophils, NK cells, monocytes, alveolar macrophages, and peribronchiolar fibroblasts shifting toward active signaling hubs (Fig. 7a). Notably, the directionality of these interactions shifted markedly toward AT2 cells after DT treatment, identifying neutrophils, monocytes, and peribronchiolar fibroblasts as the predominant injury-induced signal sources (Fig. 7b). To identify potential chemotactic cues orchestrating AT2 cell recruitment for bronchial repair, we used CellChat to quantify relative information flow across ligand-receptor pathways, enabling systematic comparison of signaling dynamics between homeostatic and injured states. This analysis revealed a consistent and robust induction of SPP1 signaling targeting AT2 cells, primarily emanating from diverse immune cell populations following DT-mediated bronchial damage (Extended Data Fig. 15e). In contrast, peribronchiolar fibroblasts did not show a discernible injury-induced enhancement in chemotactic signaling (Extended Data Fig. 15e). Instead, the peribronchiolar fibroblasts significantly upregulated a wide range of ECM-related genes, including multiple collagens (Extended Data Fig. 15f). Of note, gene set enrichment analysis confirmed enhanced extracellular matrix organization (Extended Data Fig. 15g). SPP1 is a well-characterized secreted chemotactic factor that binds to integrins and CD44 receptors on the cell surface, activating multiple pathways–including PI3K/AKT/mTOR, Rho/Cdc42, and RAS/MAPK–to promote proliferation and migration

of recipient cells (Pang et al., *Pharmacol Res*, 2019; Yim et al., *Immunol Rev*, 2022; Li et al., *Int J Cancer*, 2025) (Extended Data Fig. 15h).

These findings suggest that the rapid infiltration of myeloid cells serves as a signal amplifier, secreting high levels of Spp1 to establish a chemotactic gradient following DT-induced bronchial injury. This biochemical bridge effectively traverses the spatial gap between the injured bronchioles and the adjacent alveolar regions. Ligand–receptor interaction analysis further revealed that DT treatment significantly intensified interaction probabilities between immune cells-derived SPP1 and specific integrin heterodimers (e.g., *Itgav+Itgb6* and *Itga5+Itgb1*) on AT2 cells (Fig. 7c). Activation of the Spp1-Integrin axis appeared to prime downstream PI3K/AKT/mTOR, Rho/Cdc42, and RAS/MAPK signaling, as evidenced by marked upregulation of migration-related and S-phase gene signatures in AT2 cells following injury (Extended Data Fig. 15h,i). Consistent with this migratory phenotype, expression of key Rho GTPases, including *Rhoa*, *Rac1*, and *Cdc42*, was significantly elevated and positively correlated with migration signaling scores (Extended Data Fig. 15j,k). Collectively, we propose that the rapid infiltration of $Spp1^{high}$ immune cells establishes a chemotactic gradient, serving as the critical "injury-sensing" signal. This signaling gradient triggers downstream activation of PI3K/AKT, Rho, and RAS pathways in AT2 cells, initiating their directed migration toward the bronchioles.

Our scRNA-seq analysis revealed a response of multiple cell types to DT injury, with the most pronounced interaction strength changes observed in the immune compartments (Fig. 7a). Specifically, cell-cell communication signaling analysis identified SPP1 as a central ligand, primarily secreted by immune cells and potentially signaling to AT2 cells via specific ligand-receptor interactions (Fig. 7c and Extended Data Fig. 15e). While these data suggest that SPP1-mediated chemotaxis may drive the recruitment of AT2 cells toward the injured bronchioles, scRNA-seq lacks the spatial resolution to dissect whether these signaling events are localized to the injury site. To determine whether these responsive immune cells are strategically positioned to establish a chemotactic gradient for AT2 migration, we performed high-resolution spatial transcriptomic sequencing (Stereo-seq) on lung tissues from *Scgb1a1-DTR-GFP* mice at day 7 post-DT injury, with wildtype mice as controls. Initially, we identified major lung cell types in both control and DT groups, including immune cells, peribronchiolar fibroblasts, pericytes, smooth muscle cells, endothelial cells, AT1 cells, AT2 cells, and ciliated cells (Fig. 7d). To characterize the regionalized response to bronchial injury, we utilized H&E staining on sister sections to delineate airway and alveolar structures, subsequently defining "peribronchiolar region" (within ~200 μm of the bronchi) and "alveolar region" for localized transcriptomic analysis (Extended Data Fig. 16a). We observed a significant (~3-fold) and localized increase in immune cell infiltration within the peribronchiolar region following DT injury (Fig. 7e). To identify the molecular signals potentially driving AT2 recruitment, we employed Hotspot analysis to identify spatially coherent gene modules. Under homeostasis, gene modules associated with leukocyte activation and chemokine signaling (e.g., Modules 7 and 20) showed no specific correlation with bronchial structures (Extended Data Fig. 16b,c). In contrast, DT-injured lungs exhibited the emergence of modules related to leukocyte activation and chemotaxis (e.g., Modules 9 and 26), which were highly concentrated within the bronchial lumen and peribronchiolar areas (Extended Data Fig. 16b,c and Fig. 7 h). Notably, module 9 was enriched for pro-inflammatory and chemokine-related genes such as *Spp1* and *Ccl6*. Concurrently, module 26 was characterized by the expression of key mediators of chemokine response and leukocyte chemotaxis (e.g. *Cxcl9* and *Ccl17*). Consistently, *Spp1* expression was

significantly upregulated in peribronchiolar immune cells after DT injury (Fig. 7f). Moreover, we observed a profound enrichment of chemotaxis-related gene sets in immune cells localized within the peribronchiolar regions after DT-induced injury (Fig. 7g). Collectively, these spatial findings complement our single-cell data by demonstrating that bronchial injury triggers a localized accumulation of immune cells that secrete potent chemotactic factors such as SPP1. This localized inflammatory microenvironment likely serves as key mediators that transmit bronchial injury signals to AT2 cells and establish the chemotactic gradient necessary to drive their directed migration.

To test this hypothesis, we first examined SPP1 expression in immune cells by immunostaining. Lungs from *Scgb1a1-DTR-GFP* mice were collected on days 3, 7, 14, and 28 following DT injury (Extended Data Fig. 17a). Compared with PBS-treated controls, a large number of $CD45^+$ immune cells infiltrated the bronchial lumen after injury and showed high SPP1 expression (Fig. 7i and Extended Data Fig. 17b). Quantification revealed that the mean fluorescence intensity of SPP1 in infiltrated immune cells (yellow arrows) was significantly higher than that in peribronchiolar $CD45^+$ immune cells (white arrows, Fig. 7i,j). The high expression of SPP1 in the bronchi is consistent with our spatial transcriptomics analysis results (Fig. 7f-h). The number of immune cells infiltrating the bronchial lumen decreased over time after injury. During the first 7 days following DT treatment, immune cells rapidly responded to injury and infiltrated the bronchial lumen, whereas after day 7, infiltration declined rapidly (Fig. 7k). Accordingly, we defined the first 7 days as the early injury-response stage and the period after day 7 as the late injury-response stage (Fig. 7k). Using *Sftpc-CreER;R26-tdT;Scgb1a1-DTR-GFP* mice to trace AT2 cell lineage (AT2-tracer1) migration toward the bronchi following DT injury, we found that tdT^+ AT2 lineage cells began migrating toward the bronchiole as early as the early response stage, and the proportion of the bronchiole covered by migrated tdT^+ cells increased with repair time (red line, Fig. 7l). Immune cell infiltration peaked during the early response phase (blue line), suggesting that SPP1 secreted by these immune cells induces AT2 cell lineage migration (Fig. 7l). We previously showed that after DT injury, AT2 lineage cells enter the bronchiole via two routes: the natural bronchioalveolar duct junction (BADJ, route 1) and channels formed by AT2 cells through the bronchiolar wall (route 2) (Fig. 1n-p). Further immunofluorescence staining of lung sections from *Sftpc-CreER;R26-tdT;Scgb1a1-DTR-GFP* mice on day 3 post-DT injury revealed that infiltrating $SPP1^+MMP9^+$ immune cells were distributed near migrating AT2-derived cells at both the terminal bronchioles (adjacent to the BADJ) and channel sites, suggesting that these immune cells may participate in AT2 cell migration toward the bronchioles (Extended Data Fig. 17h-j). We then examined an alternative bronchiolar injury model induced by naphthalene. In wild-type mice treated with naphthalene, we similarly observed massive infiltration of $SPP1^{high}$ immune cells into the bronchiolar lumen, with the number of infiltrated cells gradually decreasing as repair progressed (Extended Data Fig. 17k-n). Based on the immune cell response, we again defined the first 7 days as the early response stage and the period after day 7 as the late response stage (Extended Data Fig. 17n). We used *Scgb1a1-CreER;Sftpc-DreER;R26-NR* mice to specifically examine the contribution of ZsG^+ AT2 cells (AT2-tracer2) to the bronchiolar epithelium following naphthalene injury. Immunostaining and statistical analysis revealed that ZsG^+ cells began migrating to the bronchiolar epithelium during the early stage when immune cell infiltration was high, and that their coverage of the bronchiolar epithelium increased with repair time (Extended Data Fig. 17o-q). Together, these findings suggest a positive correlation between $SPP1^{high}$ immune cells and AT2 cell migration.

We next analyzed Spp1 function through *in vitro* and *in vivo* experiments. We used *in vitro* scratch and Transwell migration assays to determine whether SPP1 secreted by immune cells promotes AT2 cell migration. Using the AT2 cell line (MLE-12), we found that wound closure was detectable 24 hours after scratching, and quantitative analysis showed that the addition of recombinant SPP1 significantly accelerated wound closure (Extended Data Fig. 18a,b). To further confirm the pro-migratory effect of SPP1, we conducted Transwell migration assays. MLE-12 cells were seeded into the upper chamber of Transwell inserts, and recombinant SPP1 was added to the lower chamber as a chemoattractant. After 16 hours of incubation, non-migrated cells were removed from the upper surface of the membrane, while migrated cells on the lower surface were fixed, stained with crystal violet, and counted under a microscope. Consistent with the scratch assay results, recombinant SPP1 also enhanced cell migration in the Transwell assay (Extended Data Fig. 18c,d). To further verify that soluble factors secreted by immune cells drive cell migration, we added immune cells to the lower chamber and found that this markedly increased MLE-12 cell migration. Moreover, the addition of an SPP1 inhibitor significantly suppressed this immune-cell-induced migratory effect (Extended Data Fig. 18e-g). Together, these *in vitro* data demonstrate that SPP1 secreted by immune cells promotes alveolar epithelial cell migration. Next, we validated the regulatory role of SPP1 *in vivo*. We treated *Sftpc-CreER;R26-tdT;Scgb1a1-DTR-GFP* mice with DT and administered an SPP1 inhibitor every other day. Lungs were collected at 4 weeks after DT injury for analysis (Fig. 7m). Immunostaining and statistical analysis showed that, compared with the control group, the coverage of tdT^+ cells migrating to the bronchiolar was significantly reduced in the SPP1 inhibitor-treated group (Fig. 7n.o). In addition, the *Scgb1a1-CreER;Sftpc-DreER;R26-NR* mice were subjected to naphthalene injury and treated with the SPP1 inhibitor (Extended Data Fig. 18h). Analysis of lung samples collected on day 28 similarly revealed that SPP1 inhibition significantly reduced the coverage of ZsG^+ cells migrating to the bronchiole (Extended Data Fig. 18i,j). Together, these experiments demonstrate that SPP1 secreted by immune cells acts as a chemoattractant for AT2 cell migration toward injured bronchioles (Fig. 7p).

Our scRNA-seq analysis revealed a robust interaction between immune cell-derived *Spp1* and the integrin receptor *Itgb1* expressed on AT2 cells (Fig. 7c). We previously used *Sftpc-CreER;R26-tdT;Scgb1a1-DTR-GFP;Itgb1*$^{flox/flox}$ mice to specifically knock out *Itgb1* in AT2 cells. Immunostaining and statistical analyses of the lungs at 28 days after DT injury showed that, compared with control mice *Sftpc-CreER;R26-tdT;Scgb1a1-DTR-GFP;Itgb1*$^{flox/+}$, *Itgb1* knockout significantly reduced AT2 cell migration toward the bronchioles (Fig. 7q-r). We agree with the reviewer's concern that the observed reduction in migration upon *Itgb1* knockout in AT2 cells cannot be unequivocally attributed solely to impaired cell migration, as other cellular processes may also be affected. To further test whether Itgb1 specifically regulates AT2 cell migration, we performed *in vitro* scratch and Transwell assays in the revised manuscript. For scratch assays, we found that the addition of an anti-Itgb1 antibody significantly inhibited wound closure (Extended Data Fig. 18k,l). We then performed Transwell assays, which can effectively exclude interference from other cellular behaviors such as proliferation and thus provide a relatively specific measurement of cell migration. Using this system, we confirmed that the addition of the anti-Itgb1 antibody significantly reduced cell migration from the upper to the lower chamber (Extended Data Fig. 18m,n). Together, these bioinformatic and experimental data suggest that Itgb1 could play a role in mediating chemotactic signal reception in AT2 cells, thereby contributing to their migration toward the damaged bronchial epithelium.

In summary, through a series of new experiments described above, we propose the following potential mechanism: following bronchiolar injury (in both DT and naphthalene models), a large number of immune cells infiltrate the bronchiolar lumen and express SPP1. The secreted SPP1 then diffuses to form a concentration gradient centered on the bronchioles. This SPP1 acts as a ligand that binds to integrin receptors on peribronchiolar AT2 cells, thereby initiating their directional migration toward the bronchiolar region with high SPP1 concentration (Fig. 7u and Extended Data Fig. 20). These data and discussion have been added to the revised manuscript. For details, please refer to revised Figure 7, Extended Data Figs. 15-18, Page 17, Paragraph 3, line 498; and Pages 18-20 of the revised manuscript.

6. Based on the current data, AT2s contribute to multiple cell populations within lung epithelium, which suggests that AT2s are multipotent. Authors need to discuss this further and emphasize this in the results and discussion sections.

Response: We thank the reviewer for this suggestion. In the present study, our fate-mapping data show that after DT- or naphthalene-induced bronchial epithelial injury, alveolar AT2 cells migrate to the bronchioles and differentiate into multiple cell types, including club cells, ciliated cells, and AT1 cells (Figs. 1m, 2r, 3o). In the revised manuscript, we further detected a very small number of AT2-derived BASC-like cells in the distal bronchioles near the BADJ region in the DT injury model (Extended Data Fig. 2n). These cells co-express Sftpc and GFP (representing Scgb1a1), which is consistent with the definition of BASC markers (Kim et al., *Cell*, 2005; Liu et al., *Nat Genet*, 2019 Salwig et al., *EMBO J*, 2019). The ability of AT2 cells to give rise to multiple cell types—including AT1 cells, BASC-like cells, club cells, and ciliated cells—demonstrates their multipotency. Following the reviewer's suggestion, we have added these data and discussion in the Results and Discussion sections of the revised manuscript. For details, please refer to revised Figs. 1,2,3, Extended Data Fig. 2; Page 5, Line136; Page 7, Paragraph 1; Page 21, Paragraph 2 of the revised manuscript.

7. There are some AT2-lineage derived AT1s in bronchioles Fig-1m and 2l. What is the fate of these cells at late times?

Response: We thank the reviewer for raising this important question regarding the fate of bronchiolar AT1 cells. In our study, we utilized two different injury models to induce the clearance of Scgb1a1^{+} cells—DT (via *Scgb1a1-DTR-GFP* in Fig. 1) and naphthalene (in Fig. 2)—to investigate the contribution of AT2 cells to bronchiolar epithelial repair. In both injury models, we observed that AT2 cells migrate into the bronchiolar region, contributing to club cell regeneration while also partially differentiating into AT1 cells that integrate into the bronchiolar layer (Figs 1j and 2j; corresponding to Figs 1m and 2l in the previous version). To explore the subsequent fate of these AT2-derived bronchiolar AT1 cells, we first established an AT1-specific genetic tracing tool. Notably, single recombinase-driven reporter systems—*Hopx-2A-DreER;Rosa26-RSR-tdT* and *Ager-CreER;Rosa26-tdT*—fail to specifically label AT1 cells, as *Hopx-2A-DreER* also labels club cells and *Ager-CreER* labels AT2 cells (Extended Data Fig. 7a-d). Therefore, we employed the intersectional dual-recombinase-driven reporter system Rosa26-rox-stop-rox-loxp-stop-loxp-tdTomato (*R26-RSR-LSL-tdT*) together with the *Hopx-2A-DreER* and *Ager-CreER* tools to construct *Hopx-2A-DreER;Ager-CreER;R26-RSR-LSL-tdT* triple-positive mice, and successfully

verified its ability to specifically trace alveolar resident AT1 cells, but not any AT2 cells or club cells (Extended Data Fig. 7e-g).

Using *Hopx-2A-DreER;Ager-CreER;R26-RSR-LSL-tdT;Scgb1a1-DTR-GFP* quadruple-positive mice, we could simultaneously trace AT1 cells and deplete Scgb1a1$^+$ cells (Extended Data Fig. 7h). In our initial experimental design, we first administered tamoxifen to the quadruple-genotype mice to label alveolar AT1 cells, followed by DT injury. Analysis of the lungs at 4 weeks post DT injury showed that pre-labeled alveolar AT1 cells did not migrate into the bronchiolar region to participate in bronchiolar repair (Extended Data Fig. 7i-m). Similarly, in *Hopx-2A-DreER;Ager-CreER;R26-RSR-LSL-tdT* triple-positive mice, tamoxifen induction followed by naphthalene injury revealed that alveolar AT1 cells did not migrate to the bronchiolar region after bronchiolar damage (Fig. 3p-s). These experiments demonstrated that alveolar resident AT1 cells did not migrate to the bronchiolar regions.

To investigate the fate of AT2-derived bronchiolar AT1 cells after injury, we modified the administration sequence of our experimental strategy in the revised manuscript (Extended Data Fig. 9a-c). Following DT injury and a subsequent 4-week repair period, *Hopx-2A-DreER;Ager-CreER;R26-RSR-LSL-tdT;Scgb1a1-DTR-GFP* mice were administered tamoxifen to label the bronchiolar AT1 cells that had appeared post-injury. Lungs were then collected for analysis at 1 week, 4 weeks, and 3 months after tamoxifen induction (Extended Data Fig. 9b). Immunostaining of lung sections 1 week after tamoxifen induction revealed flattened tdT$^+$ cells in the bronchiolar epithelium, resembling the morphology of alveolar AT1 cells. Further immunostaining for tdT, GFP, AGER, Sftpc, and Ace-Tub demonstrated that tdT$^+$ cells expressed AGER but not markers of other epithelial cell types (Extended Data Fig. 9d,e). These results confirm that our strategy successfully genetically labels AT2-derived bronchiolar AT1 cells during bronchiolar repair (Extended Data Fig. 9c). Although this approach also labels alveolar resident AT1 cells, we already demonstrated that alveolar resident AT1 cells do not migrate to bronchiolar regions or contribute to bronchiolar repair after injury, thereby avoiding interference with the fate mapping analysis of bronchiolar AT1 cells (Extended Data Fig. 7h-m). Subsequent immunostaining and quantitative analysis of lungs collected at 4 weeks and 3 months post-tamoxifen showed that tdT signals in bronchiolar regions remained exclusively associated with AT1 cells, with no labeling of other epithelial lineages (Extended Data Fig. 9d,e). These results indicate that AT2-derived bronchiolar AT1 cells do not undergo further fate conversion and maintain their AT1 identity from 4 weeks to 3 months (Extended Data Fig. 9f).

In parallel, we examined the fate of AT2-derived bronchiolar AT1 cells after naphthalene injury (Extended Data Fig. 9g,h). *Hopx-2A-DreER;Ager-CreER;R26-RSR-LSL-tdT* triple-positive mice were subjected to naphthalene injury and, after a 4-week repair period, received tamoxifen induction. The lungs were then collected at 1 week, 4 weeks, and 3 months post-induction for analysis (Extended Data Fig. 9g). Examination at 1 week confirmed successful tdT labeling of AT2-derived bronchiolar AT1 cells post naphthalene injury, with no detectable marking of other bronchiolar cell types such as club cells, ciliated cells, or AT2 cells (Extended Data Fig. 9i,j). Subsequent analysis at 4 weeks and 3 months further revealed that tdT-labeled AT1 cells did not convert into other cell types (Extended Data Fig. 9i-k). Collectively, our *in vivo* genetic fate mapping results demonstrate that AT2-derived bronchiolar AT1 cells do not undergo significant fate changes and remain as AT1 cells after DT or naphthalene injury. We have added these data and

discussion to the revised manuscript. For details, please refer to revised Fig. 3, Extended Data Figs. 7 and 9; Page 10, Line 287; and Page 11, Paragraph 1 of the revised manuscript.

8. scRNA-seq data in Fig-4S shows that very few AT2-lineage derived cells contribute to Ciliated cells at 6 months compared to 4 months. Are they lost by 6 months and replenished by other lineages (BASCs or club cells)?

Response: We thank the reviewer for raising this question. The single-cell data shown in our previous Fig. 4S (now moved to Extended Data Fig. 11c) represent AT2-derived cell types at 6 months after naphthalene injury. The UMAP plot reveals a small cluster of AT2-derived ciliated cells at this time point (Extended Data Fig. 11b). We did not perform single-cell RNA sequencing at 4 months; we suspect the reviewer is referring to the 4-week time point (Fig. 4c), where no distinct AT2-derived ciliated cell cluster was detected. Chronologically, from 4 weeks to 6 months after naphthalene injury, the AT2-derived ciliated cell population transitions from absent to present on the UMAP. Collectively, our data suggest that the contribution of AT2 cells to ciliated cells progressively increases over time rather than being lost. We have added these data and discussion to the revised manuscript. For details, please refer to the revised Fig. 4, Extended Data Fig. 11; Page 11, Paragraph 2; and Page 12, Paragraph 2 of the revised manuscript.

9. Are AT2-lineage derived cells indispensable? In Sftpc-DreER/Rbpj-KO lungs, does the lung have any defects in regeneration and physiology. Same in ITGB1-KO?

Response: We thank the reviewer for raising this important point regarding the AT2-lineage derived cells in lung regeneration and physiology. Our previous study found that after bronchial club cells are depleted, alveolar AT2 cells migrate to the bronchioles and differentiate into functional club cells, thereby participating in bronchial repair following injury. Furthermore, using lineage tracing, we further demonstrated that specific knockout of *Rbpj* or *Itgb1* in AT2 cells inhibits the AT2-to-club cell transition, leading to impaired regeneration of bronchial club cells (Figs. 5a-m,7q-t). However, we lack a systematic assessment of the lung's physiopathological function after impaired club cell regeneration. Club cells, as airway secretory and progenitor cells in bronchioles, play multiple physiological roles in maintaining airway homeostasis, repairing injury, regulating lung mechanics, and defending against infection (Hao et al., *Physiological Reviews*, 2025; Blackburn et al., *Am J Physiol Lung Cell Mol Physiol*, 2023). Therefore, in the revised manuscript, we have added multidimensional assessments of bronchiolar tissue structure, cell proliferation, pulmonary function parameters, and host defense to systematically evaluate the functional and histological consequences of the DT model. First, we evaluated the impact of Scgb1a1^{+} cell ablation on bronchiolar tissue structure in *Scgb1a1-DTR-GFP* mice post-DT. Lung sections were collected at multiple time points after DT injury (days 3, 7, 14, and 28) and subjected to H&E staining and statistical analysis (Extended Data Fig. 13g). Compared with the control group (PBS-treated), bronchiolar wall thickness began to increase in response to injury on day 3 and gradually decreased over time as repair progressed (Extended Data Fig. 13h,i). Furthermore, PDGFRa and Ki67 immunostaining and quantification revealed that injury stimulated the activation and proliferation of PDGFRa^{+} peribronchiolar mesenchymal cells, leading to adventitial thickening (Extended Data Fig. 13j-l). Our scRNA-seq analysis revealed that peribronchiolar fibroblasts from day 7 DT-injured lungs significantly upregulated a wide range of ECM-related genes, including multiple collagens (*Col1a1*, *Col3a1*, *Col4a1*, *Col6a1*, etc.), as well as *Tnc*, *Postn*, and *Vim* (Extended Data Fig. 15f).

Gene set enrichment analysis confirmed enhanced extracellular matrix organization (Extended Data Fig. 15g). These molecular changes provide a mechanistic basis for the adventitial thickening and airway wall remodeling seen after club cell ablation, consistent with our histological observations. As repair continued, the proportion of proliferating peribronchiolar mesenchymal cells gradually decreased, and the thickness of the mesenchymal layer gradually recovered (Extended Data Fig. 13j-l). Together, these data indicate that club cell ablation induces structural remodeling of the bronchioles.

Next, we used a pulmonary function testing system to assess the impact of club cell ablation-induced airway remodeling on lung respiratory function. We measured six expiratory parameters for lung function. (1) Functional residual capacity (FRC): reflects alveolar inflation or small airway ventilation. A reduced value suggests expiratory limitation or small airway obstruction. (2) Peak expiratory flow/forced vital capacity (PEF/FVC): indicates the degree of airway obstruction. A reduced ratio suggests expiratory limitation, often seen in small airway dysfunction or bronchial wall thickening. (3) Maximal mid-expiratory flow/FVC (MMEF/FVC): represents the flow rate during the middle 50% of the forced expiratory curve and reflects small airway function. A reduced ratio indicates increased small airway resistance. (4) Forced expiratory volume in 100 ms/FVC (FEV100/FVC): a commonly used indicator of airway obstruction in mouse lung function tests. A reduced ratio suggests increased airway resistance and expiratory limitation. (5) Forced expiratory volume in 75 ms/FVC (FEV75/FVC): reflects the very early, rapid phase of expiration and is sensitive to changes in small airway resistance. A reduced ratio indicates obstruction during the initial phase of expiration. (6) Airway hyperresponsiveness to acetylcholine challenge: assessed by measuring inspiratory resistance. An increase in inspiratory resistance indicates enhanced airway hyperresponsiveness, increased sensitivity of airway smooth muscle to contractile stimulation, and airway narrowing. We performed *in vivo* measurements in living *Scgb1a1-DTR-GFP* mice on day 7 after DT injury, with PBS-treated mice as controls, to capture real-time pulmonary function (Extended Data Fig. 13m). Compared with the control group, the DT group showed a significant increase in FRC and significant decreases in PEF/FVC, MMEF/FVC, FEV100/FVC, and FEV75/FVC (Extended Data Fig. 13n). In addition, airway hyperresponsiveness was significantly increased in the DT group (Extended Data Fig. 13o). These data demonstrate that DT-induced Scgb1a1$^+$ cell ablation leads to airway remodeling, airway obstruction, and significant impairment of lung respiratory function, suggesting that structural airway remodeling contributes to the observed pulmonary function deficits in mice.

We also evaluated whether Scgb1a1$^+$ cell ablation affects pulmonary antibacterial defense. Previous studies have reported that club cells promote the clearance of *Pseudomonas aeruginosa* (*P. aeruginosa*) infection by secreting antimicrobial proteins (Sahu et al., *Sci Immunol* ,2023; Guan et al., *J Adv Res*, 2025). Therefore, we examined the efficiency of pulmonary *P. aeruginosa* clearance in the DT model. *Scgb1a1-DTR-GFP* mice were first subjected to DT injury (PBS-treated as controls). Seven days later, mice were infected via the trachea with *P. aeruginosa* at a dose of 2×10^5 Colony-Forming Unit (CFU)/g. After 24 hours, lungs were collected, homogenized, and plated on *P. aeruginosa* selective medium. Following 12-16 hours of culture, samples were analyzed (Extended Data Fig. 13p). Photographs and statistical analysis of single colonies showed that the CFU count in the DT group was significantly higher than that in the control group, indicating that Scgb1a1$^+$ cell ablation severely impaired *P. aeruginosa* clearance (Extended Data Fig. 13q,r).

These data further demonstrate that DT-induced ablation of Scgb1a1^{+} cells impairs pathogen clearance, leading to significant alterations in lung function.

Having established that club cell ablation causes structural and functional deficits, we next asked whether blocking AT2-to-club cell regeneration affects the recovery of these parameters. We found that specific knockout of either *Rbpj* or *Itgb1* in AT2 cells significantly inhibited AT2 contribution to club cells (Figs. 5j-m,7q-t). To determine whether partial blockade of club cell regeneration delays the restoration of lung tissue structure and function, we performed comparative analyses of the pulmonary parameters described above in both knockout models. We first used *Sftpc-CreER;R26-tdT;Scgb1a1-DTR-GFP;Rbpj*$^{flox/flox}$ mice (knockout group) to delete the *Rbpj* gene specifically in AT2 cells, with *Sftpc-CreER;R26-tdT;Scgb1a1-DTR-GFP;Rbpj*$^{flox/+}$ mice as controls. Lung function was assessed on day 28 after DT injury (Extended Data Fig. 13s). Compared with the control group, the knockout group exhibited significantly higher FRC, significantly lower PEF/FVC, MMEF/FVC, FEV100/FVC, and FEV75/FVC, and significantly enhanced airway hyperresponsiveness (Fig. 5n-p and Extended Data Fig. 13t). In addition, *P. aeruginosa* infection experiments revealed significantly higher CFU counts in the experimental group compared with controls (Fig. 5q-s). These pulmonary function data indicate that blocking club cell regeneration significantly delays functional recovery. Consistent with these functional deficits, histological analysis revealed structural abnormalities. Immunostaining and statistical analysis of lung sections showed that the peribronchiolar mesenchymal layer was significantly thicker in the knockout group than in the control group (Extended Data Fig. 13u,v). H&E staining and quantification also revealed significantly increased bronchial wall thickness in the knockout group (Extended Data Fig. 13w,x). These histological findings suggest that impaired club cell regeneration leads to persistent activation of the peribronchiolar mesenchymal layer, thereby slowing its return to baseline. We next evaluated the impact of *Itgb1* knockout on lung tissue structure and function. Experimental mice were *Sftpc-CreER;R26-tdT;Scgb1a1-DTR-GFP;Itgb1*$^{flox/flox}$, and control mice were *Sftpc-CreER;R26-tdT;Scgb1a1-DTR-GFP;Itgb1*$^{flox/+}$. Mice were subjected to DT injury and analyzed on day 28 (Extended Data Fig. 18o). Lung function measurements showed that, compared with controls, the *Itgb1* knockout group had significantly higher FRC and airway hyperresponsiveness, and significantly lower PEF/FVC, MMEF/FVC, FEV100/FVC, and FEV75/FVC (Extended Data Fig. 18p,q). Histological assessment of lung sections also revealed that the peribronchiolar mesenchymal layer and bronchial wall thickness were significantly increased in the *Itgb1* knockout group compared with controls (Extended Data Fig. 18r-u). Moreover, *P. aeruginosa* clearance was significantly impaired in the *Itgb1* knockout group relative to controls (Extended Data Fig. 18v-x).

In summary, our findings demonstrate that club cell ablation leads to bronchial structural remodeling and pulmonary dysfunction, and that impaired club cell regeneration resulting from *Rbpj* and *Itgb1* knockout delays the recovery of bronchial structure and lung function. We have added these experimental data and discussion to the revised manuscript. For details, please refer to revised Figs. 5,7, Extended Data Figs. 13,15,18; Page 5, Paragraph 1; Page 15, Paragraph 2; Page 20, Paragraph 1 and Line 588 of the revised manuscript.

10. How far AT2-lineage derived cells migrate along bronchioles? Show images from different branches.

We thank the reviewer for raising this question. In our DT injury model (*Sftpc-CreER;R26-tdT;Scgb1a1-DTR-GFP* mice), tdT^{+} AT2-lineage-derived cells migrated into the injured

bronchiolar epithelium (Fig. 1). Similarly, in the naphthalene injury model (*Scgb1a1-CreER;Sftpc-DreER;R26-NR* and *Scgb1a1-CreER;Sftpc-DreER;R26-TLR* mice), ZsG$^+$ AT2-derived cells were also detected in the bronchiolar epithelium after injury (Figs. 2, 3). To assess how far these cells migrate along the bronchial tree, we performed immunostaining and panoramic imaging of lung sections at day 28 post-injury, covering different bronchial branches (Extended Data Fig. 3a,b and Fig. 1 to Reviewers). In the DT model, tdT$^+$ AT2-derived cells were widely distributed throughout bronchioles from proximal to distal regions (Extended Data Fig. 3a and Fig. 1a,b to Reviewers). Their spatial distribution was relatively uniform, and we did not detect any preferential migration toward specific bronchial branches. Large numbers of tdT$^+$ cells were present in terminal bronchioles adjacent to the BADJ, and they also appeared in more proximal, larger diameter bronchi. Quantification showed that at 28 days after DT injury, 71.21 ± 6.29% of the bronchial epithelium was populated by tdT$^+$ cell lineages (Extended Data Fig. 3b). The maximum migration distance of tdT$^+$ AT2-derived cells from the BADJ, measured along the airway lumen, was 3.12 ± 0.27 mm. (Fig. 1c to Reviewers). Similarly, in the naphthalene injury model, whole-mount immunofluorescence scanning images of *Scgb1a1-CreER;Sftpc-DreER;R26-NR* mouse lungs at day 28 post-injury revealed that ZsG$^+$ AT2-derived cells had also migrated and covered most of the bronchial epithelium (Fig. 1d,e to Reviewers). Their distribution was also uniform across different branches, with no obvious branch-selective preference. The maximum migration distance from the BADJ (measured along the airway lumen) in the naphthalene model was 2.76 ± 0.28 mm (Fig. 1f to Reviewers).

We speculate that the difference in maximum migration distance between the DT and naphthalene models may be related to the severity of tissue injury. Previous studies have shown that after naphthalene injury, some naphthalene-resistant Scgb1a1$^+$ cells survive (Reynolds et al., *Am J Pathol*, 2000). These cells are distributed near NE cells and the BADJ (i.e., BASCs) and can serve as reserve stem cells to participate in bronchial epithelial repair (Rawlins et al., *Cell Stem Cell*, 2009; Liu et al., *Nat Genet*, 2019). In contrast, the DT model ablates all Scgb1a1$^+$ cells, including resistant club cells and BASCs. This more severe injury may create an environment that promotes AT2-derived cell migration during bronchiolar repair. Additionally, the formation of "channel" structures in the DT model (but not in the naphthalene model) may further accelerate AT2 cell migration into the bronchioles. Collectively, out data demonstrate that after bronchial injury, AT2-lineage-derived cells can migrate into most bronchial branches. We have added these experimental data and discussion to the revised manuscript. Because our Extended Data Figures now total 20 after revision, we have included some of these data in the Figure to reviewers. These data can be considered for publication, along with review comments and response, at the reviewer and editor's discretion. For details, please refer to revised Figs. 1, 2,3 Extended Data Figs. 3 and 8, Fig. 1 to Reviewers; Page 21, Paragraph 1 of the revised manuscript.

11. In Fig-2I, the authors show Acetylated tubulin to identify ciliated cells. While this is a specific marker of ciliated cells, its not clear whether cilia belong to AT2-lineage derived cells? FOXJ1 would be a better marker to confirm AT2-labeled cells make ciliated cells.

Response: We thank the reviewer for this constructive suggestion on the ciliated cell marker. Acetylated tubulin is a well-established marker for ciliated cells due to its strong and specific labeling of the ciliary axoneme. We also agree with the reviewer that FOXJ1, as a master transcription factor for ciliated cell differentiation, provides more definitive evidence of cell identity.

First, we enlarged the ciliated cell image from the original Fig. 2l; this enlarged view (now Fig. 2m) shows more clearly than before that the cilia structures at the apical surface of ZsG^+ ciliated cells (indicated by white arrows in Fig. 2m). To directly address the reviewer's concern, we have added co-immunostaining for FOXJ1 on lung sections. Indeed, after DT or naphthalene injury, we detected a minimal number of AT2-derived cells expressing FOXJ1, confirming their differentiation into ciliated cells (Figs. 1l, 2j,n, 3j,m and Extended Data Fig. 2k). Quantitative analysis showed that in *Sftpc-CreER;R26-tdT;Scgb1a1-DTR-GFP* mice at 4 weeks post-DT injury, $FOXJ1^+$ cells accounted for 0.27 ± 0.07% of AT2-derived bronchiolar cells (Fig. 1l and Extended Data Fig. 2k). In *Scgb1a1-CreER;Sftpc-DreER;R26-NR* mice at 4 weeks after naphthalene injury, $FOXJ1^+$ cells represented 0.79 ± 0.13% of AT2-derived bronchiolar cells (Fig. 2j). In *Scgb1a1-CreER;Sftpc-DreER;R26-TLR* mice at 4 weeks after naphthalene injury, the proportion was 0.87 ± 0.14% (Fig. 3j). These new data are added to the revised manuscript. We thank the reviewer again for helping us strengthen this part of the study. For details, please refer to revised Figs. 1,2,3, Extended Data Fig. 2, Page 5, Line 129; Page 9, Line 236; Page 10, Line 281; and Page 21, Paragraph 2 of the revised manuscript.

12. How long does it take to fully replenish the lost club cells in bronchioles?

Response: We thank the reviewer for raising this question. In our study, we used both naphthalene and DT injury models to ablate club cells. To address the reviewer's question, we examined the regeneration kinetics of bronchiolar club cells after naphthalene and DT injury, respectively (Fig. 2 to Reviewers). First, adult mice were treated with naphthalene (corn oil as control), and lung samples were collected at multiple time points after injury, including days 3, 7, 14, 28, and months 3 and 6 (Fig. 2a to Reviewers). Immunostaining showed that $Scgb1a1^+$ club cells were rapidly depleted by day 3 after naphthalene injury, with only a few naphthalene-resistant club cells remaining. As repair progressed, increasing numbers of club cells became visible (Fig. 2b to Reviewers). Using the club cell density in control mouse bronchial epithelium as the steady-state baseline, we evaluated the recovery of club cells by comparing the density at different time points to that of controls. Club cell density was quantified as the number of club cells per 100 μm of bronchial epithelium. The densities in control mice and at days 3, 7, 14, 28, and months 3 and 6 after naphthalene injury were 10.36 ± 0.70, 0.33 ± 0.07, 1.35 ± 0.32, 3.43 ± 0.76, 6.13 ± 0.72, 8.40 ± 0.89, and 9.66 ± 0.70, respectively, indicating continuous club cell regeneration after injury (Fig. 2c to Reviewers). Further statistical comparison showed that club cell densities at days 3, 7, 14, 28, and month 3 were significantly different from controls, and the difference was only lost at month 6, suggesting that the repair process is prolonged (Fig. 2c to Reviewers).

We also evaluated club cell regeneration kinetics in the DT model. Lung samples from *Scgb1a1-DTR-GFP* mice were collected at days 3, 7, 14, 28, and months 3 and 6 after DT injury, with PBS treatment as control (Fig. 2d to Reviewers). Immunostaining showed that GFP^+ club cells were efficiently ablated by day 3 post-DT, and GFP signal gradually reappeared as repair progressed (Fig. 2e to Reviewers). Quantification of club cell density showed that in steady-state controls and at days 3, 7, 14, 28, and months 3 and 6 post-DT, the densities were 10.16 ± 0.54, 0.00 ± 0.00, 0.35 ± 0.17, 1.54 ± 0.27, 3.41 ± 0.48, 4.93 ± 1.03, and 5.95 ± 1.07, respectively, indicating ongoing regeneration of GFP^+ club cells (Fig. 2f to Reviewers). However, further statistical analysis revealed that even at 6 months after DT injury, GFP^+ club cell density remained significantly different from controls, suggesting slower recovery in the DT model compared to the naphthalene model (Fig. 2f to Reviewers).

The distinct rates of club cell recovery between the two injury models likely arise from differences in the extent of epithelial damage. Naphthalene injury spares a subpopulation of Scgb1a1^{+} cells that are resistant to ablation, including naphthalene-resistant club cells and BASCs. Indeed, we observed a small number of residual Scgb1a1^{+} cells in the bronchial epithelium at day 3 after naphthalene injury (Fig. 2b to Reviewers). These surviving cells have been previously characterized as reserve stem cells capable of driving bronchial epithelial repair (Reynolds et al., *Am J Pathol*, 2000; Rawlins et al., *Cell Stem Cell*, 2009; Liu et al., *Nat Genet*, 2019). In contrast, the DT model ablates virtually all Scgb1a1^{+} cells, including resistant club cells and BASCs. This more severe injury likely delays club cell regeneration. Further studies are needed to elucidate the microenvironmental differences between these two injury models. Collectively, these data show that in the naphthalene injury model, club cells take approximately 6 months to fully recover, whereas in the DT model, even longer time may be required. We have added these experimental data and discussion to the revised manuscript. Because our Extended Data Figures now total 20 after revision, we have included these data in the Figure to reviewers. These data can be considered for publication, along with review comments and response, at the reviewer and editor's discretion. For details, please refer to Fig. 2 to Reviewers, Page 21, Paragraph 1 of the revised manuscript.

Minor comments:

1. In Fig-5u and in text, the authors referred the process of conversion of AT2 cells into club cells as "Differentiation". Based on classical definition, this should be called "Transdifferentiation". Authors should review the nomenclature and change that accordingly.

Response: We thank the reviewer for this important terminological clarification. We fully agree that the conversion of AT2 cells into club cells represents transdifferentiation rather than differentiation (differentiation typically refers to the maturation of a progenitor cell into a committed cell type). Accordingly, we have revised the nomenclature throughout the manuscript, replacing "differentiation" with "transdifferentiation" where the AT2-to-club cell transition is described (e.g., in the Results section, Fig. 6i,w, and the Discussion). We have also carefully reviewed the rest of the text to ensure consistent and accurate use of these terms. We thank the reviewer for helping us improve the precision of our language. For details, please refer to revised Fig. 6, Page 2, Line 26 and 35; Page 4, Line 80, 86, 98, 104; Page 5, Line 127; Page 6, Line165; Page 7, Line 170; Page 9 ,Line236, 250, 255; Page 10, Line259; Page 12, Line 329; Page 13, Line 360; Page 16, Line 443 445; Page 17, 485; Page 18, Line 502; Page 20, Line 581, 584, 585; Page 21, Line 614; Page 22, Line 619, 622, 627, 634, 644, 647; Page 23, Line 649, 635 of the revised manuscript.

References

Basil, M.C., Cardenas-Diaz, F.L., Kathiriya, J.J., Morley, M.P., Carl, J., Brumwell, A.N., Katzen, J., Slovik, K.J., Babu, A., Zhou, S., et al. (2022). Human distal airways contain a multipotent secretory cell that can regenerate alveoli. Nature. 10.1038/s41586-022-04552-0.

Beppu, A.K., Zhao, J., Yao, C., Carraro, G., Israely, E., Coelho, A.L., Drake, K., Hogaboam, C.M., Parks, W.C., Kolls, J.K., and Stripp, B.R. (2023). Epithelial plasticity and innate immune activation promote lung tissue remodeling following respiratory viral infection. Nat Commun 14, 5814. 10.1038/s41467-023-41387-3.

Blackburn, J.B., Li, N.F., Bartlett, N.W., and Richmond, B.W. (2023). An update in club cell biology and its potential relevance to chronic obstructive pulmonary disease. Am J Physiol Lung Cell Mol Physiol 324, L652-L665. 10.1152/ajplung.00192.2022.

Guan, J., Yao, W., Zhang, L., Xie, H., Li, L., Wen, Y., Chen, H., Huang, Y., Wen, J., Ou, C., et al. (2025). Contribution of Pseudomonas aeruginosa - mediated club cell necroptosis to the bias of type 17 inflammation and steroid insensitivity in asthma. J Adv Res 75, 137-149. 10.1016/j.jare.2024.10.020.

Habermann, A.C., Gutierrez, A.J., Bui, L.T., Yahn, S.L., Winters, N.I., Calvi, C.L., Peter, L., Chung, M.I., Taylor, C.J., Jetter, C., et al. (2020). Single-cell RNA sequencing reveals profibrotic roles of distinct epithelial and mesenchymal lineages in pulmonary fibrosis. Sci Adv 6, eaba1972. 10.1126/sciadv.aba1972.

Hao, D., Liu, Y., Li, L., Stripp, B.R., and Chen, H. (2026). Immunological and regenerative properties of lung stem cells. Physiol Rev 106, 485-527. 10.1152/physrev.00056.2024.

Kadur Lakshminarasimha Murthy, P., Sontake, V., Tata, A., Kobayashi, Y., Macadlo, L., Okuda, K., Conchola, A.S., Nakano, S., Gregory, S., Miller, L.A., et al. (2022). Human distal lung maps and lineage hierarchies reveal a bipotent progenitor. Nature. 10.1038/s41586-022-04541-3.

Kim, C.F., Jackson, E.L., Woolfenden, A.E., Lawrence, S., Babar, I., Vogel, S., Crowley, D., Bronson, R.T., and Jacks, T. (2005). Identification of bronchioalveolar stem cells in normal lung and lung cancer. Cell 121, 823-835. 10.1016/j.cell.2005.03.032.

Kobayashi, Y., Tata, A., Konkimalla, A., Katsura, H., Lee, R.F., Ou, J., Banovich, N.E., Kropski, J.A., and Tata, P.R. (2020). Persistence of a regeneration-associated, transitional alveolar epithelial cell state in pulmonary fibrosis. Nat Cell Biol 22, 934-946. 10.1038/s41556-020-0542-8.

Kumar, Pooja A., Hu, Y., Yamamoto, Y., Hoe, Neo B., Wei, Tay S., Mu, D., Sun, Y., Joo, Lim S., Dagher, R., Zielonka, Elisabeth M., et al. (2011). Distal Airway Stem Cells Yield Alveoli In Vitro and during Lung Regeneration following H1N1 Influenza Infection. Cell 147, 525-538. 10.1016/j.cell.2011.10.001.

Liu, K., Meng, X., Liu, Z., Tang, M., Lv, Z., Huang, X., Jin, H., Han, X., Liu, X., Pu, W., et al. (2024). Tracing the origin of alveolar stem cells in lung repair and regeneration. Cell. 10.1016/j.cell.2024.03.010.

Liu, Q., Liu, K., Cui, G., Huang, X., Yao, S., Guo, W., Qin, Z., Li, Y., Yang, R., Pu, W., et al. (2019). Lung regeneration by multipotent stem cells residing at the bronchioalveolar-duct junction. Nature Genetics. 10.1038/s41588-019-0346-6.

Li, X., Lian, J., and Lu, H. (2025). The role of SPP1(+)TAMs in cancer: Impact on patient prognosis and future therapeutic targets. Int J Cancer 157, 1763-1771. 10.1002/ijc.70018.

Lv, Z., Liu, Z., Liu, K., Lin, X., Pu, W., Li, Y., Zhao, H., Xi, Y., Sui, P., Vaughan, A.E., et al. (2024).

Alveolar regeneration by airway secretory-cell-derived p63(+) progenitors. Cell Stem Cell. 10.1016/j.stem.2024.08.005.

Pang, X., Gong, K., Zhang, X., Wu, S., Cui, Y., and Qian, B.Z. (2019). Osteopontin as a multifaceted driver of bone metastasis and drug resistance. Pharmacol Res 144, 235-244. 10.1016/j.phrs.2019.04.030.

Pezet, M.G., Torres, J.A., Thimraj, T.A., Matkovic, I., Schrode, N., Murray, J.W., Saqi, A., Beaumont, K.G., and Snoeck, H.W. (2025). Human respiratory airway progenitors derived from pluripotent cells generate alveolar epithelial cells and model pulmonary fibrosis. Nat Biotechnol. 10.1038/s41587-025-02569-0.

Rawlins, E.L., Okubo, T., Xue, Y., Brass, D.M., Auten, R.L., Hasegawa, H., Wang, F., and Hogan, B.L. (2009). The role of Scgb1a1+ Clara cells in the long-term maintenance and repair of lung airway, but not alveolar, epithelium. Cell Stem Cell 4, 525-534. 10.1016/j.stem.2009.04.002.

Reynolds, S.D., Giangreco, A., Power, J.H.T., and Stripp, B.R. (2000). Neuroepithelial Bodies of Pulmonary Airways Serve as a Reservoir of Progenitor Cells Capable of Epithelial Regeneration. The American Journal of Pathology 156, 269-278. 10.1016/s0002-9440(10)64727-x.

Sahu, S.K., Ozanturk, A.N., Kulkarni, D.H., Ma, L., Barve, R.A., Dannull, L., Lu, A., Starick, M., McPhatter, J., Garnica, L., et al. (2023). Lung epithelial cell-derived C3 protects against pneumonia-induced lung injury. Sci Immunol 8, eabp9547. 10.1126/sciimmunol.abp9547.

Salwig, I., Spitznagel, B., Vazquez-Armendariz, A.I., Khalooghi, K., Guenther, S., Herold, S., Szibor, M., and Braun, T. (2019). Bronchioalveolar stem cells are a main source for regeneration of distal lung epithelia in vivo. EMBO J 38. 10.15252/embj.2019102099.

Snippert, H.J., van der Flier, L.G., Sato, T., van Es, J.H., van den Born, M., Kroon-Veenboer, C., Barker, N., Klein, A.M., van Rheenen, J., Simons, B.D., and Clevers, H. (2010). Intestinal Crypt Homeostasis Results from Neutral Competition between Symmetrically Dividing Lgr5 Stem Cells. Cell 143, 134-144. 10.1016/j.cell.2010.09.016.

Strunz, M., Simon, L.M., Ansari, M., Kathiriya, J.J., Angelidis, I., Mayr, C.H., Tsidiridis, G., Lange, M., Mattner, L.F., Yee, M., et al. (2020). Alveolar regeneration through a Krt8+ transitional stem cell state that persists in human lung fibrosis. Nat Commun 11, 3559. 10.1038/s41467-020-17358-3.

Vaughan, A.E., Brumwell, A.N., Xi, Y., Gotts, J.E., Brownfield, D.G., Treutlein, B., Tan, K., Tan, V., Liu, F.C., Looney, M.R., et al. (2015). Lineage-negative progenitors mobilize to regenerate lung epithelium after major injury. Nature 517, 621-625. 10.1038/nature14112.

Yim, A., Smith, C., and Brown, A.M. (2022). Osteopontin/secreted phosphoprotein-1 harnesses glial-, immune-, and neuronal cell ligand-receptor interactions to sense and regulate acute and chronic neuroinflammation. Immunol Rev 311, 224-233. 10.1111/imr.13081.

Zuo, W., Zhang, T., Wu, D.Z., Guan, S.P., Liew, A.A., Yamamoto, Y., Wang, X., Lim, S.J., Vincent, M., Lessard, M., et al. (2015). p63(+)Krt5(+) distal airway stem cells are essential for lung regeneration. Nature 517, 616-620. 10.1038/nature13903.

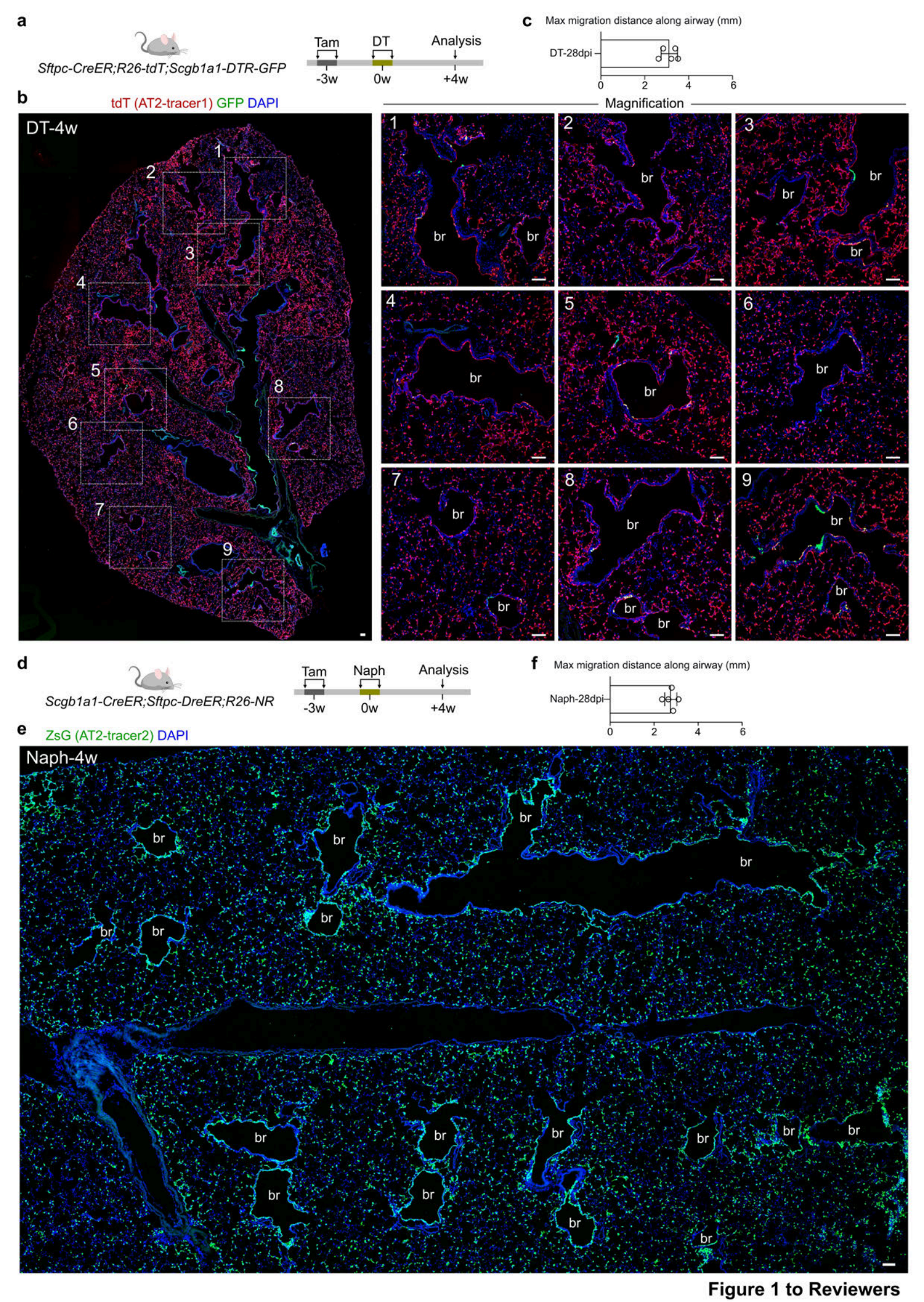


Figure 1 to Reviewers

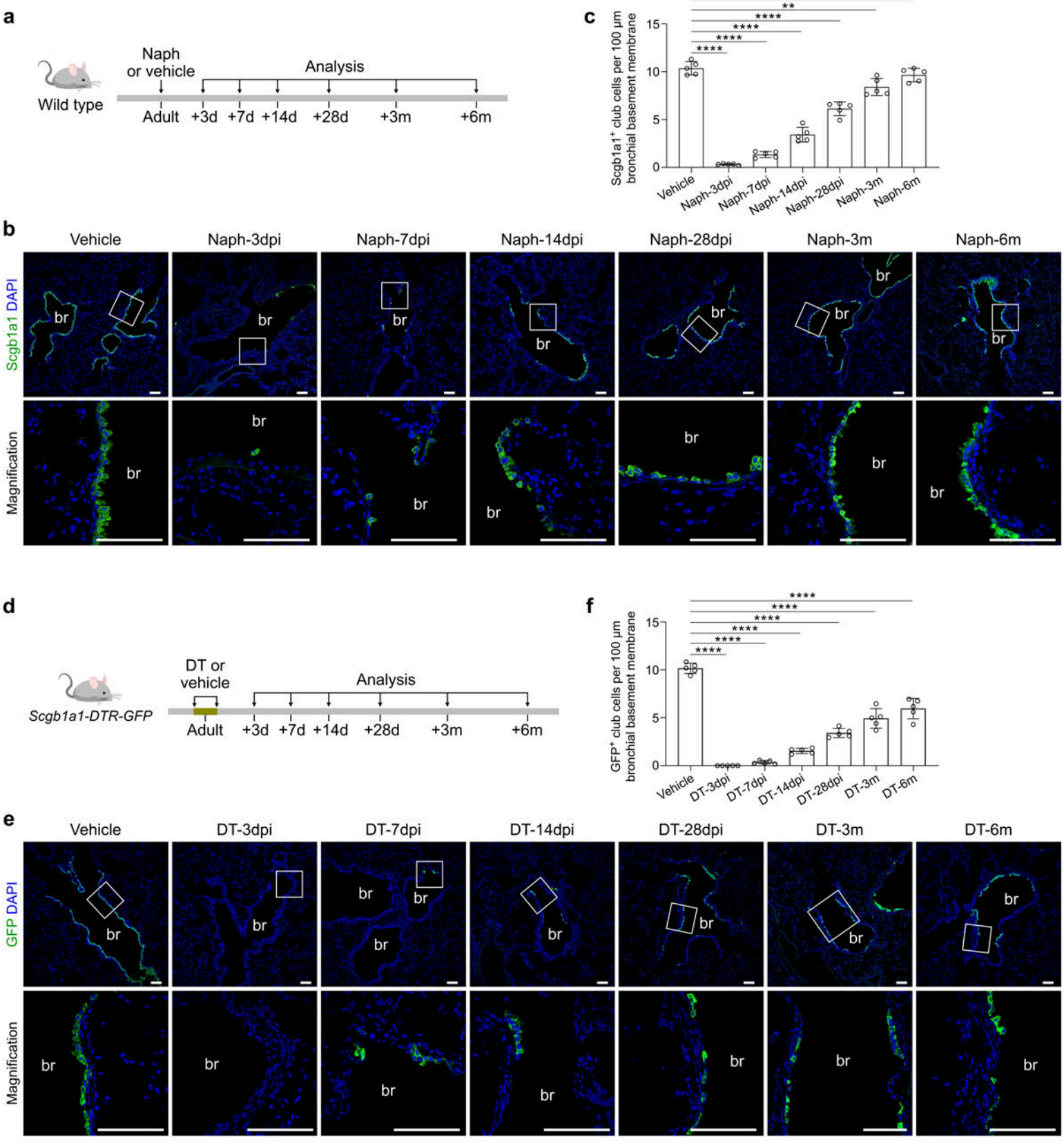


Figure 2 to Reviewers

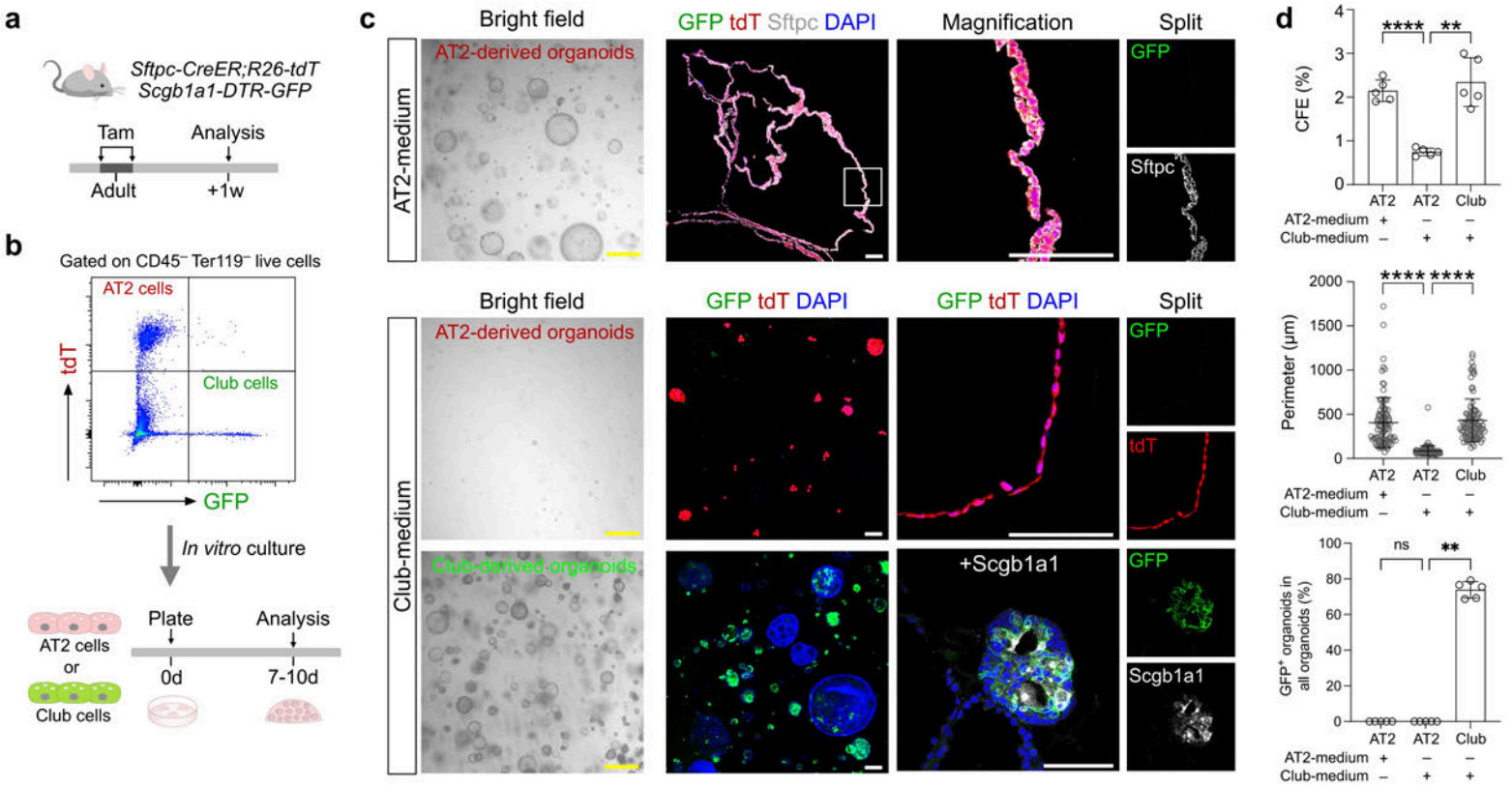


Figure 3 to Reviewers

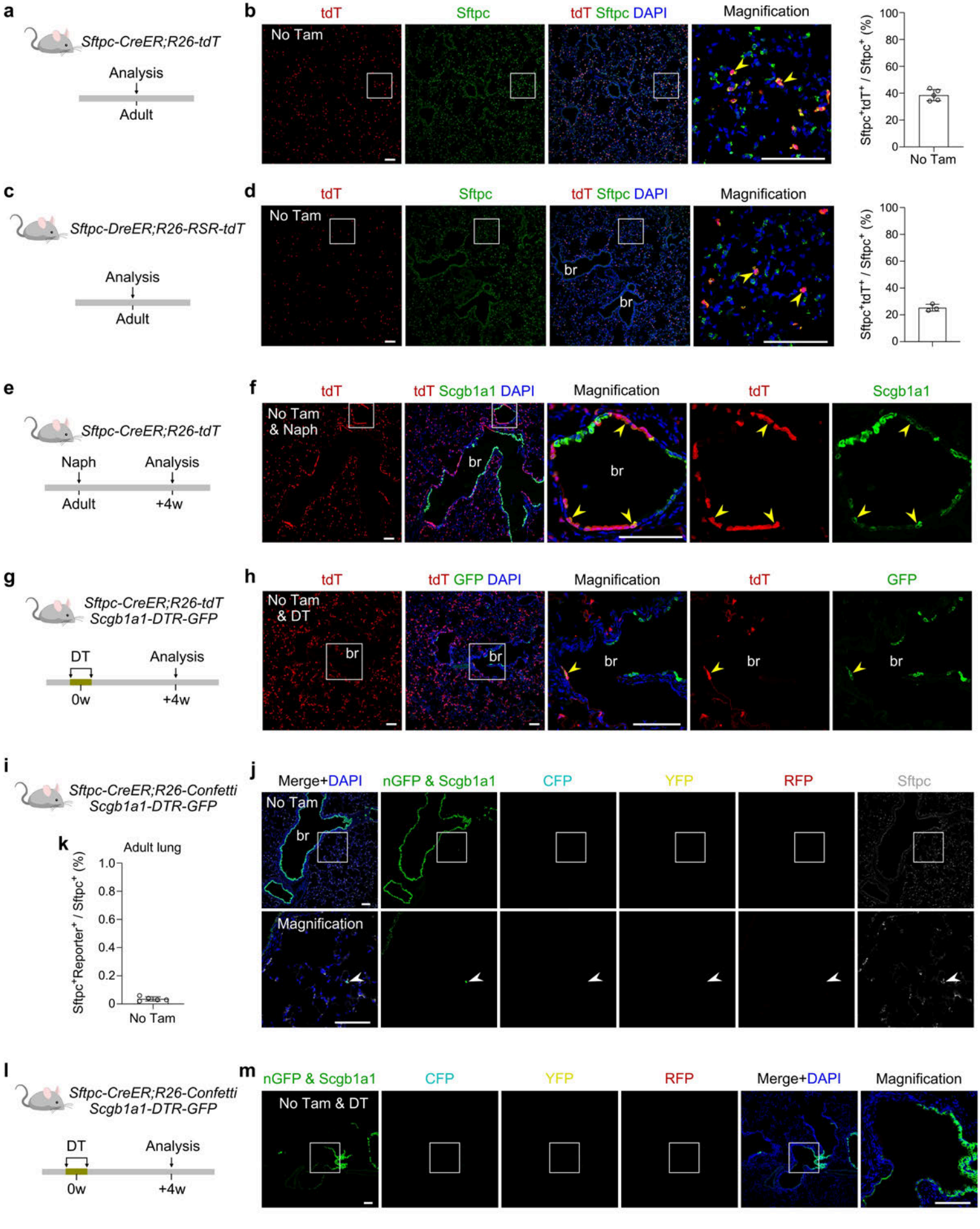


Figure 4 to Reviewers

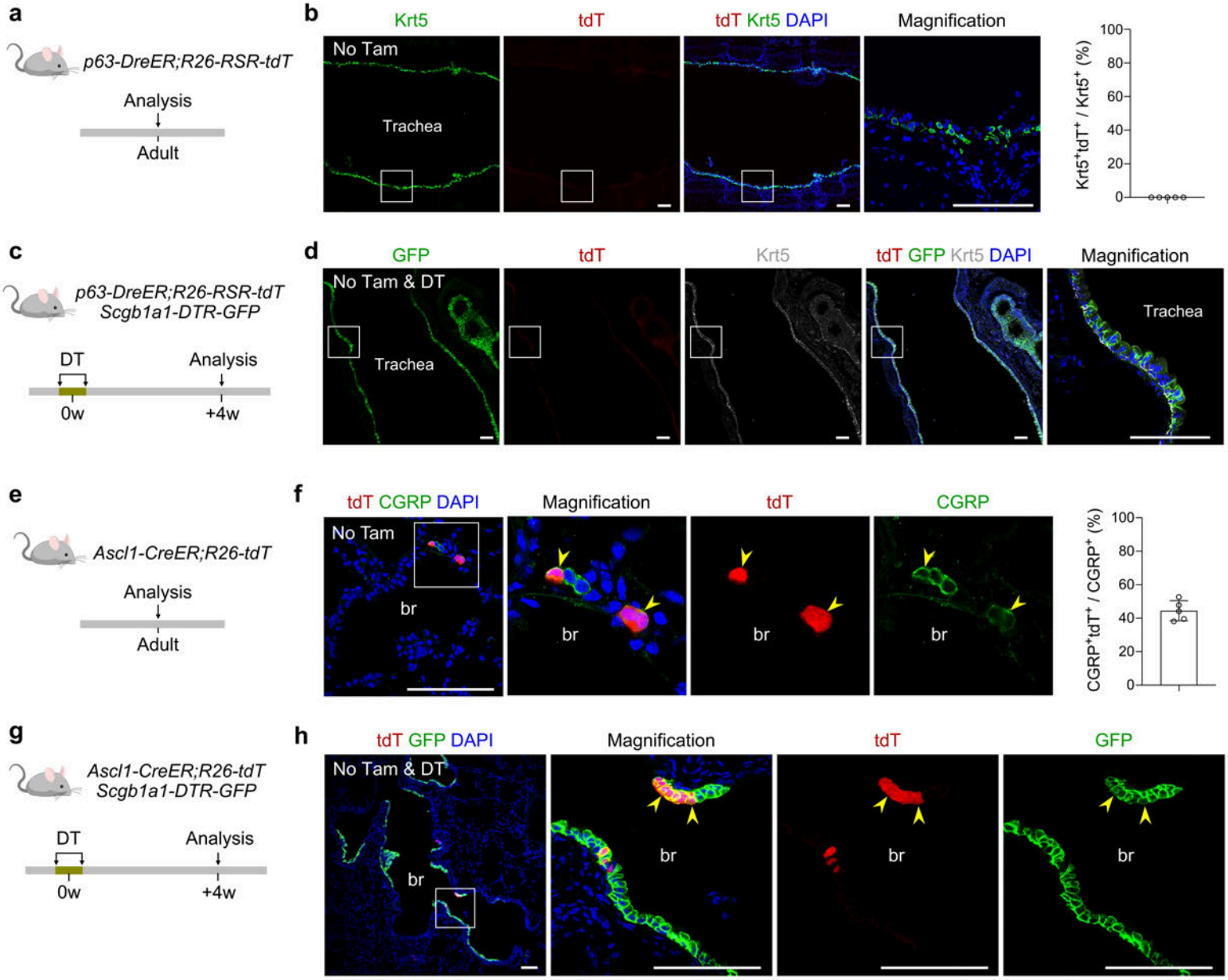


Figure 5 to Reviewers

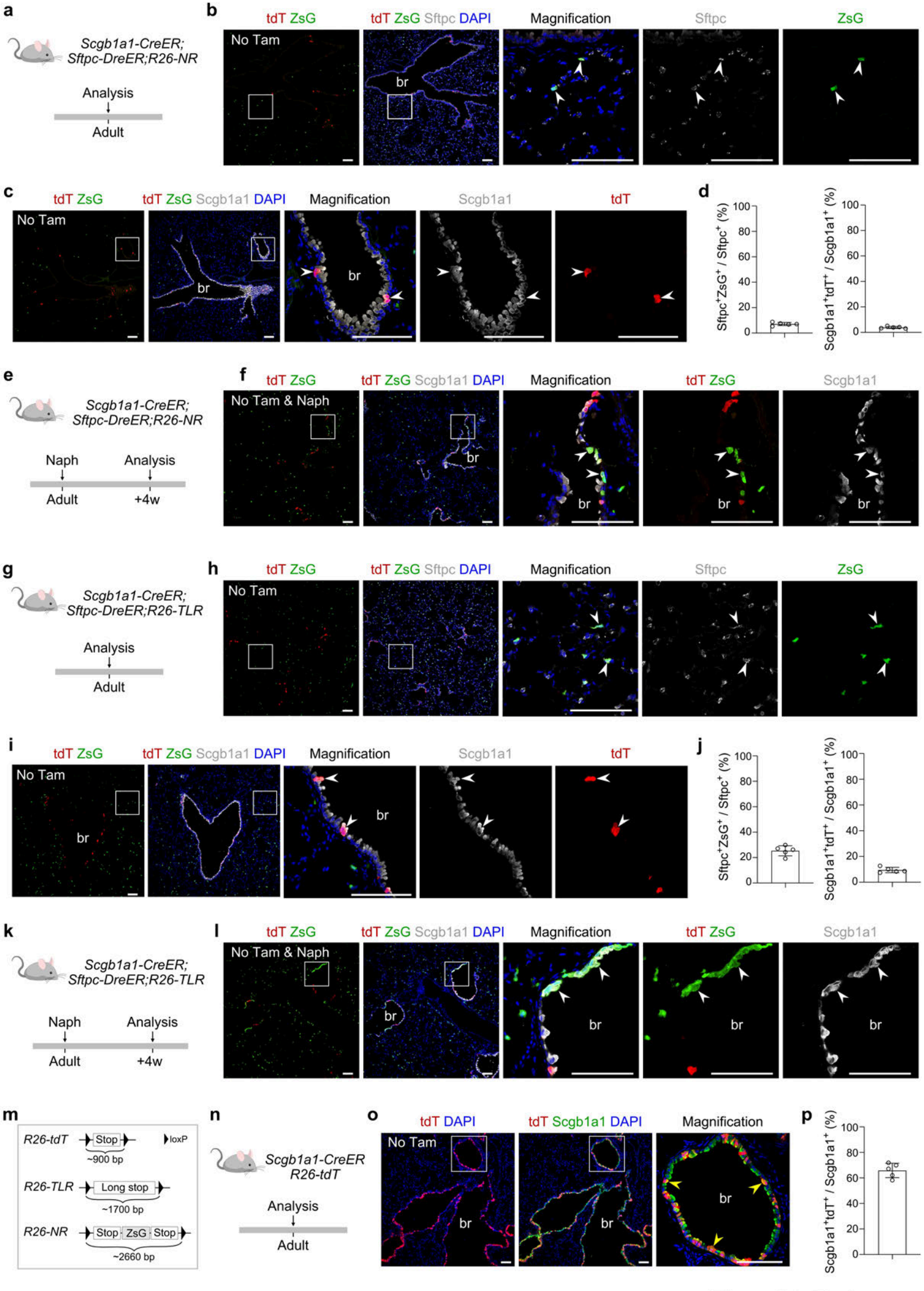


Figure 6 to Reviewers

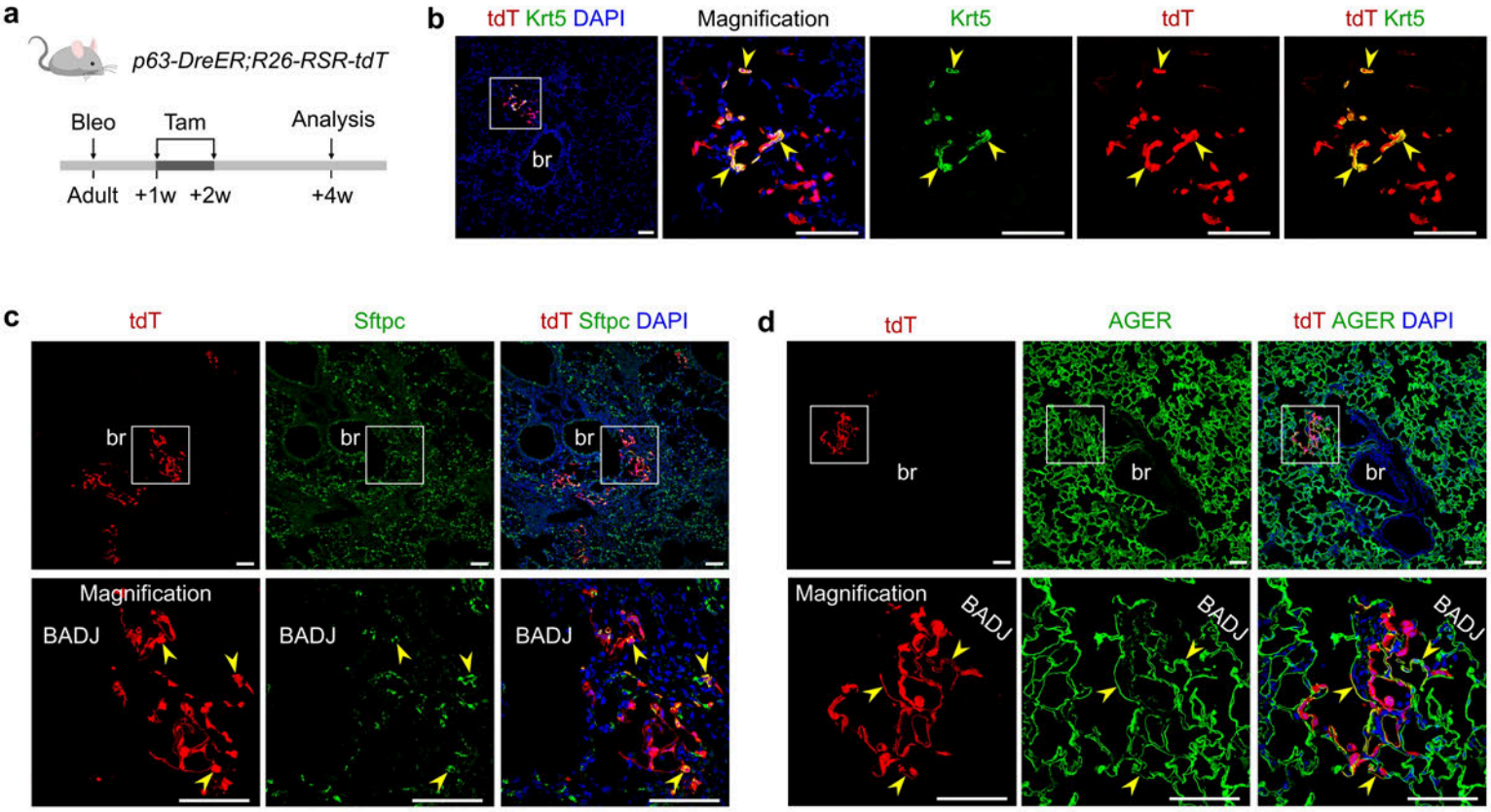


Figure 7 to Reviewers

Legends for Figure to Reviewers

Fig. 1 to Reviewers | AT2 cells migrate to bronchioles and contribute to bronchial epithelial repair following DT or naphthalene injury

a, A schematic diagram illustrating the experimental design. **b**, Whole-mount immunofluorescence scanning images of *Sftpc-CreER;R26-tdT;Scgb1a1-DTR-GFP* mice at day 28 after DT injury (left panel). Boxed regions of the lung sections are magnified in right panel. **c**, Quantification of the maximum migration distance from the BADJ along the airway. n = 5. Data are presented as mean ± SD. **d**, A schematic diagram illustrating the experimental design. **e**, Whole-mount immunofluorescence scanning images of *Scgb1a1-CreER;Sftpc-DreER;R26-NR* mouse lungs at day 28 after naphthalene injury. **f**, Quantification of the the maximum migration distance from the BADJ along the airway. n = 5. Data are presented as mean ± SD. DT, diphtheria toxin. br, bronchiole. Tam, Tamoxifen. Scale bars, 100 μm.

Fig. 2 to Reviewers | Club cells exhibit different recovery rates after naphthalene injury versus DT injury

a, A schematic diagram illustrating the experimental design. **b**, Immunostaining for Scgb1a1 on lung sections of wild type mice at different timepoints after naphthalene injury. **c**, Quantification of Scgb1a1$^+$ club cells per 100 μm of bronchiolar basement membrane at various timepoints after naphthalene or vehicle treatment in (**b**). n = 5 at each timepoint. $^{**}P = 0.0048$. $^{****}P < 0.0001$. ns, non-significant. **d**, A schematic diagram illustrating the experimental design. **e**, Immunostaining of GFP on lung sections of *Scgb1a1-DTR-GFP* mice at different timepoints after DT treatment. **f**, Quantification for GFP$^+$ club cells per 100 μm of bronchiolar basement membrane at various timepoints after DT or vehicle treatment in (**e**). n = 5 at each timepoint. $^{****}P < 0.0001$. DT, diphtheria toxin. br, bronchiole. Naph, naphthalene. Scale bars, 100 μm.

Fig. 3 to Reviewers | Club medium fails to induce AT2-to-club cell fate conversion

a, A schematic diagram illustrating the experimental design. **b**, FACS gating strategy and schematic diagram for organoid culture. **c**, Bright field image of organoids and immunostaining of whole organoid or organoid sections for tdT, GFP, Sftpc (upper panel), and Scgb1a1 (lower panel). **d**, Quantification of the CFE of organoids in (**c**) (top panel). n = 5. Data are presented as mean ± SD. $^{**}P = 0.0026$. $^{****}P < 0.0001$. Quantification of the perimeter of organoids in (**c**) (middle

panel). n = 5. Each individual dot represents one organoid. Data are presented as mean ± SD. ****$P < 0.0001$. Quantification of the percentage of organoids expressing GFP in (**c**) (bottom panel). n = 5. Data are presented as mean ± SD. **$P = 0.0079$. ns, non-significant. ****$P < 0.0001$. Tam, tamoxifen. CFE, colony-forming efficiency. Each image is representative of 5 individual biological samples. White scale bars, 100 μm. Yellow scale bars, 500 μm.

Fig. 4 to Reviewers | Leakiness in Sftpc-tracing mice (no tamoxifen) is reporter-dependent

a, A schematic diagram illustrating the experimental design. **b**, Immunostaining for tdT and Sftpc on lung sections of *Sftpc-CreER;R26-tdT* mice without Tam (left panel). Yellow arrowheads indicate tdT^+Sftpc^+ AT2 cells. Quantification of the percentage of $Sftpc^+$ AT2 cells expressing tdT without Tam (right panel) (n = 5). Data are presented as mean ± SD. **c**, A schematic diagram illustrating the experimental design. **d**, Immunostaining for tdT and Sftpc on lung sections of *Sftpc-DreER;R26-RSR-tdT* mice without Tam (left panel). Yellow arrowheads indicate tdT^+Sftpc^+ AT2 cells. Quantification of the percentage of $Sftpc^+$ AT2 cells expressing tdT without Tam (right panel) (n = 3). Data are presented as mean ± SD. **e**, A schematic diagram illustrating the experimental design. **f**, Immunostaining for tdT and Scgb1a1 on lung sections of *Sftpc-CreER;R26-tdT* mice after naphthalene treatment without Tam. Yellow arrowheads indicate $tdT^+Scgb1a1^+$ club cells. **g**, A schematic diagram illustrating the experimental design. **h**, Immunostaining of tdT and GFP on lung sections of *Sftpc-CreER;R26-tdT;Scgb1a1-DTR-GFP* mice after DT treatment without Tam. Yellow arrowheads indicate $tdT^+Scgb1a1^+$ club cells. **i**, A schematic diagram illustrating the experimental design. **j**, Immunostaining for RFP, GFP (Scgb1a1), CFP, YFP, and Sftpc on lung sections of *Sftpc-CreER;R26-Confetti;Scgb1a1-DTR-GFP* mice without Tam. White arrowheads indicate $nGFP^+Sftpc^+$ AT2 cells. **k**, Quantification of the percentage of $Sftpc^+$ AT2 cells expressing reporters without Tam (n = 5). Data are presented as mean ± SD. **l**, A schematic diagram illustrating the experimental design. **m**, Immunostaining for RFP, GFP (Scgb1a1), CFP, YFP, and Sftpc on lung sections of *Sftpc-CreER;R26-Confetti;Scgb1a1-DTR-GFP* mice after DT treatment without Tam. DT, diphtheria toxin. br, bronchiole. Tam, Tamoxifen. Naph, naphthalene. Scale bars, 100 μm.

Fig. 5 to Reviewers | Leakiness assessment in *p63-DreER* and *Ascl1-CreER* mice without tamoxifen

a, A schematic diagram illustrating the experimental design. **b**, Immunostaining for tdT and Krt5 on lung sections of *p63-DreER;R26-RSR-tdT* mice without Tam treatment (left panel). Quantification of the percentage of $Krt5^+$ basal cells expressing tdT without Tam treatment (right panel) (n = 5). Data are presented as mean ± SD. **c**, A schematic diagram illustrating the experimental design. **d**, Immunostaining for tdT, GFP, and Krt5 on lung sections of *p63-DreER;R26-RSR-tdT;Scgb1a1-DTR-GFP* mice after DT treatment without Tam. **e**, A schematic diagram illustrating the experimental design. **f**, Immunostaining for tdT and CGRP on lung sections of *Ascl1-CreER;R26-tdT* mice without Tam (left panel). Yellow arrowheads indicate tdT^+CGRP^+ cells. Quantification of the percentage of $CGRP^+$ expressing tdT without Tam (right panel) (n = 5). Data are presented as mean ± SD. **g**, A schematic diagram illustrating the experimental design. **h**, Immunostaining for tdT and GFP on lung sections of *p63-DreER;R26-RSR-tdT;Scgb1a1-DTR-GFP* mice after DT treatment without Tam. Yellow arrowheads indicate tdT^+GFP^+ club cells. DT, diphtheria toxin. br, bronchiole. Tam, Tamoxifen. Each image is representative of 5 individual biological samples. Scale bars, 100 μm.

Fig. 6 to Reviewers | Leakiness in Scgb1a1-tracing mice (no tamoxifen) is reporter-dependent
a, A schematic diagram illustrating the experimental design. **b,c**, Immunostaining for tdT, ZsG, Sftpc (**b**) or Scgb1a1 (**c**) on lung sections of *Scgb1a1-CreER;Sftpc-DreER;R26-NR* mice without Tam. White arrowheads indicate ZsG^+Sftpc^+ AT2 cells (**b**). White arrowheads indicate $tdT^+Scgb1a1^+$ club cells (**c**). **d**, Quantification of the percentage of $Sftpc^+$ AT2 cells expressing ZsG (left panel) or $Scgb1a1^+$ club cells expressing tdT (right panel) (n = 5). Data are presented as mean ± SD. **e**, A schematic diagram illustrating the experimental design. **f**, Immunostaining for tdT, ZsG, and Scgb1a1 on lung sections of *Scgb1a1-CreER;Sftpc-DreER;R26-NR* mice at 4 weeks after naphthalene treatment without Tam treatment. White arrowheads indicate $ZsG^+Scgb1a1^+$ club cells. **g**, A schematic diagram illustrating the experimental design. **h,i**, Immunostaining for tdT, ZsG, Sftpc (**h**) or Scgb1a1 (**i**) on lung sections of *Scgb1a1-CreER;Sftpc-DreER;R26-TLR* mice without Tam. White arrowheads indicate ZsG^+Sftpc^+ AT2 cells (**h**) or $tdT^+Scgb1a1^+$ club cells (**i**). **j**, Quantification of the percentage of $Sftpc^+$ AT2 cells expressing ZsG (left panel) or $Scgb1a1^+$ club cells expressing tdT (right panel) in (**h**) and (**i**) (n = 5). Data are presented as mean ± SD. **k**, A schematic diagram illustrating the experimental design. **l**, Immunostaining for tdT, ZsG and Scgb1a1 on lung sections of *Scgb1a1-CreER;Sftpc-DreER;R26-TLR* mice at 4weeks after

naphthalene treatment without Tam. White arrowheads indicate $tdT^{-}ZsG^{+}Scgb1a1^{+}$ club cells. **m**, Comparison of the stop sequence length in different reporters including *R26-tdT*, *R26-TLR* and *R26-NR*. **n**, A schematic diagram illustrating the experimental design. **o**, Immunostaining for tdT and Scgb1a1 on lung sections of *Scgb1a1-CreER;R26-tdT* mice without Tam. Yellow arrowheads indicate $tdT^{+}Scgb1a1^{+}$ club cells. **p**, Quantification of the percentage of $Scgb1a1^{+}$ club cells expressing tdT in (**o**) (n = 5). Data are presented as mean ± SD. Naph, naphthalene. br, bronchiole. Tam, tamoxifen. Each image is representative of 5 individual biological samples. Scale bars, 100 μm.

Fig. 7 to Reviewers | *p63-DreER* mice trace injury-emerging $p63^{+}$ transient cells that differentiate into alveolar epithelium post-bleomycin

a, A schematic diagram illustrating the experimental design. **b-d**, Immunostaining for tdT and Krt5 (**b**), Sftpc (**c**) or AGER (**d**) on lung sections of *p63-DreER;R26-RSR-tdT* mice after bleomycin and tamoxifen treatment. Yellow arrowheads indicate $tdT^{+}Krt5^{+}$ cells (**b**), $tdT^{+}Sftpc^{+}$ cells (**c**) or $tdT^{+}AGER^{+}$ AT1 cells (**d**). Tam, tamoxifen. Bleo, Bleomycin. Each image is representative of 5 individual biological samples. Scale bars, 100 μm.

Fig. 8 to Reviewers | No AT1 cells are present in bronchial epithelium of uninjured or aged mice

a, A schematic diagram illustrating the experimental design. **b**, Immunostaining for tdT, GFP, AGER and T1a on lung sections of uninjured or aged *Sftpc-CreER;R26-tdT;Scgb1a1-DTR-GFP* mice. White arrowheads indicate $GFP^{+}AGER^{-}$ or $GFP^{+}T1a^{-}$ cells. **c**, Quantification of the number of $AGER^{+}$ or $T1a^{+}$ AT1 cells in bronchioles of uninjured lung and older lung in (**b**) (n = 5). Data are presented as mean ± SD. **d**, A schematic diagram illustrating the experimental design. **e**, Immunostaining for tdT, ZsG, AGER, and T1a on lung sections of uninjured or aged *Scgb1a1-CreER;Sftpc-DreER;R26-NR* mice. White arrowheads indicate $tdT^{+}AGER^{-}$ or $tdT^{+}T1a^{-}$ cells. **f**, Quantification of the number of $AGER^{+}$ or $T1a^{+}$ AT1 cells in bronchioles of uninjured lung and older lung in (**e**) (n = 5). Data are presented as mean ± SD. **g**, A schematic diagram illustrating the experimental design. **h**, Immunostaining of tdT, ZsG, AGER, and T1a on lung sections of uninjured or aged *Scgb1a1-CreER;Sftpc-DreER;R26-TLR* mice. White arrowheads indicate $ZsG^{+}AGER^{-}$ or $ZsG^{+}T1a^{-}$ cells. **i**, Quantification of the number of $AGER^{+}$ or $T1a^{+}$ AT1 cells in

bronchioles of uninjured lung and older lung in (**h**) (n = 5). Data are presented as mean ± SD. Tam, Tamoxifen. br, bronchiole. Each image is representative of 5 individual biological samples. White scale bars, 100 μm.

Response Letter to Reviewers

We sincerely thank the reviewers for their valuable time and insightful comments. Their constructive suggestions have greatly helped us enhance the quality of our manuscript. Below, we provide point-by-point responses to their comments. The reviewers' original remarks are in black text, and our responses follow in blue. The references cited in the response, the figures to reviewers, and their legends are listed at the end of this letter.

Referees' comments:
Referee #1 (Remarks to the Author):

In the reviewed manuscript, Liu et al. demonstrate that AT2 cells can migrate to the bronchioles and transdifferentiate into club cells, ciliated cells, and AT1 cells, using multiple lineage-tracing approaches across different injury models. To investigate the regulatory mechanisms governing AT2 cell transdifferentiation, single-cell sequencing was performed, revealing a transient cell population characterised by high Cldn4 expression between club and AT2 cells. Further analyses indicated that Notch signalling is activated during this transdifferentiation process, and that inhibition of the Notch pathway blocks AT2 cell fate conversion. In addition, ciliated cells were shown to express the Notch ligands Jag1/2, whereas AT2 cells express the corresponding receptors during this process. Finally, the authors propose that immune cells secrete Spp1, which binds to Itgb1 on AT2 cells and promotes their migration towards the bronchioles.
Although the study presents an interesting concept, the current evidence remains insufficient to fully support several key conclusions:
Author's Response: We sincerely thank the reviewer for their recognition of our work and for the constructive comments. To address the concerns regarding the conceptual advance, we have now performed additional experiments and included new data that further strengthen the evidence supporting the transdifferentiation of AT2 cells into club cells after bronchiolar injury. We believe that with these revisions, the revised manuscript provides a more solid conceptual advance in the field of lung regeneration.

1. In this manuscript, most immunostaining used to quantify the proportions of AT2 and club cells relies on single-marker staining. However, as noted by the authors, BASCs located at the BADJ co-express both AT2 and club cell markers and can differentiate into club cells following injury. Therefore, double-marker staining is essential to ensure that lineage-labelled cells are accurately identified as bona fide AT2 or club cells. A similar concern applies to the organoid culture experiments.
Authors' Response: We thank the reviewer for raising this important point. Previous studies have demonstrated that BASCs, located at the bronchioalveolar duct junctions, are characterized by the co-expression of the club cell marker Scgb1a1 and the AT2 cell marker Sftpc (Kim et al., *Cell*, 2005; Liu et al., *Nat Genet*, 2019; Salwig et al., *EMBO J*, 2019). In our study, we aimed to show that alveolar AT2 cells can transdifferentiate into bronchiolar club cells following airway injury. As the reviewer correctly noted, our initial quantification of AT2 and club cell proportions relied on

single-marker staining, which indeed does not permit definitive cell-type identification, especially given the existence of BASCs. As suggested by the reviewer, we have now incorporated double-marker immunostaining in the revised manuscript.

In our *Scgb1a1-DTR-GFP* mice, Scgb1a1$^+$ cells express both DTR and the GFP reporter; thus, GFP expression denotes Scgb1a1$^+$ cells, and DT administration efficiently ablates the GFP$^+$Scgb1a1$^+$ cells (Extended Data Fig. 1l-q). Our previous data showed that, in *Sftpc-CreER;R26-tdT;Scgb1a1-DTR-GFP* mice treated with tamoxifen to label AT2 cells with tdT and then challenged with DT, the bronchiolar epithelium was repopulated by GFP$^+$ cells that were also tdT$^+$ after a 4-week repair period (Fig. 1i). To validate whether the GFP reporter faithfully reflects Scgb1a1 expression, we first performed immunostaining for tdT, GFP, and Scgb1a1 on lung sections, confirming that these tdT$^+$GFP$^+$ cells co-expressed Scgb1a1, thus proving that GFP inserted downstream of the *Scgb1a1* promoter faithfully reports Scgb1a1 expression (Extended Data Fig. 2a,b). We then used GFP as a surrogate for Scgb1a1 and performed double staining together with the AT2 markers Sftpc or Lamp3. Immunostaining revealed that the vast majority of bronchiolar tdT$^+$GFP$^+$ cells did not express Sftpc or Lamp3 (Extended Data Fig. 2c,d). Quantification based on double-marker immunostaining further showed that, among the tdT$^+$ cells that had migrated to the bronchioles, 38.18 ± 4.55% were GFP$^+$Sftpc$^-$ club cells and 14.61 ± 2.62% were GFP$^-$Sftpc$^+$ AT2 cells, demonstrating that these cells are *bona fide* AT2 or club cells (Fig. 1l). In addition, our quantification based on double-marker immunostaining indicated that 77.42 ± 4.71% of the newly formed bronchiolar GFP$^+$Sftpc$^-$ club cells were tdT$^+$, revealing that AT2 cells contributed to the majority of club cell regeneration at the terminal bronchioles (Fig. 1k). Beyond the DT model, we also observed that AT2 cells can contribute to club cells after naphthalene-induced airway injury; we therefore performed the same double-immunostaining experiments in this model. In *Scgb1a1-CreER;Sftpc-DreER;R26-NR* mice, AT2 cells are specifically labelled as ZsGreen$^+$tdTomato$^-$ (ZsG$^+$tdT$^-$) (Fig. 2a-e). Lung sections harvested 28 days after naphthalene injury were immunostained for ZsG, tdT, Scgb1a1 and Sftpc or Lamp3 (Extended Data Fig. 8a). The results showed that the majority of bronchiolar ZsG$^+$tdT$^-$ cells derived from AT2 cells expressed Scgb1a1 but were negative for Sftpc or Lamp3 (Extended Data Fig. 8a). Quantitative analysis based on double-marker immunostaining revealed that among the bronchiolar ZsG$^+$tdT$^-$ cells, 62.31 ± 4.98% were Scgb1a1$^+$Sftpc$^-$ club cells and 9.45 ± 1.43% were Scgb1a1$^-$Sftpc$^+$ AT2 cells (Fig. 2k). Furthermore, double-marker immunostaining and quantitative analyses revealed that 42.93 ± 5.60% of the newly formed bronchiolar Scgb1a1$^+$Sftpc$^-$ club cells were ZsG$^+$, demonstrating a significant contribution of AT2 cells to club cell regeneration following naphthalene injury (Fig. 2h). Furthermore, we also used *Sftpc-CreER;R26-tdT;Scgb1a1-DTR-GFP;R26-NICD* mice to overexpress NICD specifically in AT2 cells and found that Notch pathway activation promotes AT2-to-club cell fate conversion in vitro (Fig. 5t-y). We therefore performed the same double-marker staining on organoid cultures. In control organoids derived from tdT$^+$ AT2 cells (sorted from *Sftpc-CreER;R26-tdT;Scgb1a1-DTR-GFP* mice), robust Sftpc and Lamp3 expression was observed (Fig. 1a-c to Reviewers). In contrast, double-marker staining showed that the majority of tdT$^+$GFP$^+$ cells in NICD-overexpressing organoids were negative for Sftpc and Lamp3 (Fig. 1d to Reviewers). Quantitative analysis confirmed that 94.00 ± 1.97% of tdT$^+$GFP$^+$ cells were negative for Sftpc, suggesting that they had undergone transdifferentiation into club cells (Fig. 1e to Reviewers; also in Extended Fig. 13y,z).

Taken together, our *in vivo* and *in vitro* experiments collectively demonstrate that the major bronchiolar cell type contributed by AT2 cells is the club cell, rather than AT2 cells or BASCs. We have added these new data and the corresponding discussion to the revised manuscript; in particular, the statistical graphs based on the double-marker staining have been included. Because our Extended Data Figures now total 20 after revision, we have included some of these additional data in the Figure to Reviewers. These data can be considered for publication, along with review comments and response, at the reviewer and editor's discretion. For details, please refer to revised Figures 1,2; Extended Data Figs. 1,2,8,13; Page 5, Paragraph 2 of the revised manuscript.

2. To demonstrate AT2 cell migration toward the bronchioles, the authors present examples of AT2 cell clones (route 1) and putative channels (route 2). In route 1, lineage-labelled cells could also localise to the BADJ and differentiate into BASCs. In route 2, AT2 cells may transiently reside in this region or migrate away from it; thus, the data in Extended Fig. 3f do not provide clear evidence to support the direction of migration as the arrow showed. Furthermore, in Fig. 1o, it is unclear how lineage-labelled cells observed in the bronchioles can be definitively assigned to either route 1 or route 2 based solely on immunostaining. In addition, in Fig. 1p, the authors propose that the channel is formed by AT1 cells, yet no direct evidence is provided to confirm that these channel-forming cells are indeed AT1 cells.

Authors' Response: We thank the reviewer for raising this important concern. We previously found that after DT-induced airway injury, AT2 cells can enter the bronchiolar region through two routes: the natural bronchioalveolar duct junction (BADJ, route 1) and channels that appear on the bronchiolar wall (route 2) (Fig. 1n). We acknowledge that defining these two routes is somewhat subjective. As the reviewer noted, the migratory route and direction of AT2-lineage cells after they enter the bronchioles are difficult to determine, and it is therefore not possible to definitively assign these cells to route 1 or route 2. In response, we have removed the directional arrows from Extended Fig. 3f (now Extended Fig. 3g in the revised figures) and retained only the channels indication. We recognize that precisely distinguishing between these two routes would likely require *in vivo* live imaging, a technical platform we currently do not have available to record the entire migration process. We acknowledge this as a limitation of our study and have addressed it in the Discussion section.

Nevertheless, we have sought to further characterize these two routes. Because AT2-lineage cells from both routes may meet and mingle in the bronchiolar epithelium at later repair stages, making them indistinguishable, we analyzed samples from early time points after DT injury. We previously detected that AT2-lineage cells can enter the bronchioles through route 1 or route 2 as early as day 3 after DT injury (Fig. 1n,o). We therefore performed serial sectioning and immunostaining on lung sections at this time point. For AT2-lineage cells traversing the BADJ (route 1), consecutive images of serial sections did not reveal any channel on the bronchiolar wall in the surrounding area (Extended Data Fig. 3b). Similarly, for cells traversing the channel (route 2), consecutive imaging did not reveal any route 1 event in the vicinity (Extended Data Fig. 3c). These data suggest that, at least at the early repair stage, AT2-lineage cells entering the bronchioles through route 1 or route 2 are relatively independent and distinguishable. To ensure rigor, we have removed the statistical analyses of route events at late repair time points from Fig. 1o and retained the data from early time points (pDT 3d and pDT 7d), when the lineage-labelled cells extended over shorter distances (Fig. 1o). From these early data, it can still be inferred that the predominant route

for AT2-lineage cells entering the bronchiolar region is route 1, likely because it represents a natural connection between the bronchioles and alveoli, whereas route 2 would require additional processes to form channels on the bronchiolar wall (Fig. 1o). Regarding the reviewer's concern that no direct evidence was provided to confirm the channel-forming cells are AT1 cells (Fig. 1p), we previously proposed in Fig. 1p that the channel is formed by AT1 cells. To address this, we performed co-immunostaining for tdT and the AT1 marker AGER. We found that the tdT^+ flattened cells lining the inner wall of the channel expressed AGER, indicating that these channel-forming cells are AT1-like cells (Extended Data Fig. 3h,i). However, due to the extremely low abundance of this cell population, it is technically challenging to sort them and compare their gene expression signature with that of *bona fide* alveolar AT1 cells. We have therefore labelled them as "AT1-like" cells in revised Fig. 1p. These data and the corresponding discussion have been added to the revised manuscript. For details, please refer to revised Figure 1, Extended Data Fig. 3; Page 6, Line 175; Page 21, Line 681 of the revised manuscript.

3. On page 5, the authors state that only a small proportion of BASCs are detected following injury repair. This raises an important question: if AT2 cells can migrate to the bronchioles via the BADJ and subsequently differentiate into club cells, why do they not first adopt a BASC state, given that BASCs are both anatomically and developmentally closer to AT2 cells than club cells? The authors should address this point directly to strengthen the biological plausibility of their model.

Authors' Response: We thank the reviewer for raising this interesting question on the state of BASCs. Our lineage tracing data detected tdT-labelled GFP(Scgb1a1)$^+$Sftpc$^+$ BASC-like cells in the lungs of *Sftpc-CreER;R26-tdT;Scgb1a1-DTR-GFP* mice after DT injury. This observation naturally raises whether AT2 cells transit through a BASC-like state during their conversion into club cells, as the reviewer has pointed out. BASCs are commonly defined by the dual expression of Scgb1a1 and Sftpc (Kim et al., *Cell*, 2005; Liu et al., *Nat Genet*, 2019; Salwig et al., *EMBO J*, 2019); however, these two markers do not allow us to distinguish a putative AT2-derived BASC-like transient state from AT2-derived club cells, as both would activate the same set of markers. Addressing this question requires a unique gene marker specifically expressed in BASCs but not in AT2 cells or club cells, in combination with dual recombinase-mediated lineage-tracing systems to specifically capture AT2-derived cells that transit through a BASC-like state. We outline a potential future strategy if such a marker is identified: a BASC promoter-driven loxP-Stop-loxP-Dre (*BASC-LSL-Dre*) mouse line could be generated and crossed with the *R26-NR2* dual-reporter mouse (carrying the construct CAG-rox-loxP-Stop-loxP-ZsG-Stop-rox-tdT) together with *Sftpc-CreER* and *Scgb1a1-DTR-GFP*, yielding *Sftpc-CreER;Scgb1a1-DTR-GFP;BASC-LSL-Dre;R26-NR2* quadruple transgenic mice (Fig. 2a,b to Reviewers). Upon tamoxifen induction, Cre-loxP recombination would occur at the BASC gene locus in all Sftpc$^+$ cells, excising the loxP-flanked Stop cassette to convert *BASC-LSL-Dre* into *BASC-Dre*. Cre-loxP recombination at the *R26-NR2* locus would also label all Sftpc$^+$ cells with ZsG. Subsequent DT administration would specifically ablate all Scgb1a1$^+$ cells, including club cells and BASCs (Fig. 2 to Reviewers). We have already demonstrated that AT2 cells contribute to club cell regeneration after DT injury. If AT2 cells pass through a BASC-like intermediate state, *BASC-Dre* would be expressed and mediate Dre-rox recombination at the *R26-NR2* locus, excising the ZsG and stop sequences flanked by the two rox sites and activating tdT expression, thereby labelling these cells with red fluorescence. In contrast, AT2-lineage cells that do not undergo a BASC-like intermediate would remain ZsG$^+$ (Fig. 2 to

Reviewers). This genetic strategy would thus allow specific tracing of AT2-lineage cells that have experienced a BASC-like intermediate state. It would also enable quantification of the proportion of AT2-to-club transdifferentiation events that occur through a BASC-like state. Unfortunately, no unique BASC-specific gene marker has yet been identified; therefore, we are currently unable to generate the genetic system described above to quantify the proportion of AT2 cells that contribute to club cells through the BASC state.

Nevertheless, our scRNA-seq pseudotime analysis indicated that the AT2-to-club transdifferentiation process is accompanied by a progressive decrease in *Sftpc* expression and a corresponding increase in *Scgb1a1* expression (Fig. 4c-f), suggesting that the Sftpc^{+}Scgb1a1^{+} BASC-like state may represent a transitional stage during this fate conversion. In the revised manuscript, we have performed additional double-marker immunostaining for BASC-like cells at multiple time points (days 3, 7, 14, and 28 after DT injury) to further characterize the kinetics of BASC-like cell appearance (Extended Data Fig. 2n-p). Immunostaining and quantification revealed that at day 3 after injury, tdT^{+} AT2-lineage cells did not express GFP (Scgb1a1) or Sftpc, suggesting that at this early stage, AT2-lineage cells may be primarily responding to injury and migrating toward the bronchioles, rather than undergoing transdifferentiation into BASC-like or club cells (Extended Data Fig. 2n,p). At days 7, 14, and 28 after DT injury, we did detect AT2-derived GFP^{+}Sftpc^{-} club cells as well as GFP^{+}Sftpc^{+} BASC-like cells, with the latter predominantly localized near the BADJ (Extended Data Fig. 2o). Quantitative analysis showed that BASC-like cells accounted for $0.87 \pm 0.15\%$, $0.70 \pm 0.16\%$, and $0.33 \pm 0.08\%$ of tdT^{+} cells at days 7, 14, and 28, respectively (Extended Data Fig. 2p). The relatively low proportion of BASC-like cells we observed may be due to the BASC-like intermediate state being highly dynamic and transient during AT2-to-club transdifferentiation (Fig. 4f). Thus, our quantification of immunostaining data may underestimate the actual contribution of AT2 cells to club cells via the BASC state. Nevertheless, the observed increase and subsequent decrease in BASC-like cell proportions over the course of repair suggest that these cells may represent an intermediate state during AT2-to-club transdifferentiation. However, definitive genetic evidence will ultimately depend on the future identification of a unique BASC gene marker that is not expressed in either AT2 cells or club cells. We have acknowledged this as a limitation of our current study in the Discussion. We have added these data and the corresponding discussion to the revised manuscript. For details, please refer to revised Figure 4, Extended Data Fig. 2; Figure 2 to Reviewers, Page 6, Paragraph 1, Line 160; Page 23, Line 731 of the revised manuscript.

4. The authors report that all Scgb1a1^{+} cells are ablated , and excluding alternative sources of club cells, including basal cells, neuroendocrine cells, and AT1 cells. However, in Fig. 1j and 1k, approximately 20% of club cells are negative for AT2 lineage tracing. Additional evidence is required to clarify the origin of these AT2 lineage-negative club cells.

Authors' Response: We thank the reviewer for this careful observation. We agree that in Fig. 1j and 1k, approximately 20% of the newly formed distal bronchiolar club cells were negative for AT2 lineage tracing in *Sftpc-CreER;R26-tdT;Scgb1a1-DTR-GFP* mice after DT injury. This confirms that AT2 cells contribute to the majority, but not all, of bronchiolar club cell regeneration following injury. Our study has demonstrated that the remaining club cells likely arise from other known sources, including basal cells, Scgb3a2^{+}Scgb1a1^{-} intralobular serous (IS) cells, and neuroendocrine

(NE) cells; AT1 cells have not been found to contribute to club cell regeneration. We provided the following detailed analysis of these potential sources.

One source is distal bronchiolar basal cells. Previous studies have reported that airway basal cells function as stem cells responsible for airway injury repair (Pellegrini et al., *PNAS*, 2001; Rock et al., *PNAS*, 2009), and that a rare population of $p63^+$ cells exists in distal bronchioles and can expand after alveolar injury (Kumar et al., *Cell*, 2011; Vaughan et al., *Nature*, 2015; Zuo et al., *Nature*, 2015). Using *p63-DreER;R26-RSR-tdT* mice, we detected that basal cells are predominantly distributed in the trachea and main bronchi, with a small number of basal cells also present in the distal bronchioles (Extended Data Fig. 5a-c). Immunostaining and quantitative analysis of lung sections from *p63-DreER;R26-RSR-tdT;Scgb1a1-DTR-GFP* mice at 28 days after DT treatment revealed that, following club cell ablation, basal cells were primarily responsible for the regeneration of proximal club cells in the trachea and main bronchi (Extended Data Fig. 5d-j). In the distal bronchioles, these sparsely labelled basal cells underwent clonal expansion and contributed to $0.59 \pm 0.37\%$ of distal club cells (Extended Data Fig. 5h-j).

A second source is the recently described $Scgb3a2^+Scgb1a1^-$ distal airway secretory cells, termed IS cells (Beppu et al., *Nat Commun*, 2023). Our results indicated that, under homeostasis, club cells exhibit heterogeneity, with the majority being bulk club cells expressing both Scgb1a1 and Scgb3a2, while a small subset expressed only Scgb3a2 (Extended Data Fig. 6a-d). We found that these $Scgb3a2^+Scgb1a1^-$ cells survived DT injury, proliferated in response to injury, and acquired GFP expression, suggesting that they can convert into $Scgb1a1^+$ club cells (Extended Data Fig. 6e-j). However, due to the lack of a Scgb3a2-specific tracing tool, we are currently unable to quantify the specific contribution of $Scgb3a2^+Scgb1a1^-$ cells to newly formed club cells after DT injury, and we acknowledge this as a limitation of our study. Future studies using *Scgb3a2-CreER;R26-tdT;Scgb1a1-DTR-GFP* mice could address this.

A third source is NE cells. Previous studies have reported that NE cells can function as stem cells and differentiate into club cells after bronchial injury (Reynolds et al., *Am J Pathol*, 2000; Song et al., *PNAS*, 2012; Ouadah et al., *Cell*, 2019). Using *Ascl1-CreER* to efficiently label NE cells, we analyzed lung sections from *Ascl1-CreER;R26-tdT;Scgb1a1-DTR-GFP* mice at 28 days after DT injury and found that NE cells contributed to $4.59 \pm 1.36\%$ of distal club cells (Extended Data Fig. 6k-s).

Additionally, using *Hopx-DreER;Ager-CreER;R26-RSR-LSL-tdT;Scgb1a1-DTR-GFP* mice to specifically label AT1 cells while ablating $Scgb1a1^+$ cells, our lineage tracing results confirmed that AT1 cells do not contribute to club cells after DT injury (Extended Data Fig. 7). Beyond the sources discussed above, we cannot exclude the possibility that other as-yet-unidentified cell types may also contribute to club cell regeneration after DT injury.

Taken together, based on the currently available data, the approximately 20% of club cells that are not derived from AT2 cells likely originate from basal cells, $Scgb3a2^+Scgb1a1^-$ cells, NE cells, and possibly other uncharacterized sources. We have added these data and the discussion to the revised manuscript. For details, please refer to revised Extended Data Figs. 5,6,7; Page 7, Paragraph 3; Page 8, Paragraph 1-3; Page 23, Line 747 of the revised manuscript.

5. Club cells and ciliated cells are arranged in an alternating pattern within the bronchioles. Based on the authors' model, migrating AT2 cells would frequently encounter ciliated cells and potentially differentiate into club cells. However, the quantification data indicate that the majority of lineage-

labelled cells remain as AT2 or AT1 cells. This apparent discrepancy should be clarified to improve the coherence of the proposed model.

Authors' Response: We thank the reviewer for raising this important question. We previously evaluated the contribution of AT2 cells to bronchiolar regeneration in two injury models (DT and naphthalene) and apologize that our previous presentation of the quantitative data may not have been sufficiently clear. In the DT injury model using *Sftpc-CreER;R26-tdT;Scgb1a1-DTR-GFP* mice at 28 days post-injury, our quantitative data showed that, among the tdT^+ AT2-lineage cells that had migrated to the bronchioles, 38.18 ± 4.55% were club cells, 14.61 ± 2.62% were AT2 cells, and 18.90 ± 4.48% were AT1 cells (Fig. 1l). Together, AT2 and AT1 cells accounted for approximately one-third of the lineage labeled cells, representing a minor fraction. In the naphthalene injury model using *Scgb1a1-CreER;Sftpc-DreER;R26-NR* mice at 28 days post-injury, among the ZsG^+ AT2-lineage cells that had migrated to the bronchioles, 62.31 ± 4.98% were club cells, 9.45 ± 1.43% were AT2 cells, and 6.63 ± 1.91% were AT1 cells (Fig. 2k). Together, AT2 and AT1 cells accounted for approximately 16%, also representing a minor fraction of the lineage labeled cells. Thus, in both injury models, club cells constituted the major cell type derived from AT2 cells. Our previous model proposed that after AT2 cells migrate to the bronchiolar region, they need to contact ciliated cells and activate Notch signaling to promote their transdifferentiation into club cells (Extended Data Fig. 20). However, as the reviewer noted, a portion of AT2 cells that migrated to the bronchioles remained as AT2 cells or differentiated into AT1 cells, rather than uniformly becoming club cells. This appears to conflict with our model. To address this, we have incorporated additional experiments in the revised manuscript that offer a reasonable explanation for this observation.

First, we re-evaluated the status of ciliated cells after bronchiolar injury. We collected lung sections from *Scgb1a1-DTR-GFP* mice under control conditions (PBS) and at days 3 and 28 after DT injury (Extended Data Fig. 2i). Immunostaining for GFP together with the ciliated cell markers FOXJ1 and Ace-Tub revealed that ciliated cells and GFP^+ club cells were arranged in an alternating pattern in control mice. At day 3 after DT injury, GFP^+ club cells were ablated, and ciliated cells were also sparse and scattered within the bronchiolar epithelium. At day 28, ciliated cells remained sparse in some areas; the residual ciliated cells were often found in clusters, and GFP^+ club cells were frequently observed near these clusters (Extended Data Fig. 2j; and Fig. 3a,b to Reviewers). This observation supports our model that AT2-lineage transdifferentiation into club cells requires contact with ciliated cells to activate Notch signaling (Fig. 6). Quantitative analysis further showed that, compared with controls, the density of ciliated cells in the bronchiolar epithelium was significantly reduced at day 3 after DT injury and, although partially recovered by day 28, had not returned to baseline levels (Extended Data Fig. 2j; and Fig. 3c to Reviewers). TUNEL staining also detected apoptotic signals in ciliated cells after club cell ablation (Fig. 3d to Reviewers). These data indicate that club cell ablation does not occur in isolation but instead triggers collateral damage to neighboring ciliated cells, likely reflecting the intricate intercellular crosstalk and homeostatic regulatory networks inherent to the *in vivo* airway epithelial niche. Further immunostaining for tdT, GFP, FOXJ1, and Ace-Tub on lung sections from *Sftpc-CreER;R26-tdT;Scgb1a1-DTR-GFP* mice at day 28 after DT injury demonstrated that AT2-derived tdT^+GFP^+ club cells (yellow arrows) were often distributed in the vicinity of ciliated cells (white arrows), whereas bronchiolar epithelial regions devoid of ciliated cells were covered by non-club cells, such as tdT^+ flattened AT1-like cells (Extended Data Fig. 2l,m; and Fig. 3e,f to Reviewers). These data suggest that the actual number of

ciliated cells accessible to AT2 cells that have migrated to the bronchiolar region is significantly lower than that under steady-state conditions, greatly limiting the opportunity for Notch signaling activation and subsequent club cell differentiation. Second, AT1 cells are the natural progeny of AT2 cells. Those AT2 cells that fail to contact ciliated cells may be more inclined to either remain in the AT2 state or follow their intrinsic differentiation trajectory, giving rise to flattened, spread AT1 cells ideally suited to rapidly resurface denuded airway, rather than adopting a club cell fate.

We also performed assessments of ciliated cell status after naphthalene-induced club cell injury. Lung sections from wild-type mice under control conditions and at days 3 and 28 after naphthalene injury were immunostained for FOXJ1 and Scgb1a1 (Fig. 3g,h to Reviewers). The results similarly showed that at day 3 after naphthalene injury, when club cells underwent extensive apoptosis, ciliated cell density was also significantly reduced and remained below steady-state levels even at day 28 (Fig. 3i to Reviewers). TUNEL staining also detected apoptotic ciliated cells after naphthalene injury (Fig. 3j to Reviewers). The observation that bronchiolar ciliated cell density is reduced after naphthalene injury is consistent with previous reports (Gharib et al., *Am J Respir Cell Mol Biol*, 2013). Analysis of *Scgb1a1-CreER;Sftpc-DreER;R26-NR* mice at day 28 after naphthalene injury further demonstrated that ciliated cell numbers had not fully recovered, and that not all ZsG^+ AT2-lineage cells that had migrated to the bronchioles were able to contact ciliated cells to receive Notch signals (Fig. 3k,l to Reviewers).

Taken together, our data provide a plausible explanation for why a considerable proportion of lineage-labelled cells in the bronchiolar region still manifest as AT2 or AT1 cells. We believe that there is no substantive contradiction between our model predictions and the quantitative data. We have added these data and the corresponding discussion to the revised manuscript to further refine our injury and regeneration model. Because our Extended Data Figures now total 20 after revision, we have included some of these data in the Figure to Reviewers. These data can be considered for publication, along with review comments and response, at the reviewer and editor's discretion. For details, please refer to revised Figures 1,2,6; Extended Data Figs. 2,3,20; Figure 3 to Reviewers, Page 5, Paragraph 2; Page 6, Paragraph 1; Page 21, Line 681 of the revised manuscript.

6. The authors state that AT2 cells can differentiate into AT1 cells within the bronchioles and exclude the possibility that AT1 cells migrate into this region. However, in Fig. 2j and Extended Fig. 2i, j, some AT1 cells do not express RFP, indicating that they are not derived from the AT2 lineage. These seemingly contradictory observations require further clarification.

Authors' Response: We thank the reviewer for this careful observation. We agree with the reviewer's summary that our lineage tracing results demonstrate that, after bronchial injury, AT2-lineage cells that migrate to the bronchiolar region can differentiate not only into club cells but also partially into AT1 cells (Fig. 1j,l), whereas alveolar AT1 cells themselves show minimal migration into the bronchiolar region (Extended Data Fig. 7h-m). We apologize that the layout of our previous figures may have caused some confusion. In the revised manuscript, we have reorganized the figure layout, provided higher-magnification views of the relevant regions, and included additional statistical analyses that further support our conclusions.

First, Fig. 2j shows immunostaining for AGER, ZsG, and tdT on lung sections from *Scgb1a1-CreER;Sftpc-DreER;R26-NR* mice at 28 days after naphthalene injury. In this system, AT2 cells are specifically labelled with ZsG (Fig. 2a-e). As shown in the image, the newly appeared $AGER^+$ AT1 cells in the bronchiolar epithelium were positive for ZsG (Fig. 2j). Furthermore,

immunostaining for the additional AT1 markers Hopx and T1a confirmed that $Hopx^+$ and $T1a^+$ cells in the bronchioles were also positive for ZsG (Extended Data Fig. 8b). Quantification revealed that $99.64 \pm 0.49\%$ of bronchiolar AT1 cells were ZsG^+, indicating that virtually all bronchiolar AT1 cells were derived from AT2 cells after naphthalene injury (Extended Data Fig. 8c).

Second, Extended Data Fig. 2i, j (now renumbered as Extended Data Fig. 2e, f) shows immunostaining for T1a, Hopx, and tdT on lung sections from *Sftpc-CreER;R26-tdT;Scgb1a1-DTR-GFP* mice at 28 days after DT injury. In this system, AT2 cells are specifically labelled with tdT (RFP). High-magnification views of the bronchiolar epithelium clearly revealed that $T1a^+$ and $Hopx^+$ AT1 cells co-expressed tdT (Extended Data Fig. 2e, f). In addition, co-staining for tdT and AGER revealed that $AGER^+$ cells appearing in the bronchioles were labelled with tdT (Fig. 1j). Quantitative analysis showed that $98.99 \pm 0.56\%$ of bronchiolar AT1 cells were tdT^+, confirming their AT2 cell origin (Extended Data Fig. 2g).

We acknowledge that the newly formed bronchiolar AT1 cells are adjacent to alveolar AT1 cells and separated by the bronchiolar wall, which can occasionally make their distinction challenging in immunostained sections. Nevertheless, our lineage tracing data consistently and robustly demonstrate that these bronchiolar AT1 cells are efficiently labeled by the AT2 lineage. We have added these data and the corresponding discussion to the revised manuscript. For details, please refer to revised Figures 1,2, Extended Data Figs. 2,7,8; Page 5, Line 130; Page 9, Line 307 of the revised manuscript.

7. In the injury models used, club cells are specifically ablated by genetic or chemical methods, whereas ciliated cells remain intact. The authors also show that AT2 cells can differentiate into AT1 cells upon migration to the bronchioles. Given that AT1 cells have a substantially larger surface area, this raises the question of how ciliated cells are accommodated within regions covered by AT1 cells. If ciliated cells are also lost, this would call into question the validity of the injury models employed. The authors should address this issue explicitly.

Authors' Response: We thank the reviewer for raising this important question. As the reviewer noted, we used genetic (DT) and chemical (naphthalene) approaches to ablate club cells. As detailed in our response to Comment 5, club cell ablation indirectly affects the survival of neighboring ciliated cells; thus, ciliated cells do not remain intact in our injury models (Fig. 3 to Reviewers). This is consistent with previous reports that ciliated cell density is significantly reduced following naphthalene injury (Gharib et al., *Am J Respir Cell Mol Biol*, 2013). In both injury models, we readily detected AT2-to-club transdifferentiation, indicating that residual ciliated cells, though reduced in number, are sufficient to provide the Notch signals required for this fate conversion.

Regarding the reviewer's concern about the coexistence of AT1 cells and ciliated cells in the bronchiolar region, we note that at day 28 after injury, AT1 cells accounted for $18.90 \pm 4.48\%$ of the AT2-derived lineage within the bronchioles in the DT model (Fig. 1l), compared with $6.63 \pm 1.91\%$ in the naphthalene model (Fig. 2k). Thus, AT1 cells represented a relatively small proportion of the repaired epithelium and did not cover the entire bronchiolar area. Immunostaining revealed that the repaired epithelium consists of a monolayer composed of AT2-derived AT1 cells, residual ciliated cells, and other cell types such as AT2 and club cells (Fig. 1j,l; Fig. 3f to Reviewers). We further characterized the cellular dynamics in the injury models. At day 3 after DT injury in *Scgb1a1-DTR-GFP* mice, ciliated cell numbers were reduced, and the residual ciliated cells were scattered randomly throughout the bronchioles; by day 28, the residual ciliated cells were frequently

observed in clusters (Extended Data Fig. 2j; also in Fig. 3a,b to Reviewers). Analysis of *Sftpc-CreER;R26-tdT;Scgb1a1-DTR-GFP* mice showed that AT2-lineage cells had just begun to migrate into the bronchioles at day 3 after DT injury (Fig. 1n); by day 28, AT2-derived club cells were detected in the vicinity of clustered ciliated cells, whereas bronchiolar regions devoid of ciliated cells were often covered by tdT^+ flattened AT1 cells or other non-club cells (Extended Data Fig. 2l,m; Fig. 3f to Reviewers). We acknowledge that direct visualization of how residual ciliated cells converge and how AT2 cells choose between club and AT1 fates would ideally require *in vivo* live imaging, a technology we currently lack. Based on our data, we offer the following explanation: AT2 cells that migrate to the bronchioles and encounter residual ciliated cells receive Notch signals and differentiate into club cells, whereas those that do not encounter ciliated cells tend to remain as AT2 cells or differentiate into AT1 cells to rapid resurface denuded airway epithelium. Thus, fate choice appears to be largely influenced by the spatial distribution of residual ciliated cells. Our lineage tracing data further showed that these AT2-derived AT1 cells, once formed, stably maintain their AT1 identity and do not transdifferentiate into other cell types (Extended Data Fig. 9). Therefore, even if these terminally differentiated AT1 cells later encounter ciliated cells, they do not undergo fate conversion. Given their relatively larger surface area, we speculate that AT1 cells may physically compete for space with neighboring ciliated cells, potentially contributing to the clustering of residual ciliated cells observed at day 28—which would explain why ciliated cells transition from a scattered distribution at day 3 to clustered aggregates at day 28. Taken together, the repaired bronchiolar epithelium exhibits a coexistence of club cells, ciliated cells, AT1 cells, and AT2 cells—a finding that reflects the involvement of alveolar stem cells in bronchiolar repair (Extended Data Fig. 20).

Regarding the reviewer's concern about whether ciliated cell loss calls into question the validity of the injury models, we acknowledge that ciliated cells are partially reduced but not completely ablated; a substantial population persists throughout the repair process (Fig. 3 to Reviewers). Importantly, the primary target—club cells—is efficiently eliminated, and AT2-to-club transdifferentiation was readily detected in both models, confirming that residual ciliated cells, though reduced in number, remain sufficient to support this process. Furthermore, club cells and ciliated cells are closely associated and functionally interdependent. Under both homeostasis and repair conditions, ciliated cells are maintained through differentiation from club cells, which serve as their progenitor pool. Therefore, it is plausible that the loss of club cells may affect the survival of neighboring ciliated cells. This is consistent with previous studies documenting ciliated cell damage following naphthalene injury (Gharib et al., *Am J Respir Cell Mol Biol*, 2013). Epithelial repair is inherently a dynamic, multicellular process—changes in ciliated cell number and morphology during repair reflect this *in vivo* biological complexity rather than a flaw in the models themselves. We have added these data and the corresponding discussion to the revised manuscript and believe that our injury models remain valid for studying club cell regeneration and AT2 cell plasticity. For details, please refer to revised Figures 1,2,6; Extended Data Figs. 2,3,20; Figure 3 to Reviewers, Page 5, Paragraph 2; Page 6, Paragraph 1; Page 21, Line 681 of the revised manuscript.

8. The interaction strength between peribronchial fibroblasts and AT2 cells appears to be substantially greater than that between immune cells and AT2 cells. Therefore, investigating signalling pathways mediated by peribronchial fibroblasts may be more relevant for understanding AT2 cell migration. The authors should justify their focus on immune-derived signals to improve

the interpretability of their findings.

Authors' Response: We thank the reviewer for this insightful comment and for prompting us to clarify the rationale underlying our focus on immune-cell-derived signals. We agree that in the aggregate CellChat interaction-strength analysis, peribronchial fibroblasts exhibit strong outgoing interaction strength toward AT2 cells after DT injury (Fig. 7a, b). However, this aggregate metric integrates communication probabilities across the entire repertoire of detected ligand–receptor pathways and therefore does not identify which specific signals underlie directional chemotactic recruitment. To address this question, we decomposed the aggregate signal into pathway-level relative information flow (Extended Data Fig. 15e), which revealed a clear qualitative distinction between fibroblast- and immune-derived signals.

The DT-induced pathways dominating peribronchial fibroblast signaling toward AT2 cells were overwhelmingly structural, adhesion- and morphogen-related—including laminin, fibronectin, JAM, ephrin–Eph (EPHA/EPHB), and Wnt/ncWnt (Extended Data Fig. 15e)—consistent with fibroblasts' canonical role in elaborating and remodeling the extracellular matrix (ECM) scaffold rather than generating a directional migratory cues. This interpretation is reinforced by the marked DT-induced upregulation of fibrillar collagen genes (*Col1a1*, *Col1a2*, *Col3a1*, *Col4a1/2*, *Col5a1/2*, *Col6a1–3*) and other ECM components (*Tnc*, *Postn*) in peribronchial fibroblasts (Extended Data Fig. 15f), together with strong enrichment of the "extracellular matrix organization" gene set in this population after injury (Extended Data Fig. 15g). In contrast, the chemotactic SPP1 pathway emerged as one of the most robustly and consistently DT-induced pathways directed at AT2 cells across all four immune populations examined—neutrophil, monocyte, NK cell, and alveolar macrophage—despite these cell types exhibiting generally lower aggregate interaction strength (Extended Data Fig. 15e; Fig. 7b). This convergent, pathway-specific induction across multiple independently responding immune populations nominated SPP1, rather than the numerically larger but functionally heterogeneous fibroblast-derived signal, as the most directly supported chemoattractant candidate. Corroborating this inference, spatial transcriptomics independently and unbiasedly identified an Spp1-enriched gene module (Module 9) that emerged following injury and was spatially restricted to the bronchiolar lumen and peribronchiolar region (Fig. 7h; Extended Data Fig. 16b). Additionally, SPP1 was selectively elevated in $CD45^{+}$ immune cells infiltrating the bronchiolar lumen rather than in peribronchial stromal cells (Fig. 7f, i-j; Extended Data Fig. 17b, g). Supported by this convergent evidence, we proceeded to functionally validate SPP1 as the key chemoattractant. Treatment with recombinant SPP1, immune-cell co-culture, and pharmacological SPP1 inhibition collectively established a direct causal relationship between immune-cell-derived SPP1 and AT2 cell migration *in vitro* (Extended Data Fig. 18a–g). Furthermore, both pharmacological SPP1 blockade and AT2-specific Itgb1 deletion significantly impaired AT2 migration toward injured bronchioles in two independent injury models *in vivo* (Fig. 7m–s; Extended Data Fig. 18h–j).

In summary, we do not contend that peribronchial fibroblasts are uninvolved in bronchiolar repair. Rather, our data suggest their principal contribution lies in remodeling the local ECM niche and providing structural support to the bronchiolar wall—a process distinct from, yet potentially complementary to, the immune-cell-driven chemotactic recruitment step we describe here. We have revised the manuscript to articulate this distinction explicitly and have added the above data and the corresponding discussion. For details, please refer to revised Figure 7, Extended Data Figs. 15,18; Page 18, Paragraph 2, Line 596; Page 23, Line 751 of the revised manuscript.

Referee #2 (Remarks to the Author):

The authors addressed all my technical concerns, and then some. It is a tour-de-force. There is no doubt that the observed trajectories occur in mice.

The connection to human lung regeneration remains tenuous however, as this extrapolation is based on expression of Cldn4 in both the transitional cells studied here and in AT0 cells in the data of the Tata group (Nature 2022). The trajectory of the heterogenuous TRB population in humans is furthermore quite controversial, which does not help the argument, and the authors picked the one trajectory that fits their argument. The only way to resolve this issue is to do studies on well-characterized and pure human cells, and correlate with rigorous trajectory analysis in human lung injury. This is admittedly beyond the scope of this already very extensive manuscript.

Authors' response: We sincerely thank the reviewer for the highly positive assessment of our technical work and for this important caution regarding human relevance. We agree that extrapolating our mouse AT2-to-club transdifferentiation findings to human lung regeneration based solely on CLDN4 expression and single trajectory analysis is premature and risks overinterpretation. As the reviewer correctly noted, the heterogeneity of the human TRB population and the ongoing controversy surrounding its trajectory make such extrapolation even more tenuous. We recognize that definitively addressing this question would require well-controlled studies on purified human cells, coupled with rigorous trajectory analysis in the context of human lung injury—an undertaking that is beyond the scope of the present manuscript. To ensure rigor and avoid unsupported claims, we have removed the data and discussion pertaining to human AT0 cells and CLDN4 expression, as well as statements attempting to link our mouse findings to human lung regeneration. We fully acknowledge whether an evolutionarily conserved AT2-to-club transdifferentiation program exists in humans remains an open question for future investigation. We have therefore added a corresponding discussion to the revised manuscript. For details, please refer to Page 24, Line 779 of the revised manuscript.

Referee #3 (Remarks to the Author):

All my prior concerns were addressed and congratulations to the authors for accomplishing this.

Authors' Response: We sincerely thank the Reviewer for the positive feedback and for confirming that all our previous concerns have been adequately addressed. We are also grateful for the reviewer's time and constructive suggestions throughout the review process.

Referee #3 (Remarks on code availability):

NA

References

Beppu, A.K., Zhao, J., Yao, C., Carraro, G., Israely, E., Coelho, A.L., Drake, K., Hogaboam, C.M., Parks, W.C., Kolls, J.K., and Stripp, B.R. (2023). Epithelial plasticity and innate immune activation promote lung tissue remodeling following respiratory viral infection. Nat Commun 14, 5814. 10.1038/s41467-023-41387-3.

Gharib, S.A., Altemeier, W.A., Van Winkle, L.S., Plopper, C.G., Schlesinger, S.Y., Buell, C.A., Brauer, R., Lee, V., Parks, W.C., and Chen, P. (2013). Matrix metalloproteinase-7 coordinates airway epithelial injury response and differentiation of ciliated cells. Am J Respir Cell Mol Biol 48, 390-396. 10.1165/rcmb.2012-0083OC.

Kim, C.F., Jackson, E.L., Woolfenden, A.E., Lawrence, S., Babar, I., Vogel, S., Crowley, D., Bronson, R.T., and Jacks, T. (2005). Identification of bronchioalveolar stem cells in normal lung and lung cancer. Cell 121, 823-835. 10.1016/j.cell.2005.03.032.

Kumar, Pooja A., Hu, Y., Yamamoto, Y., Hoe, Neo B., Wei, Tay S., Mu, D., Sun, Y., Joo, Lim S., Dagher, R., Zielonka, Elisabeth M., et al. (2011). Distal Airway Stem Cells Yield Alveoli In Vitro and during Lung Regeneration following H1N1 Influenza Infection. Cell 147, 525-538. 10.1016/j.cell.2011.10.001.

Liu, Q., Liu, K., Cui, G., Huang, X., Yao, S., Guo, W., Qin, Z., Li, Y., Yang, R., Pu, W., et al. (2019). Lung regeneration by multipotent stem cells residing at the bronchioalveolar-duct junction. Nature Genetics. 10.1038/s41588-019-0346-6.

Ouadah, Y., Rojas, E.R., Riordan, D.P., Capostagno, S., Kuo, C.S., and Krasnow, M.A. (2019). Rare Pulmonary Neuroendocrine Cells Are Stem Cells Regulated by Rb, p53, and Notch. Cell 179, 403-416 e423. 10.1016/j.cell.2019.09.010.

Pellegrini, G., Dellambra, E., Golisano, O., Martinelli, E., Fantozzi, I., Bondanza, S., Ponzin, D., McKeon, F., and De Luca, M. (2001). p63 identifies keratinocyte stem cells. Proc Natl Acad Sci U S A 98, 3156-3161. 10.1073/pnas.061032098.

Reynolds, S.D., Giangreco, A., Power, J.H.T., and Stripp, B.R. (2000). Neuroepithelial Bodies of Pulmonary Airways Serve as a Reservoir of Progenitor Cells Capable of Epithelial Regeneration. The American Journal of Pathology 156, 269-278. 10.1016/s0002-9440(10)64727-x.

Rock, J.R., Onaitis, M.W., Rawlins, E.L., Lu, Y., Clark, C.P., Xue, Y., Randell, S.H., and Hogan, B.L.M. (2009). Basal cells as stem cells of the mouse trachea and human airway epithelium. P Natl Acad Sci USA 106, 12771-12775. 10.1073/pnas.0906850106.

Salwig, I., Spitznagel, B., Vazquez-Armendariz, A.I., Khalooghi, K., Guenther, S., Herold, S., Szibor, M., and Braun, T. (2019). Bronchioalveolar stem cells are a main source for regeneration of distal lung epithelia in vivo. EMBO J 38. 10.15252/embj.2019102099.

Song, H., Yao, E., Lin, C., Gacayan, R., Chen, M.H., and Chuang, P.T. (2012). Functional characterization of pulmonary neuroendocrine cells in lung development, injury, and tumorigenesis. Proc Natl Acad Sci U S A 109, 17531-17536. 10.1073/pnas.1207238109.

Vaughan, A.E., Brumwell, A.N., Xi, Y., Gotts, J.E., Brownfield, D.G., Treutlein, B., Tan, K., Tan, V., Liu, F.C., Looney, M.R., et al. (2015). Lineage-negative progenitors mobilize to regenerate lung epithelium after major injury. Nature 517, 621-625. 10.1038/nature14112.

Zuo, W., Zhang, T., Wu, D.Z., Guan, S.P., Liew, A.A., Yamamoto, Y., Wang, X., Lim, S.J., Vincent, M., Lessard, M., et al. (2015). p63(+)Krt5(+) distal airway stem cells are essential for lung regeneration. Nature 517, 616-620. 10.1038/nature13903.

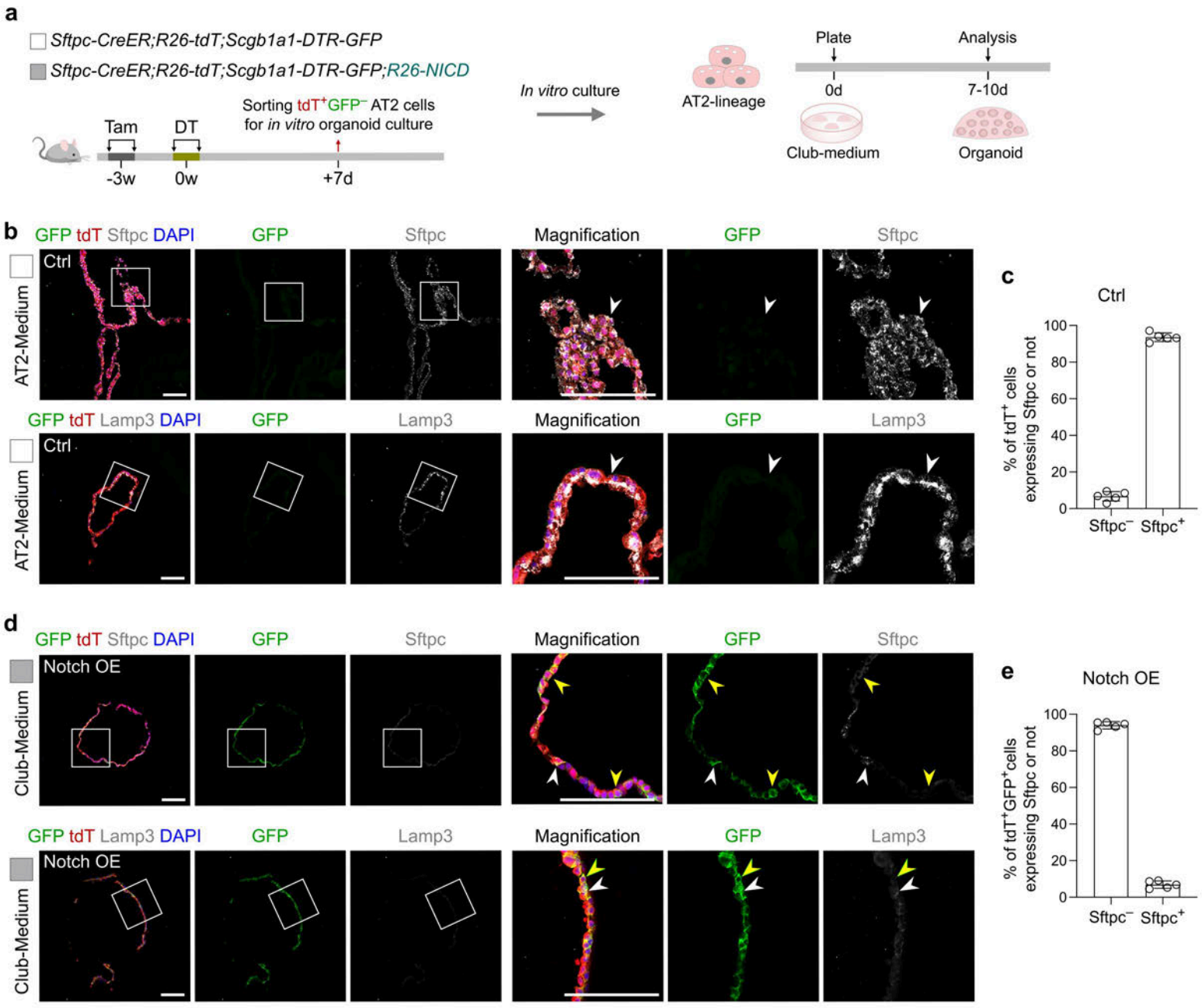


Figure 1 to Reviewers

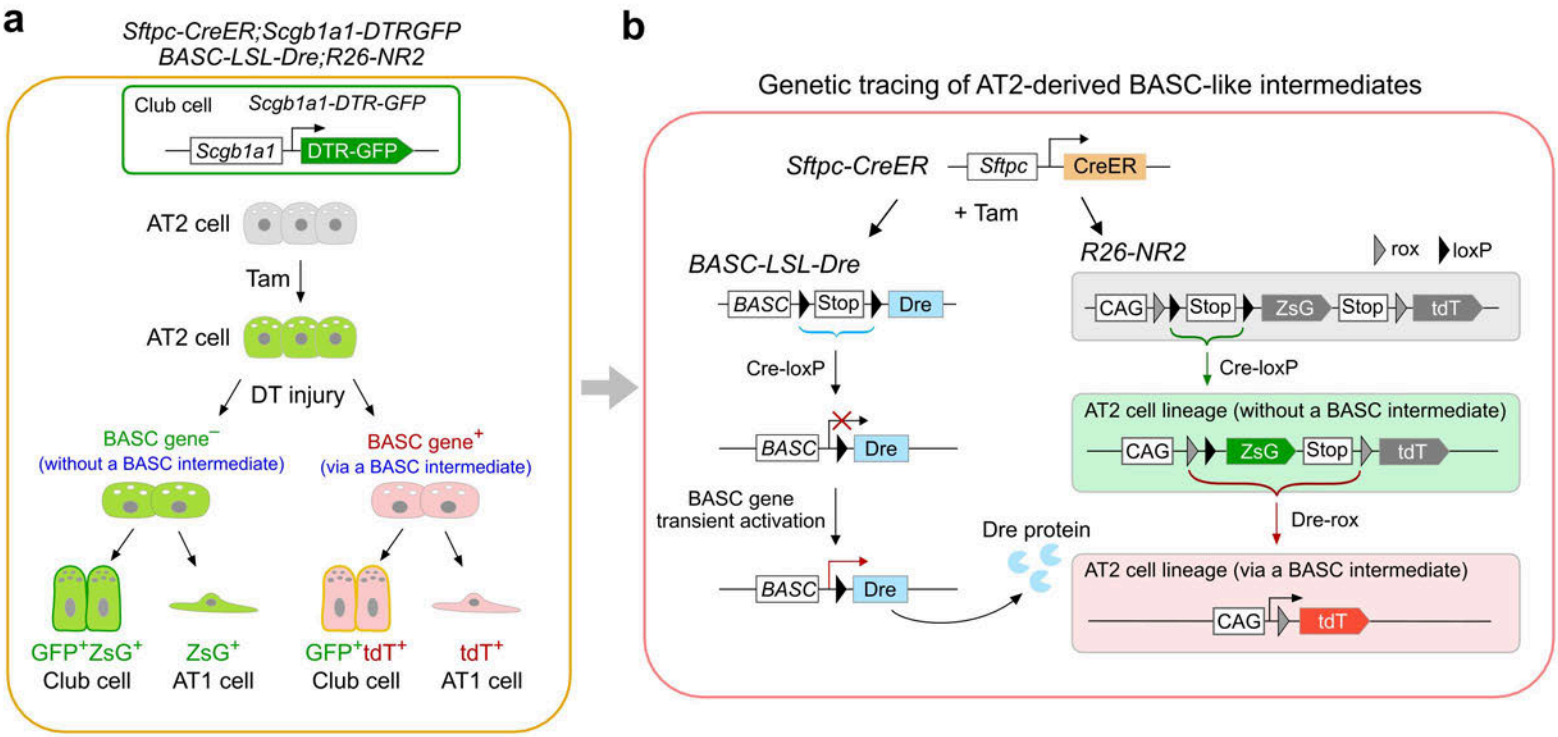


Figure 2 to Reviewers

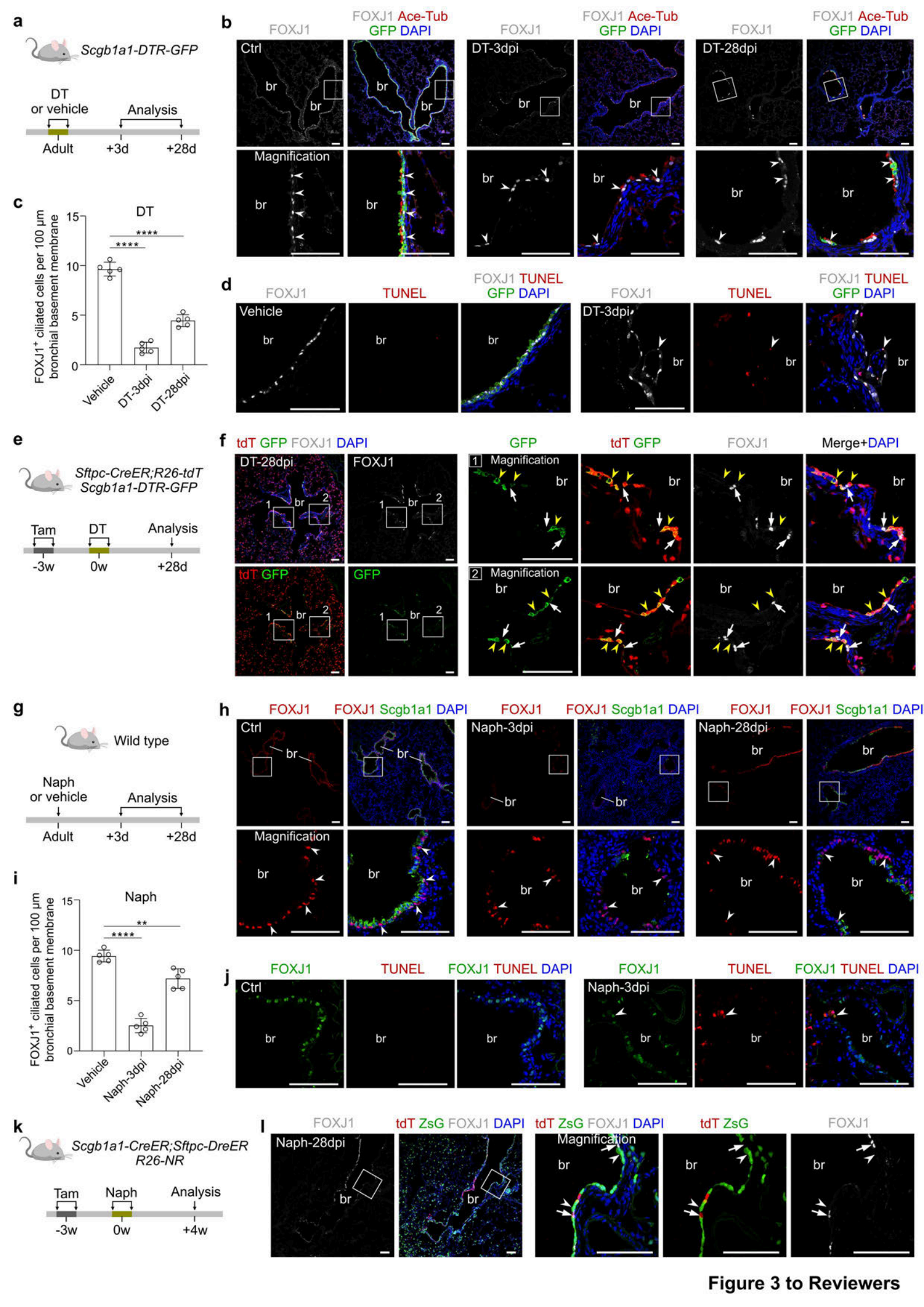


Figure 3 to Reviewers

Figure to Reviewers legends

Fig. 1 to Reviewers | Notch overexpression drives AT2-to-club cell transition *in vitro*

a, A schematic diagram illustrating the experimental design. **b**, Immunostaining for tdT, GFP, and Sftpc or Lamp3 on organoid sections in ctrl group. **c**, Quantification of the percentage of tdT^+ cells that are $Sftpc^-$ or $Sftpc^+$ from the organoids in (b) (n=5). Data are presented as mean ± SD. **d**, Immunostaining for tdT, GFP, and Sftpc or Lamp3 on organoid sections in NICD overexpression group. **e**, Quantification of the percentage of tdT^+GFP^+ cells that are $Sftpc^-$ or $Sftpc^+$ from the organoids in (d) (n=5). Data are presented as mean ± SD. Ctrl, control group. NICD OE, NICD overexpression group. Tam, tamoxifen. DT, diphtheria toxin. White scale bars, 100 μm.

Fig. 2 to Reviewers | A theoretical genetic approach for specifically tracing AT2-derived BASC-like intermediate cells

a,b, In the conception, a BASC promoter-driven loxP-Stop-loxP-Dre (*BASC-LSL-Dre*) mouse line would be generated and crossed with the *R26-NR2* dual-reporter mouse (carrying the construct CAG-rox-loxP-Stop-loxP-ZsG-Stop-rox-tdT) together with *Sftpc-CreER* and *Scgb1a1-DTR-GFP*, yielding *Sftpc-CreER;Scgb1a1-DTR-GFP;BASC-LSL-Dre;R26-NR2* quadruple transgenic mice (a). Theoretically, upon tamoxifen induction, Cre-loxP recombination would occur at the BASC gene locus in all $Sftpc^+$ cells, excising the loxP-flanked Stop cassette to convert *BASC-LSL-Dre* into *BASC-Dre*. Meanwhile, Cre-loxP recombination at the *R26-NR2* locus would label all $Sftpc^+$ cells with ZsG. Subsequent DT administration would specifically ablate all $Scgb1a1^+$ cells, including club cells and BASCs (a,b). If AT2 cells pass through a BASC-like intermediate state, *BASC-Dre* would be expressed and mediate Dre-rox recombination at the *R26-NR2* locus, excising the ZsG and stop sequences flanked by the two rox sites and activating tdT expression, thereby labelling these cells with red fluorescence. In contrast, AT2-lineage cells that do not undergo a BASC-like intermediate would remain ZsG^+.

Fig. 3 to Reviewers | Depletion of club cells also indirectly causes damage to ciliated cells

a, A schematic diagram illustrating the experimental design. **b**, Immunostaining for GFP, FOXJ1, and Ace-tub on lung sections at the indicated time points post-DT or vehicle treatment. **c**, Quantification of the number of $FOXJ1^+$ ciliated cells per 100 μm of bronchial basement membrane in (**b**). (n = 5). Data are presented as mean ± SD. **d**, Immunostaining for GFP, FOXJ1,

and TUNEL on lung sections after DT or vehicle treatment. **e**, A schematic diagram illustrating the experimental design. **f**, Immunostaining for tdT, GFP, and FOXJ1 on lung sections after DT treatment. **g**, A schematic diagram illustrating the experimental design. **h**, Immunostaining for FOXJ1, and Scgb1a1 on lung sections at the indicated time points post-Naph or vehicle treatment. **i**, Quantification of the number of $FOXJ1^{+}$ ciliated cells per 100 μm of bronchial basement membrane in (**h**). (n = 5). **j**, Immunostaining for GFP, FOXJ1, and TUNEL on lung sections after naphthalene or vehicle treatment. **k**, A schematic diagram illustrating the experimental design. **l**, Immunostaining for tdT, GFP, and FOXJ1 on lung sections after naphthalene treatment. Each image is representative of 5 individual biological samples. Ace-Tub, Acetylated tubulin. Tam, tamoxifen. DT, diphtheria toxin. Naph, naphthalene. br, bronchiole. White scale bars, 100 μm.